

TRANSPORT PROPERTIES OF CLUSTER-ASSEMBLED MAGNETIC NANOSTRUCTURES

THÈSE N° 4027 (2008)

PRÉSENTÉE LE 29 FÉVRIER 2008

À LA FACULTÉ DES SCIENCES DE BASE
LABORATOIRE DE NANOSTRUCTURES EN MATRICES
PROGRAMME DOCTORAL EN PHYSIQUE

ÉCOLE POLYTECHNIQUE FÉDÉRALE DE LAUSANNE

POUR L'OBTENTION DU GRADE DE DOCTEUR ÈS SCIENCES

PAR

Giulia DI DOMENICANTONIO

laurea in fisica, Università degli studi di Roma La Sapienza, Italie
et de nationalité italienne

acceptée sur proposition du jury:

Prof. R. Schaller, président du jury
Prof. C. Félix, Dr M. D. Hillenkamp, directeurs de thèse
Dr V. Dupuis, rapporteur
Prof. K. Fauth, rapporteur
Prof. H. Ronnow, rapporteur



ÉCOLE POLYTECHNIQUE
FÉDÉRALE DE LAUSANNE

Suisse
2008

Abstract

The aim of this thesis is to get a deeper understanding of magnetic properties of small clusters when they are embedded in a host material. The study was motivated by the observation of the very peculiar properties that clusters present in the gas phase or when deposited on a substrate. The intriguing perspective is that those properties would be preserved in a solid state sample that could be used for technological applications.

Preformed and well characterized clusters are used as building blocks to produce nanostructured films in which they are embedded in a host material in order to preserve them from chemical and thermal degradation when the sample is exposed to ambient conditions. For this purpose an innovative set-up has been constructed that allows the independent control of cluster size, concentration and chemical composition. In particular samples containing small magnetic clusters embedded in a non magnetic matrix have been produced in order to study the evolution of the magnetic behaviour of such cluster assembled materials.

These samples have been subsequently studied by means of magnetotransport, in particular by measuring their magneto-resistance and Hall voltage as a function of temperature in magnetic fields of up to $5T$. Additionally, a novel measurement protocol detecting the derivative of the resistance with respect to temperature as a function of magnetic field has been used to characterize the samples.

Magnetotransport is known to be an important tool for the investigation of the magnetic behaviour as the conduction electrons can be considered as microscopic probes of the state of the sample. However, even though these properties have been studied extensively, a complete and universally accepted theory on the mechanisms giving rise to the observed magneto-resistance in cluster assembled materials is still to be found.

In this work, the high quality of the produced samples allows an unequivocal identification of all the aspects that are not correctly described by the theories in use. In particular it is observed that, in the case of small clusters, the effect of magnetic interactions cannot be neglected even at very low concentrations. The consequence is twofold since both the superparamagnetic model of magnetization and the well known $(1 - m^2)$ expression for the magneto-resistance fail if a correlation between magnetic moment exists.

Furthermore we claim that the Mott hypothesis of two parallel currents adopted for electrical conduction is not sufficient to describe the details of transport in granular systems. In fact the particular differential resistance measurement introduced in this work allows an underlining of the importance of the spin-channel mixing mechanisms that are not taken into account in the Mott picture.

Keywords:

Cluster; Nanostructure; Cluster Assembled Materials; Magnetism; Spintronics; Giant Magneto Resistance; Spin mixing.

Riassunto

Il fine di questa tesi è la comprensione delle proprietà magnetiche di piccoli aggregati metallici dispersi in una matrice di diversa natura. L'interesse di questo studio deriva dalle peculiari proprietà che vengono osservate negli aggregati magnetici quando si trovano in fase gassosa o depositati su un substrato. La speranza è di poter preservare tali proprietà in un campione in stato solido che possa essere utilizzato per delle applicazioni tecnologiche.

In quest'ottica, degli aggregati dalle caratteristiche ben definite vengono utilizzati come costituenti fondamentali per la produzione di materiali granulari nanostrutturati. Più nel dettaglio, gli aggregati vengono dispersi in una matrice avente lo scopo di proteggerli dalla degradazione chimica e termica che avrebbe altrimenti luogo in condizioni ambiente. A questo scopo è stato ideato e realizzato un apparato sperimentale che permette di produrre aggregati controllandone, simultaneamente e in maniera indipendente, la taglia, la concentrazione e la composizione chimica. Nel caso particolare di questo lavoro sono stati prodotti campioni in cui piccoli cluster di cobalto sono dispersi in una matrice diamagnetica con l'intenzione di studiarne le proprietà magnetiche in funzione della loro struttura microscopica.

I campioni sono stati analizzati tramite delle misure di trasporto in funzione della temperatura e in campi magnetici fino a $5T$. L'attenzione stata, in particolar modo, focalizzata sulla magnetoresistenza e il potenziale di Hall. Per meglio caratterizzare i campioni, è stato inoltre sviluppato un altro procedimento di misura che rileva la derivata rispetto alla temperatura della resistenza in funzione del campo magnetico applicato.

Il magnetotrasporto si rivela particolarmente utile per lo studio del comportamento magnetiche dei materiali in quanto gli elettroni possono essere visti come sonde microscopiche dello stato del campione. Tuttavia, nonostante questa applicazione investigativa delle proprietà di trasporto sia in uso da molti decenni, una teoria completa e universalmente riconosciuta che descriva i meccanismi di conduzione non è stata ancora formulata.

In questo lavoro, grazie all'ottima caratterizzazione dei campioni, è stato possibile identificare univocamente tutti gli aspetti che determinano il fallimento dei modelli normalmente utilizzati. In particolare si è osservato che, nel caso di piccoli aggregati, le interazioni mag-

netiche giocano un ruolo fondamentale che non può essere trascurato. La presenza di tali interazioni ha una duplice conseguenza, infatti da una parte diviene necessario abbandonare il modello superparamagnetico e allo stesso tempo la magnetoresistenza non può più essere descritta come $(1 - m^2)$.

Si ipotizza inoltre che un'ulteriore approssimazione debba essere abbandonata: l'ipotesi di Mott di due correnti di spin separate e indipendenti che viene generalmente utilizzata per descrivere il trasporto in materiali non magnetici. In particolare la nuova tecnica di misura differenziale applicata alle nanostrutture granulari, sembra mostrare l'importanza delle collisioni che implicano un'inversione dello spin degli elettroni di conduzione, collisioni che vengono trascurate nell'immagine di Mott.

Parole chiave:

Aggregato; Nanostruttura; Materiali Granulari Nanostrutturati; Magnetismo; Spintronica; Magnetoresistenza Gigante.

Table of contents

Introduction	1
I State of the Art	5
Cluster physics	7
2.1 Clusters: from the atom to the bulk	7
2.2 Theoretical Models	11
2.2.1 Large metallic clusters	11
2.2.2 Small clusters	12
2.3 Cluster Production	13
2.4 Conclusions	16
2.4.1 Cluster Assembled Materials	16
Magnetism at the nanoscale	19
3.1 Basic phenomenology of bulk magnetism	20
3.2 The origin of atomic magnetic moment	21
3.3 The evolution of magnetic moment	22
3.3.1 Localized Moments: the Heisenberg model	23
3.3.2 Itinerant Magnetism: the Stoner model	24
3.4 Magnetic Interactions	24
3.4.1 Direct Exchange	25
3.4.2 Dipolar Interactions	25
3.4.3 Indirect exchange	26
3.4.4 Superexchange	26
3.5 Magnetism in Clusters	26

3.5.1	Clusters in the gas phase	27
3.6	Cluster Assembled Materials	30
3.6.1	Dilute systems: the superparamagnetic limit	31
3.6.2	Weak interactions: the interacting superparamagnet	32
3.6.3	Spin glasses	34
Magneto Transport		35
4.1	Magneto Resistance	36
4.1.1	MR in normal metals	37
4.1.2	MR in ferromagnets	38
4.1.3	MR in multilayers	38
4.1.4	MR in granular materials	40
4.2	The virtual-bound-state model	41
4.3	Hall effect	42
II Experimental Methods		45
Sample Preparation		47
5.1	Concept and Overview of the Apparatus	47
5.2	The Cluster Source	49
5.3	Transfer and Deflector	53
5.4	TOF Mass Spectrometer	54
5.5	Deposition	56
5.6	Residual gas analysis	59
5.7	Conclusions	60
Measurements		61
6.1	Sample characterization	61
6.1.1	X-Ray Photoelectron Spectroscopy	61
6.1.2	High Resolution Transmission Electron Microscopy	62
6.2	SQUID magnetometry	63
6.3	Transport measurements	64
6.3.1	Magneto Resistance	65
6.3.2	Hall voltage	66
6.3.3	Magneto Differential Resistance	68

III Results and Discussion	71
Magnetization and GMR	75
7.1 Results: MR and Hall voltage	75
7.1.1 Magnetic Field and Temperature	75
7.1.2 Hysteresis	76
7.1.3 The effect of size	78
7.1.4 The effect of concentration	79
7.1.5 Anisotropy	81
7.1.6 The effect of the matrix	82
7.2 Magnetotransport in the two current approximation	83
7.2.1 The origin of magneto-resistance	85
7.2.2 Zhang and Levy model	86
7.2.3 MR in the superparamagnetic limit	90
7.2.4 Interaction Mechanisms	93
7.2.5 MR for interacting superparamagnets	94
7.2.6 Beyond the superparamagnetic model	96
7.2.7 Correlated Spin Glasses	100
7.3 Conclusions	102
Beyond the Mott hypothesis	103
8.1 Experimental	103
8.1.1 Magnetic Field and Temperature	103
8.1.2 Concentration	104
8.1.3 Size	105
8.2 <i>MDR</i> in the superparamagnetic model	107
8.2.1 The importance of <i>MDR</i>	108
8.3 <i>MDR</i> and Spin-Mixing	109
8.4 Conclusions	111
Conclusions and Perspectives	116
Appendix A	121
Appendix B	125
Bibliography	136

Introduction

The constant quest for miniaturization brought about the discovery of a great number of fascinating phenomena that take place when the size of a system is reduced to the nanoscale. The challenge of nano-physics is to understand and control the mechanisms giving rise to these phenomena.

For what concerns the understanding, an important role is played by clusters: systems composed of a finite number of atoms or molecules ranging from two to many thousands. Clusters offer the unique opportunity to follow the modification of properties as the system develops from the isolated atom to bulk matter and furthermore their behaviour is unique and strongly related to the specific size. Because of this strong dependence on size, two different regimes are often distinguished: the regime of scalable size effects and that of quantum size effects. The former concerns clusters containing at least several tens of atoms and in which the energy structure is similar to the bulk. Consequently, continuum models are applicable. However, since the large fraction of surface atoms plays a determining role on the cluster properties, these will still present peculiar features and will reach the bulk behaviour in the large particle limit. The quantum regime, on the other hand, applies to clusters containing a few tens of atoms only. In this case the energy bands are not yet formed and the energy landscape is closer to a molecular one with discrete levels. As a consequence the properties can vary dramatically with the size and strong fluctuations are observed even with the addition of a single atom.

The clusters studied in this work belong to this second category and have been shown to be extremely challenging because of interesting properties such as fluorescence [Feli 01, Peys 01], enhanced catalytic activity [Sanc 99] and unusual magnetic moment [Bill 94, Lau 02, Gamb 03]. In particular interest has been focused on magnetism.

All these peculiar properties have been observed in free or supported clusters. In order to obtain results that could be useful for technological applications, it is needed to embed the clusters in a solid environment in order to protect them from thermal or chemical deterioration. A sample is then produced in which the nanoparticles are used as building blocks of a new kind of material that is expected to have peculiar properties related to those observed for free clusters.

For this purpose an innovative set-up is necessary that allows the production of well-defined small magnetic clusters with great control of their size and chemical state. The clusters can then be deposited at low energy to avoid fragmentation, together with the desired matrix in order to form a film with a controlled concentration of the magnetic particles. After this growth process the sample can be taken out of vacuum and characterized in the desired experimental facility. In the present case cluster assembled magnetic materials have been produced and characterized by means of transport measurements. This technique has in fact proven to be a successful method to probe the magnetic behaviour since transport properties are not sensitive to the total amount of magnetic material but rather to its concentration. Consequently these measurements are well suited in the present case in which, because of the low flux of clusters and their reduced dimension, the absolute amount of magnetic particle is extremely low. In particular the magneto-resistance and Hall effect have been recorded for samples with different cluster concentrations and sizes, ranging from one atom to several thousands of them. Another measurement protocol will also be presented: the magneto differential resistance (*MDR*). This technique consists in detecting the magnetic response of the first derivative of the resistance with respect to temperature. *MDR* is claimed to be important in order to understand the details of the spin dependent conduction mechanisms as it allows the elimination of all the temperature independent contributions that dominate the resistivity signal.

Nevertheless magneto transport is not only a probe of the magnetic behaviour but it is itself an interesting field of research. Great attention was attracted by this domain following the discovery of several challenging phenomena, the best known being the discovery of *GMR* by A. Fert [Baib 88] and P. Grünberg [Bina 89], awarded with the Nobel prize in Physics in 2007. The rapid technological application of *GMR* as well as the development of several devices based on magnetotransport effects, such as magnetic random access memories or the spin-polarized field effect transistor, have brought about the birth of a new science: spintronics.

Even though it has been the subject of numerous and detailed studies in the last recent years, a complete and universally accepted theory for the intriguing transport phenomena that are observed in nanostructured materials is still to be found. As much as concerns cluster assembled materials, the difficulties arise mainly from the complex effect of cluster-cluster and cluster-matrix interactions and their interplay with the conduction mechanisms. A severe limitation to the understanding of the problem comes from the experimental difficulties in producing well defined samples and in controlling each parameter independently. In this context it is expected that the sample preparation technique that was developed in this work, together with the analysis procedure and the new *MDR* measurement protocol will allow for a deeper insight on the theory of spin-dependent conduction.

Outline of the thesis

This thesis is divided into three main parts: an introduction and state of the art, a description of the experimental techniques, and the discussion of the results.

In the first part, the main aspects of cluster physics, of magnetism, and of transport properties of magnetic nanostructures are summarized and discussed. The purpose is to introduce the different fields with which this work is concerned and review the concepts and the formalism that will be useful for further discussion.

In the second part, the experimental apparatuses for both samples preparation and characterization are presented. A great deal of attention is given to the set-up for cluster production, since the construction and the optimization of this apparatus was one of the important and innovative parts of the work, as it was built and customized following an original design adapted to the specific requirements of the planned experiments. For what concerns the measuring technique, a topic that deserves particular attention is the employment of the magneto differential resistance measurement. This technique, developed in collaboration with the group of Prof. J-P. Ansermet, is extremely sensitive to the details of the sample magnetic structure allowing a further understanding of the microscopic mechanisms of magnetotransport.

Finally, the third part is devoted to experimental results, their analysis and discussion. It will be shown that the magnetic moment of small clusters does survive when embedded in the sea of conduction electrons and that, because of the mediating action of the conduction electrons themselves, the magnetic behaviour is strongly influenced by collective behaviour. Clusters cannot thus be considered as isolated entities anymore: interactions between them and with the surrounding matrix play an important role and the material has to be considered as a whole. In particular it will be shown that much of the observed behaviour can be attributed to correlations and the subsequent formation of a spin glass. In the last chapter attention is brought again to the mechanisms defining the transport properties and the potentiality of the magneto differential resistance measurement is discussed. An interpretation in terms of spin channels mixing is presented.

Part I

State of the Art

Cluster physics

In 1956 Becker and co-workers [Beck 56] reported for the first time the formation of a cluster beam. Clusters were identified as assemblies of atoms or molecules bound together by bulk-phase intermolecular forces and ranging in size from the dimer up to many millions of atoms. Since they are formed by a limited number of particles, they are traditionally referred to as the *link between the atom and the bulk*. Even if this image has been often used to over-speculate on the importance of clusters, it still contains a great amount of truth: several properties as polarizability, magnetic susceptibility, photoabsorption, etc. are considerably different from both the atomic, discrete case and the continuum limit.

The second sentence that every cluster physicist has heard and repeated an innumerable amount of times is that *at small sizes every atom counts*. The phrase refers to the fact that in the nanometric world, the energy landscape strongly depends on the electronic structure that, as we will see, can vary dramatically with the addition of a single atom.

In this chapter I will review some important features of cluster physics in order to better explain the two founding sentences presented here. A short description of the theoretical models used to interpret cluster behaviour will follow. Afterwards I will present the main experimental technique that have been developed for the production of clusters, in order to justify the choices that have been made in planning the experiment described in this work.

2.1 Clusters: from the atom to the bulk

The materials we encounter in every day life are composed of a enormous, virtually unlimited, number of particles. Their properties depend on the nature and on the geometrical arrangement of the elemental constituents: atoms or molecules. Their behaviour is defined by collective effects and also the models used to describe it are based on many-body techniques that strongly differ from the formalism used in the atomic case. But what happens if an aggregate of only a few particles is considered? Up to which extent can a molecular approach be used? And down to which limit is the bulk behaviour still valid? Those are some of the questions cluster physicists try to answer.

In modelling bulk material, an infinite number of atoms is considered. As a consequence, size and shape do not play an important role. When the dimension is reduced, the fraction of atoms located at the surface increases (cf. fig.2.1) up to becoming dominant, as it is the case for the small clusters considered in this work. The energy balance of the particle and,

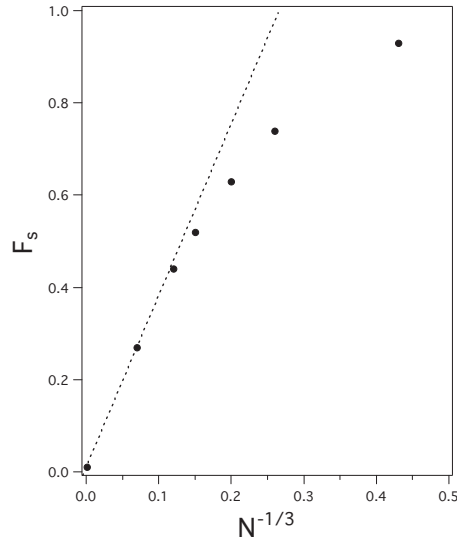


Figure 2.1 – Fraction of surface atoms (F_s) with respect to the total number of atoms (N) plotted against $N^{-1/3}$ for icosahedral geometric shell clusters. The dashed line represents the prediction in a spherical cluster approximation.

as a consequence, its behaviour, are then determined by the contribution given by surface atoms that have a lower coordination than those in the volume and are consequently more sensitive to the local geometry and environment. In the small size regime it can then be sufficient to add a single atom to induce a significant change in properties such as the melting point or the first ionization potential that are shown, as a function of size, in fig.2.2. This is the main reason why cluster behave differently than bulk, however a big difference in behaviour is observed also between small (less than a thousands atoms) and large clusters.

In the large size regime clusters can be described using adapted continuum models, while in the small size regime, their properties are closer to those of molecular systems. This fact reflects the evolution of electronic properties with the number, N , of atoms per cluster: when only a few atoms are assembled together, the cluster will present discrete energy levels and behave similarly to a molecular system; as N is increased, the energy separation between levels will reduce and become negligible with respect to thermal energy, $\Delta E \ll k_B T$, the levels can thus be considered as narrow bands, eventually approaching the continuum limit.

Let us consider, as an example, the optical absorption spectra of clusters embedded in a dielectric host. The classical description of the interaction between a spherical metallic particle and an electromagnetic wave, has been derived by G. Mie [Krei 95] solving Maxwell

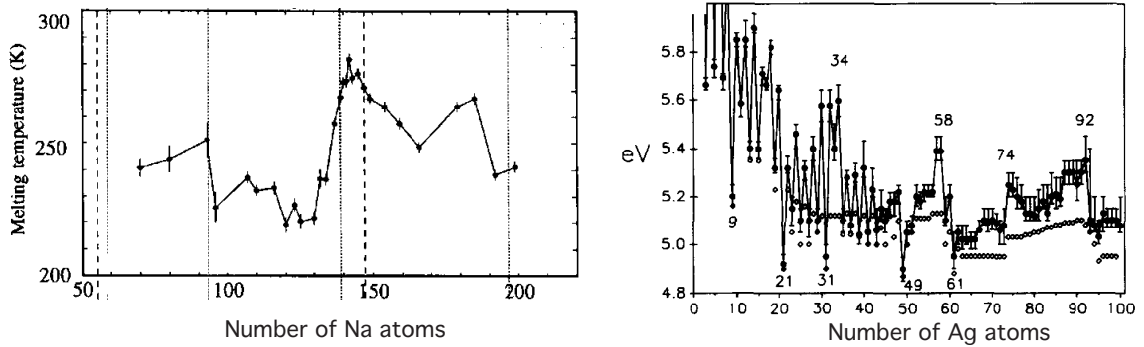


Figure 2.2 – Melting point of Na clusters [Schm 98] (on the left) and ionization potential of Ag clusters [Alam 92] (on the right) as a function of the number of atoms per cluster. Strong fluctuations are observed even if a single atom is added.

equations with adequate boundary conditions. If ϵ_m is the dielectric constant of the matrix and $\epsilon(\omega) = \epsilon_1(\omega) + i\epsilon_2(\omega)$ is the dielectric function of the bulk metal, the absorption coefficient can be written as:

$$\alpha(\omega) = 9\frac{\omega}{c}\epsilon^{3/2}V_0\frac{\epsilon_2(\omega)}{[\epsilon_1(\omega) + 2\epsilon_m]^2 + [\epsilon_2(\omega)]^2}$$

where ω_p is the surface plasmon frequency of the cluster, defined as the solution of $2\epsilon_m + \epsilon_1(\omega) = 0$ [Kres 92]. It is important to remark that this model is size independent, in

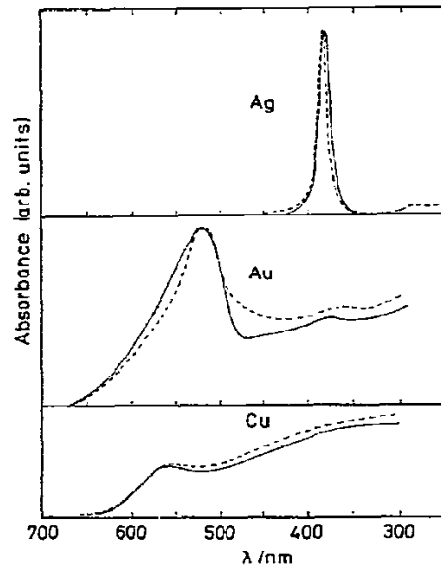


Figure 2.3 – Measured absorbance spectra of Ag, Cu and Au clusters of about 10nm diameter in solid argon matrix compared with spectra calculated with Mie theory (broken lines) [Abe 82]. The position of the peak as well as the general form of the absorbance are well reproduced by theoretical curves.

agreement with the classical principle that no size effect should be observed if the wave length of light is longer than the diameter of the particle¹. This model is also in good agreement with experimental results for clusters of intermediate size (i.e. large enough for continuum theories to be valid and sufficiently small to allow to neglect multipolar excitations) as shown in fig.2.3. However, as the size of clusters is decreased, several size effects start to appear and the classical model fails.

The first size effect, observed for clusters of some nanometers in diameter, is a shift and a broadening of the surface plasmon peak. Both the width and the position scale as $1/D$, this being a clear sign of an effect due to the cluster-matrix interface [Moli 03, Hilg 00]. It is in fact reasonable to expect the chemical nature of the matrix to have an influence on the plasmonic excitation. A more accurate theoretical description of these intermediate sizes, can be obtained in the framework of the Jellium model [Ekar 85] that will be described in the following section.

The failure of the Mie theory is much more drastic when smaller sizes are attained, as it can be seen in fig.2.4. In the sub-nanometric region several features appear that are interpreted as single electron excitations. In this case a quantum treatment of the electronic

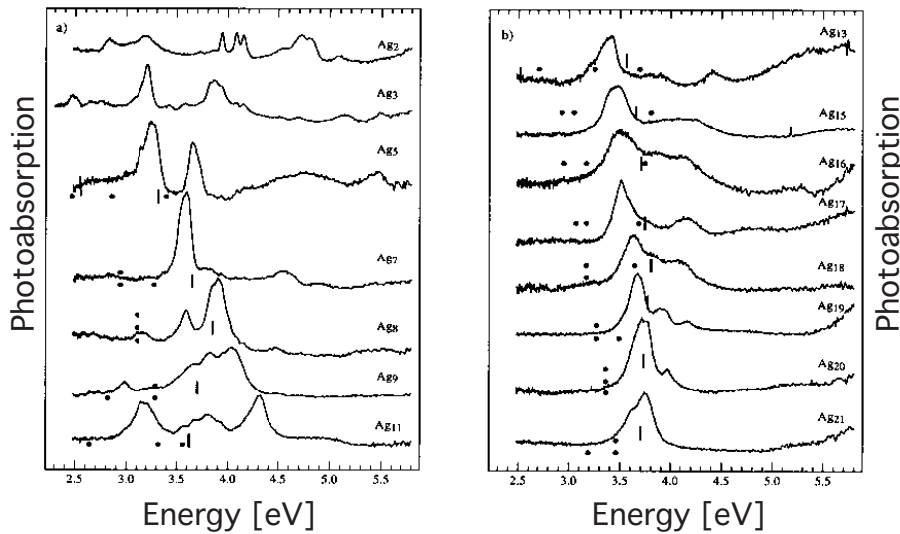


Figure 2.4 – Photoabsorption spectra of small Silver clusters in solid Argon. The points correspond to the energies calculated with the Mie theory [Fedr 93]. A transition from plasmon-like absorption to molecular transition is observed as the size is reduced.

structure of the system, taking into account the actual geometry as well as the chemical interaction with the surrounding matrix, is required.

This overview on the absorption properties underlines the importance of reduced dimensions in photoabsorption experiments. The relevant effect of interfaces in the case of

¹Since the energy range of interest is the Visible-UV, typical wave lengths are of the order of $300nm$, much bigger than the particle diameter that is less than $10nm$.

embedded clusters was also pointed out. It can be expected that size and interactions with the matrix will play an important role in determining other properties as well, in particular on the magnetic properties of cluster assembled materials, that are the subject of this work.

2.2 Theoretical Models

In the previous section, it was discussed how the size evolution implies a transition from a molecular-like to a bulk-like behaviour. As a consequence, theoretical frameworks have been developed to describe both small and large clusters: for small systems a bottom-up approach can be followed using the tools of quantum chemistry to build a model based on the atomic states, while the properties of larger particles are generally well described by continuum theories obtained starting from bulk behaviour and applying a top-down strategy. In the following the basic concepts used in each approach are presented focusing on metallic particles that are the subject of this work.

2.2.1 Large metallic clusters

Atoms in metallic clusters are kept together by bulk metallic bonds with a covalent contribution that is negligible for the *s*-type elements and becomes important in the case of transition metals [John 98].

Since the properties of large metallic clusters are defined by the delocalized valence electrons, much of their phenomenology can be explained in the frame of the **Jellium model** [Knig 84, Mart 85], which does not take into account the details of the geometrical arrangement of the atoms. In this model a cluster containing N atoms is assumed to be a sphere¹ of radius R with a uniform distribution of positive charge, n , defined by the valence charge z and the Wigner-Seitz radius r_{WS} , as being $n = z/r_{WS}$, where r_{WS} is linked to the volume of the Jellium sphere by $N r_{WS} = \frac{4}{3}\pi R^3$.

As a result the potential felt by the electrons is spherical and the respective energy levels can be labelled with a principal and an orbital quantum number. In first approximation clusters can be treated as *super atoms*. However, since in this case the positive charge is distributed over a broad volume instead of following a delta-like function as in the atomic case, the potential will have a different form influencing the structure of the energy levels.

The importance of this model relies on the fact that, with an appropriate choice of potential, several cluster properties can be explained. The most adequate choice is the Woods-Saxon potential:

$$U(R) = \frac{-U_0}{\exp[(r - R)/\sigma] + 1}$$

¹A semi-phenomenological argument as the Clemenger-Nilsson model, proves that clusters are mostly ellipsoidal rather than spherical. The Jellium model has been extended to describe this more realistic case [Laur 91].

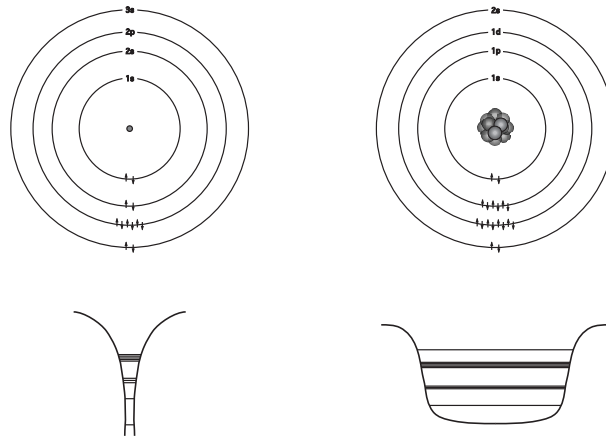


Figure 2.5 – Schematics of the energy levels of an atom and a cluster. The difference in form of the potential produces a different ordering of atomic levels, but the same type of formalism and labelling can be used.

where $U_0 = \epsilon_F + W$, W and ϵ_F being the work function and the Fermi energy of the bulk material. It is then possible to predict the apparition of *magic numbers*, i.e. particular sizes corresponding to a more stable electronic configuration due to the filling of a shell, in mass abundance spectra, ionization energy or electronic polarizability.

However the quantitative agreement is restricted to the case of alkali and noble metal atoms while the Jellium model fails in the case of three valence electron elements as well as in describing fine structure effects (as the even-odd alternations in mass spectra or ionization potential). In particular the model is not too accurate for transition metal clusters that are the subject of this work. In this case the failure can be attributed to the presence of *d*-orbitals that give rise to narrow bands with high electronic density of state, resulting in a strong dependence of the shell structure on the atomic arrangement. As a result magic numbers will appear in correspondence of stable geometrical configurations, as icosahedra, or in other favourable configurations defined by the interplay of structure and electronic shells [Mart 96].

2.2.2 Small clusters

We stated that the geometrical arrangement of atoms plays an important role in the determination of the electronic structure in many cases of interest. Models based on quantum chemistry concepts aim to the description of clusters without any crude simplification of the ionic background. The goal is to determine the structure of the cluster by the determination of the most stable configuration, i.e. by minimizing the total energy of the system [Bran 83].

Such procedure presents however several complications since it has to deal with the eigenfunctions and the eigenvalues of the complex relativistic Hamiltonian of N atoms and

ZN interacting electrons. As a consequence some approximations need to be introduced, the most important of which being the *Born-Oppenheimer approximation*. It consists in separating the nuclear and electronic problems and writing the total wave function as a product of a nuclear and electronic part:

$$\Phi_{\mathbf{R}, \mathbf{r}} = \psi(\mathbf{R})\phi(\mathbf{r}; \mathbf{R})$$

where \mathbf{R} and \mathbf{r} are the coordinates of nuclei and electrons respectively and \mathbf{R} has the role of an external parameter in ϕ . This guess is justified by the fact that the electrons dynamics are much faster than those of the nuclei so that the two problems can be considered as uncoupled. The consequence of such approximation is the well known level structure of rotational and vibrational molecular excitations.

Once the electronic and nuclear problem are decoupled, several techniques can be used to obtain reasonable approximations of the electronic wave function, the best known ones being the Hartree-Fock method and the density functional theory.

The *Hartree-Fock* method consists in writing the ZN body wave function as an anti-symmetric product of (ZN) single-body wave functions, called a Slater determinant. At this point the variational principle is applied to minimize the energy, resulting in a self-consistent problem. The use of a single Slater determinant is actually a very crude restriction of the phase space of parameters; the method can be considerably improved, engaging extra computing time, using as first guess a linear combination of Slater determinants.

While in the Hartree-Fock method the one-electron wave function is varied to determine the energy minimum, in the second technique, the *density functional* method, the energy is written as a functional of the electronic density $n(r)$. The main advantage of this technique is that $n(r)$, and hence the whole problem, depends only on three variables; the major drawback is that, on the other hand, the form of the exchange and correlation energy is not known. Several approximation can be given for such term, the best known being the local density approximation (LDA).

2.3 Cluster Production

Clusters are not only challenging systems for theorists, they are also an important laboratory for testing new experimental methods and technologies. With the growth of interest in nanotechnology, several strategies have been developed to operate in the nano-scale regime [Glei 95]. One aspect of the experimental challenge concerns the production techniques. As for the theoretical description, two different approaches are distinguished: top-down and bottom-up. As it is revealed by their names, the top-down approach consist in starting from the bulk and reducing the size, as it is done in lithography or ion milling; while in bottom-up approaches the atoms are used as building blocks to construct the nanostructures. Cluster sources belong to the latter category and they exploit various working principle in order to

satisfy different experimental needs: the beam can be chosen to be intense, cold, charged, and so on.

Almost all sources are based on the vaporization of the material and subsequent condensation. Vaporization can be obtained by Joule heating, laser ablation, sputtering, depending on the characteristics of the material (its boiling point or its electrical conductivity, for example). Once a vapour of atoms is created, they are condensed together to form larger aggregates.

Source type:	Seeded supersonic nozzle	Gas aggregation	Laser vaporization and Pulsed arc vaporization	Sputtering	Pick-up
vaporization method	Joule heating	Joule heating or sputtering	pulsed laser or pulsed arc	high energy ion bombardment	Joule heating
aggregation	hot inert seeding gas + expansion	cold inert seeding gas	inert seeding gas + expansion	preformed clusters	atoms captured in pre-formed rare gas clusters
pulsed or continuous	continuous	continuous	pulsed	continuous	continuous
typical cluster size in atoms	1-1000	1-10000	1-1000	1-100	1-100
cluster temperature	depends on the expansion	source temperature or lower	source temperature or lower	very high	low
target material	low boiling point	low boiling point	all metals	all metals	low boiling point
main reference	Hagena 91	Sattler 80	Milani 90	Begemann 89	Gough 85

For the aggregation to take place, cooling of the vapour is required to attain a supersaturated vapour state in which it is energetically possible to create a stable cluster. Cooling can be achieved by an expansion or by thermalization with an inert gas. The latter technique is advantageous if the temperature of the beam needs to be controlled, since the final temperature of the beam will be determined by that of the thermal bath. In table 2.3 the mostly employed sources are listed together with their operational principle and main features. For a comprehensive review on the subject see [Scol 88]; in the following a short description of the most used sources is given

Supersonic Nozzle Sources

In supersonic nozzle sources the material is vaporized and stored in a high pressure ($\sim 10^5 - 10^6 Pa$) stagnation chamber. The vapour is then expanded through a small nozzle with a diameter of less than $1mm$ into vacuum, thereby creating a supersonic beam. The high stagnation pressure and the small diameter of the nozzle guarantee a great number of collisions during the expansion. Furthermore, the expansion being adiabatic and isenthalpic, the vapour is cooled and becomes supersaturated allowing clusters to condense.

These sources produce intense, continuous cluster beams with narrow velocity distributions and sizes up to thousands of atoms. Clusters can be obtained from inert gases, molecules and low-boiling metals, as well as from alkali metals via prior vaporization in an oven. In this latter case an inert gas is added into the aggregation chamber in order to reach high pressures and to decrease, via collisions, the temperature of the vapour. In this case the source also exploits the **gas aggregation** principle.

Laser Vaporization and Pulsed Arc Sources

In these kinds of sources, vapour is produced by pulsed-laser ablation or by an intense electrical discharge, which produce a high temperature plasma. A pulse of cold helium cools such vapour and induces cluster formation. Further evaporative cooling can then occur.

The resulting beam can be pulsed, highly intense, and contains clusters with sizes up to several hundreds atoms, with temperatures lower than $110K$. Another advantage of these sources is that clusters can be produced out of almost any material, including refractory metals, carbon and silicon.

Ion Sputtering Sources

In ions sputtering sources, clusters are produced by bombarding a target with high energy inert gas ions. The produced beam is continuous, ionized and hot, evaporative cooling will hence take place. Clusters are generally quite small.

All conductive targets, including refractory metals and high-temperature melting materials can be used.

Pick-up Sources

In this case large rare-gas clusters are first produced in a supersonic expansion, the beam drifts then through a chamber containing low-pressure vapour of the material out of which clusters have to be produced. The gas droplet capture the atoms that aggregate inside it. The droplet that acts as a thermal bath, defining in an extremely precise way the final temperature of the clusters.

With this source it is possible to operate at very low temperatures (as liquid helium temperature, for example) and thus the technique is particularly well suited for optical studies as the analysis of vibrational spectra.

The source that has been built in this work exploits several principles of those listed above: the vaporization is obtained with magnetron sputtering and the aggregation takes place via collision with an inert gas. The whole aggregation chamber is cooled at liquid nitrogen temperature and the exit is constituted by an adjustable diaphragm which guarantees an expansion of the clusters-gas mixture. As a result, a continuous beam containing a high percentage of ionized particles is produced. Cluster sizes range between 1 and several thousands of atoms and can be obtained from any metallic material. A detailed description of the source will follow in part II.

2.4 Conclusions

The main characteristics of small clusters have been presented here. It was observed that the two key factors at the origin of their peculiarities are the *quantum confinement* and the *surface to volume ratio*.

These parameters will influence both electronic and geometrical properties of clusters. The first ones show a transition from a *discrete*, quantized energy levels, to the formation of narrow bands that are the precursors of the solid state structure. The latter ones present particular *non crystallographic symmetries* due to the fact that the rotational and translational invariances do not have to be satisfied anymore. As a consequence, cluster properties are tunable and, in the small size region they can change with the addition of a single atom.

For those reasons clusters are extremely interesting from both the scientific and technological point of view. However, in order to seek for applications, it is necessary to produce systems in which clusters are protected and supported.

2.4.1 Cluster Assembled Materials

Up to now the peculiar properties of free clusters have been discussed. However clusters can also be seen in a different way: they can be imagined as *super-atoms* and used as building blocks in order to produce a novel kind of system: cluster assembled materials [Pere 97, Jena 96]. The expectation is that some of the unique properties of clusters will be preserved and that, with the introduction of extra parameters, it will be possible to specifically tailor the characteristics of those materials. For example if in a normal crystal there is only one characteristic length, i.e. the lattice constant, in cluster assembled materials we introduce the particle size and the inter-particle distance; also the interaction landscape becomes more complex since both inter- and intra-cluster interactions need to be considered.

The basic principle consists in growing the clusters using a physical or chemical technique and assemble them with or without a bonding material (matrix).

However it should be kept in mind that such treatment can strongly affect the aggregates that could coalesce or alloy with the matrix. In the most favourable case in which clusters stay intact and independent, the embedding process still produces a modification of the geometry and of the electronic properties of the aggregates, and the resulting properties will be generally different from those observed in the gas phase [Faut 04b]. In studying cluster assembled materials, then, several additional topics have to be faced, the most important being the effect of interactions both with the matrix and with the neighbouring clusters.

If the investigation of free clusters is of fundamental interest from a scientific point of view, the production of cluster-assembled materials opens several perspectives on technological applications.

Magnetism at the nanoscale

Magnetism and the phenomena related to it have fascinated mankind since the ancient times [Berr]. First came the observation that some minerals, such as magnetite Fe_3O_4 and the magnetic iron ore $FeO - Fe_2O_3$ can attract iron.

The empirical observation of these natural phenomena led to the development of important technological applications, starting from the compass to electro-magnetic motors and, in recent times, magneto-recording. For a long time, the focus has been on macroscopic magnetism, however, in the last decades it became clear that many other challenging applications can be found if magnetism when the dimension of the system is reduced to the nanoscale.

Mother Nature is exploiting the magnetic properties of nanostructures since millions of years, for example growing magnetite nanoparticles in bacteria, insects and higher animals in order to help them to keep vertical orientation (as in the case of magnetostatic bacteria [Sche 06]) or to find their way in long migrations (as in the case of pigeons and tuna [Walk 84]).

Men also have found the way to exploit the properties of magnetic nanosystems and developed ultra-high density storage media, magnetic reading-heads, high performance permanent magnets [Skom 99, Full 98, Al O 95, Skom 93], and so on. But even more challenging are the frontiers that can be foreseen: magnetic nanostructures could be used for drug delivery, for building micro-electromechanical systems (MEMS) and for customizing new devices for spintronics.

However, magnetism is not only interesting for technological applications, but also from a fundamental point of view. In 1600 the English physicist William Gilbert publishes *De Magnete* [Gilb 00], opening the way to a scientific investigation of magnetism. But it was only in the last century, with the development of quantum mechanics that the basic phenomena of magnetism, as crystal-field interaction, exchange interaction or spin-orbit coupling were finally understood. A related question concerns the transition from macroscopic to nanoscale magnetism: in the case of reduced dimension, a rich variety of peculiar behaviours are observed as random-anisotropy scaling [Chud 86], remanence

enhancement [Coeh 88], grain boundary [Liu 00] and exchange coupling [Hadj 99] effects. These phenomena are due to the modification of *extrinsic* properties, such as the remanence magnetization or the coercivity, that strongly depend on the structure of the system and, when moving to very small size regimes, also to the change of *intrinsic* properties, like the spontaneous magnetization or the internal anisotropy.

In order to understand magnetism in cluster-assembled materials, both extrinsic and intrinsic properties need to be considered since, as it will be shown, the behaviour of such system is peculiar in both ways: on one side the reduced dimension of clusters modifies the intrinsic parameters and on the other the particular structure of the material produces peculiar extrinsic properties due to the complex interaction landscape.

3.1 Basic phenomenology of bulk magnetism

When a material is exposed to a magnetic field H , a magnetization

$$M = \chi H$$

is induced. The susceptibility χ , defining the response of the system, depends on the nature of the atoms and on the environment to which they are exposed.

In order to explain in a qualitative way the magnetic behaviour of matter, it is sufficient, in first approximation, to treat each atom as a single, independent magnetic dipole. Such dipole can be intrinsic or induced by the external field.

If the atoms do not possess a magnetic moment, the effect of an applied magnetic field will be the generation of an induced moment with opposite orientation. We speak in this case of **Larmor diamagnetism**. This effect is encountered in every material, however due to its small absolute value, it is hidden by other stronger magnetic responses and it is observable only in those materials in which all electronic shells are filled. The susceptibility is negative and of the order of 10^{-5} .

If the atoms present intrinsic magnetic moments, these will be randomly oriented if $H = 0$ but they will align when an external field is applied. This **paramagnetic** response will be positive and much stronger ($\chi \sim 10^{-3}$) with respect to the diamagnetic case. The magnetization of the system is described by a Brillouin function and, for small field to temperature ratio, the susceptibility is described by *Curie's law*:

$$\chi \propto \frac{H}{T}$$

Finally, if the intrinsic magnetic moments interact with each other, their energy is minimized for parallel (**ferromagnet**) or anti-parallel (**antiferromagnet**) alignment. However, in the ferromagnetic case a complete alignment of all magnetic moments would produce too high a total magnetostatic energy for it to be the equilibrium configuration. As a consequence, magnetic domains are created: in each domain all moments are rigidly coupled but

different domains can be oriented in different directions. The total magnetization can thus average to zero. When a magnetic field is applied, however, the domains will start to align parallel to it until a saturation magnetization, M_s , is obtained. If the field is reversed, the magnetization will not necessarily follow the same curve and eventually, when the external field is zero, a residual magnetization, M_r , can still be present due to residual coupling between domains. Consequently, a coercive field, H_c , has to be applied in order to bring the magnetization to zero. This means that the magnetic configuration depends not only on the external fields (T and H) but also on the history of the system and on its magnetic characteristics.

Until now we have assumed that every atom behaves as if it were isolated, however this condition is not satisfied in metals, where the conduction electrons are delocalized over the whole crystal. The origin of magnetic behaviour in this case is more complex and strongly related to the quantum mechanical features of the constituent atoms. In order to understand the development of magnetism in bulk metals, it is, first of all, necessary to understand the origin of the atomic magnetic moment.

3.2 The origin of atomic magnetic moment

In order to understand the origin of magnetism in bulk matter, we first need to explain the formation of magnetic moments in atoms. Let us consider an atom in a homogeneous magnetic field \vec{H} described by a vector potential $\vec{A} = -\frac{1}{2}(\vec{r} \times \vec{H})$. The Hamiltonian for the Z electrons, each having an intrinsic spin magnetic moment $\vec{m} = -2\mu_B \vec{s}$ and a momentum \vec{l} , reads:

$$\begin{aligned} \mathcal{H} &= \sum_i \frac{1}{2m} (\vec{p}_i + \frac{e}{c} \vec{A}(\vec{r}_i))^2 + \sum_i \frac{-Ze}{r_i} + \frac{1}{2} \sum_{i \neq j} \frac{e^2}{|\vec{r}_i - \vec{r}_j|} - \sum_i \vec{m}_i \vec{H} \\ &= \left[\sum_i \left(\frac{1}{2m} \vec{p}_i^2 - \frac{ze^2}{r_i} \right) + \frac{1}{2} \sum_{i \neq j} \frac{e^2}{|\vec{r}_i - \vec{r}_j|} \right] + \left[\mu_B \vec{H} \sum_i (\vec{l}_i + 2\vec{s}_i) + \frac{e^2}{8mc^2} B^2 \sum_i (x^2 + y^2) \right] \\ &= \mathcal{H}^{(0)} + \mathcal{H}^{(1)} \end{aligned}$$

Where all the terms containing the magnetic field have been grouped in $\mathcal{H}^{(1)}$, that can be treated as a perturbation of $\mathcal{H}^{(0)}$. Hence the energy of the ground state, in 2^{nd} order

perturbation theory is:

$$\begin{aligned}
E_0 &= E_0^{(0)} + \langle 0 | \mathcal{H}^{(1)} | 0 \rangle + \sum_{n \neq 0} \frac{|\langle 0 | \mathcal{H}^{(1)} | n \rangle|^2}{E_0^{(0)} - E_0^{(n)}} = \\
&= E_0^{(0)} + \mu_B \vec{H} \langle 0 | (\vec{L} + 2\vec{S}) | 0 \rangle + \\
&\quad + \frac{e^2}{8mc^2} H^2 \langle 0 | \sum_i (x_i^2 + y_i^2) | 0 \rangle + \\
&\quad + \mu_B^2 H^2 \sum_{n \neq 0} \frac{|\langle 0 | (\vec{L} + 2\vec{S}) | n \rangle|^2}{E_0^{(0)} - E_0^{(n)}}
\end{aligned}$$

Where the first term

$$E^{(p)} = \mu_B \vec{H} \langle 0 | (\vec{L} + 2\vec{S}) | 0 \rangle = -\vec{H} \vec{M}_0$$

represents the paramagnetic response and is five orders of magnitude greater than the following ones that are the diamagnetic and the van Vleck paramagnetic term respectively. These two terms describe the magnetic polarization induced by the magnetic field and give no contribution to the permanent magnetic moment. Consequently the magnetic moment of the atom can be written as:

$$\begin{aligned}
\vec{M} &= -\frac{\partial E_0(\vec{H})}{\partial \vec{H}} \simeq \\
&\simeq -\mu_B \langle 0 | (\vec{L} + 2\vec{S}) | 0 \rangle
\end{aligned}$$

This result shows that in order for the magnetic moment of an atom to be zero, both the total angular momentum \vec{L} and the total spin \vec{S} need to vanish. We can conclude that only those atoms for which all the l -sub-shells are filled with $2(2l + 1)$ electrons, do not carry a magnetic moment, and this condition is fulfilled for very few elements of the periodic table.

3.3 The evolution of magnetic moment

We just saw that most atoms possess a permanent magnetic moment, but we know from experience that this is often not the case when the same atoms are arranged to form a crystal. The fact that most materials do not show a ferromagnetic behaviour can be attributed to the quenching of the orbital moment described by two principal mechanisms:

- Quantized energy levels are replaced by bands that are normally broader than the typical energy separation produced in an atom by a magnetic field. As a result levels with different m_l values, are not filled one after the other as in the atomic case, but they rather have an equal probability to be occupied. Finally the orbital moment is averaged over all occupied states and its value diminishes.

- The potential acting on the electrons, the crystal field, is not a central potential as in the atomic case. As a consequence, the orbital angular momentum does not have the correct symmetry in order for L to be an appropriate quantum number. The effective operator that has the same symmetry as the potential, actually corresponds to very low values of the atomic orbital moment.

As a result of these effects, spontaneous ferromagnetism is mainly due to the spin contribution and it survives only in the elements in the middle of the $3d$ -series and in the rare earth elements and actinides. The magnetic behaviour of a material can be foreseen applying the Stoner criterion, a rule that states that ferromagnetism is favoured if the density of states and a parameter called *exchange integral* are large. A derivation of the Stoner criterion can be obtained in the frame of spin-density-functional theory (SDFT), however it is useful to first introduce the Heisenberg Hamiltonian in order to clarify the concept of exchange integral. Furthermore, while the Stoner model describes well itinerant magnetism, i.e. magnetism of $3d$ transition metals, ferromagnetism can also occur due to localized magnetic moment. In such a case the system is better described by the Heisenberg model.

3.3.1 Localized Moments: the Heisenberg model

In order to understand the origin of the exchange interaction, let us consider the two electron wave function describing the hydrogen molecule. The major difficulty in calculating such wave function, is due to the electron-electron correlation expressed by the fact that the atomic wave functions overlap. The consequence of such correlation together with the fact that the total wave function has to be fermionic, is that the total energy of the system will contain, additionally to the single electron atomic energies, two terms describing the Coulomb repulsion and the exchange effect. The latter is related to the anti-symmetry of the problem and will have a different value if the system is in a singlet or triplet spin configuration. Such energy difference, called *exchange energy* J , determines which spin configuration, between parallel and antiparallel, is more favourable.

This argument can be extended to a system of spins \vec{s}_i , obtaining the so called Heisenberg Hamiltonian:

$$\mathcal{H}_{Heis} = -2 \sum_{a,b} J_{ab} \vec{s}_a \cdot \vec{s}_b \quad (3.1)$$

where the sum is to be performed over all pairs of spins. Obviously such problem becomes rapidly too complex to be solved analytically as the number of spins is increased. A simplification can be introduced considering the nature of the exchange energy J_{ab} : this coupling constant is proportional to the overlap between the atomic wave functions, it will thus strongly decrease with increasing distance. Consequently the sum in 3.1 can be limited to the nearest neighbours.

3.3.2 Itinerant Magnetism: the Stoner model

The principle of SDFT consists in reducing a many particle problem into an equivalent single particle problem described by wavefunctions $\varphi_i^\pm(\vec{r})$ that are solutions of the Kohn-Sham equations[Hohe 64, Kohn 65]:

$$\left[-\frac{\hbar^2}{2m}\nabla_{\vec{r}}^2 + V_{eff}^\pm(\vec{r}) \right] \varphi_i^\pm(\vec{r}) = \epsilon_i^\pm \varphi_i^\pm(\vec{r}) \quad (3.2)$$

where the \pm refer to majority and minority spins and all the physics is hidden in the effective potential

$$V_{eff}^\pm(\vec{r}) = e^2 \int \frac{n(\vec{r}')}{|\vec{r} - \vec{r}'|}(\vec{r})d\vec{r}' + V_{ext}^\pm(\vec{r}) + \frac{\delta E_{XC}[n^+(\vec{r}), n^-(\vec{r})]}{\delta n^\pm(\vec{r})}$$

The Stoner model consists in expanding the exchange-correlation potential in terms of the magnetization density $m(\vec{r})$ leading to the approximation:

$$\begin{aligned} V_{XC}^\pm(\vec{r}) &= V_{XC}^0(\vec{r}) \mp m(\vec{r})\tilde{V}(n(\vec{r})) \\ &= V_{XC}^0(\vec{r}) \mp \frac{1}{2}IM \end{aligned}$$

where I and M are the average on the atomic cell of \tilde{V} and $m(\vec{r})$ respectively. The important parameter in Stoner theory is I , the exchange integral. It represents the difference between the potentials acting on the two spin channels. Since I is positive, the majority spins (+) will feel a more attractive potential than the minority (-) ones. Moreover, in this model the potential differs from the homogeneous one ($V_{XC}^0(\vec{r})$) only by a constant term since M is the same for all unit cells. This implies that the eigenstates of the system will not be affected by the spin-dependent perturbation that will produce, as unique effect, a splitting of the energy levels:

$$\epsilon_i^\pm = \epsilon_i^0 \mp \frac{1}{2}IM$$

Consequently the density of states will also be shifted in two opposite directions for minority and majority channels:

$$n^\pm(E) = n^0(E \pm \frac{1}{2}IM)$$

This splitting, represented schematically in fig.3.1, is of great importance in magnetotransport since, as it will be discussed in the next chapter, it is at the origin of the *GMR* effect.

3.4 Magnetic Interactions

We saw that magnetism is the result of intrinsic properties of the electron as its charge, spin and momentum and the necessity of satisfying the Pauli exclusion principle. Another important aspect of magnetism concerns the interactions between two neighbouring magnetic

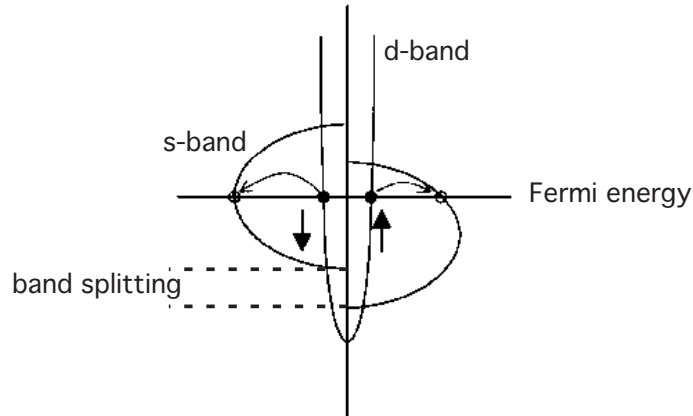


Figure 3.1 – Schematic representation of the band structure of a ferromagnet. The d -band splits and consequently the DOS at the Fermi energy is different for spin-up and spin-down carriers.

moments. These interactions can take several forms depending on the distance between the moments and the nature of the surrounding environment. It is useful at this point to summarize the different situations that can be encountered.

3.4.1 Direct Exchange

If two magnetic moments are on different sites \mathbf{i} and \mathbf{j} they will be coupled through the Heisenberg Hamiltonian in analogy with what was described in section [repar:localizedMagnetism](#) for two electronic spins:

$$\mathcal{H}_{ij} = -J_{ij} \mathbf{S}_i \mathbf{S}_j.$$

Direct exchange can take place only if the overlap between wave functions, and consequently J_{ij} is different from zero. This contribution is thus negligible for magnetic moments that are well separated and strongly localized.

3.4.2 Dipolar Interactions

Another coupling mechanism that is always present between two magnetic moments is the dipole-dipole interaction:

$$\mathcal{H}_{ij}^{dip} = \frac{1}{r_{ij}^3} \left[m_i \cdot m_j - 3 \frac{(m_i \cdot \mathbf{r}_{ij})(m_j \cdot \mathbf{r}_{ij})}{r_{ij}^2} \right]$$

The peculiarity of dipolar interaction is that it introduces a directional asymmetry since the equilibrium configuration can be parallel or antiparallel depending if the moments are collinear or perpendicular to the vector \mathbf{r}_{ij} .

3.4.3 Indirect exchange

As we saw, the direct exchange coupling has a very short range, but often magnetic interactions are observed in systems with much longer length scales, as it is the case in multilayers. This effect, normally observed in the presence of an interface between normal and magnetic metal, is due to a indirect exchange mechanism mediated by the conduction electrons of the non magnetic host: a local moment induces a damped oscillation in the polarization of conduction electron that allows a coupling with surrounding moments. This mechanism that was identified by Ruderman, Kittel, Kasuya and Yoshida, and therefore named RKKY, can be described by the Hamiltonian:

$$\mathcal{H}_{ij} = J(r)\mathbf{S}_i\mathbf{S}_j$$

where

$$J(r) = 6\pi nJ^2N(\epsilon_F) \left[\frac{\sin(2k_F r)}{(2k_F r)^4} - \frac{\cos(2k_F r)}{(2k_F r)^3} \right] \xrightarrow{\text{large } r} \frac{J_0 \cos(2k_F r + \phi)}{(2k_F r)^3}$$

n is the number of conduction electrons per atom, $N(\epsilon_F)$ is the DOS at the Fermi energy and k_F is the Fermi momentum. The J factor has two important features: its decay in r^3 is sufficiently slow to allow the coupling to survive on several nearest neighbours sites and, through the cosine, its sign is oscillatory giving a coupling that changes between parallel and antiparallel with distance.

3.4.4 Superexchange

In order to observe a RKKY-type exchange, it is necessary to have conduction electrons as mediator. In the case of a semiconductor or insulating host, however, another kind of mechanism can be found: an intervening ligand between two magnetic atoms forms a covalent mixing with the magnetic orbitals. The exchange will then take place through the hybrid orbital that is formed between the three atoms and, since the two electrons that occupy it have to respect the Pauli exclusion principle, the resulting coupling will be antiferromagnetic in character.

3.5 Magnetism in Clusters

We have reviewed the basic concepts of atomic and bulk magnetism. However the system under study do not belong to either of these two classes. When the characteristic lengths of a magnetic system are reduced to the nanometric region, both extrinsic and intrinsic properties are affected and, furthermore, surface and finite size effects need to be considered.

A comprehensive discussion of all the phenomena that originate from reducing the dimension and the dimensionality of a magnet is out of reach for this work, consequently I will focus on the behaviour of magnetic clusters and cluster-assembled materials.

3.5.1 Clusters in the gas phase

Important information on the magnetic properties of clusters, can be obtained in gas-phase experiments, since in this case no other effects are detected other than the intrinsic properties of the particles. The main experimental technique to measure the magnetic moment of free clusters is a Stern-Gerlach set-up [Gerl 22]. The idea is to apply an inhomogeneous magnetic field to the clusters beam in order to produce a deflection proportional to the magnetic moment. Clusters are then revealed with a position sensitive time-of-flight spectrometer [Bill 95] and it is possible to measure the evolution of the magnetic moment with cluster size, as it was done for several materials as Co, Ni, Fe [Doug 93, Cox 85, Bill 95].

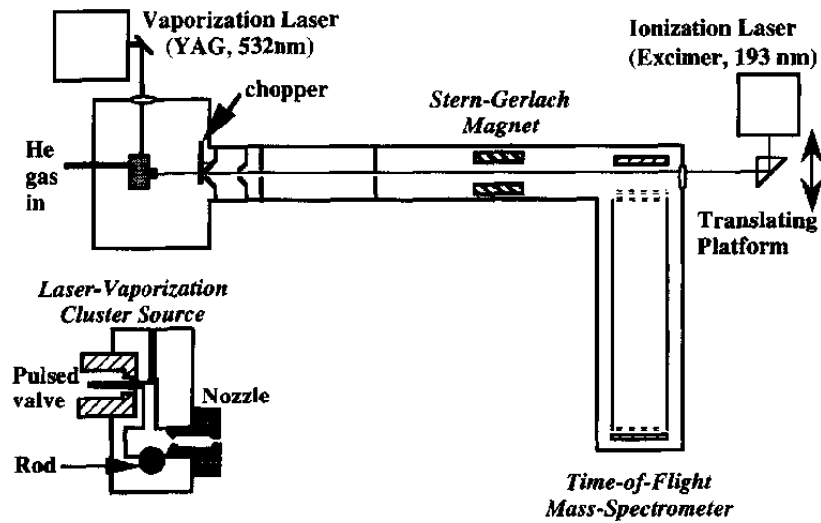


Figure 3.2 – Typical set-up for a Stern-Gerlach experiment on a cluster beam: clusters are produced in a laser vaporization source, the beam is then deflected with a magnet and the deflection is measured in a high-resolution time of flight mass spectrometer [Bill 95].

In particular it was confirmed that atomic moments in a sufficiently small cluster behave as a single giant magnetic moment, called *macrospin*. This is due to the fact that the formation of a domain requires an energy due to the misalignment of the moments in the domain wall. If the particle is smaller than a critical size¹ this energy cost will be not compensated by the energy gain due to the formation of domains [Brow 68, Kitt 46].

But the most important result was that the magnetic moment per atom is greatly enhanced with respect to the bulk value for the same material. In the case of cobalt, for example, values up to $2.4\mu_B$ per atom are found; such a magnetic moment is considerably higher than the bulk value of $1.7\mu_B$. In addition to that, it can be seen from figure 3.3 that the magnetic moment per atom undergoes strong fluctuation with size. This is due to

¹The critical size for the creation of domains depends on the considered element and is normally of the order of $\sim 100\text{\AA}$ in diameter.

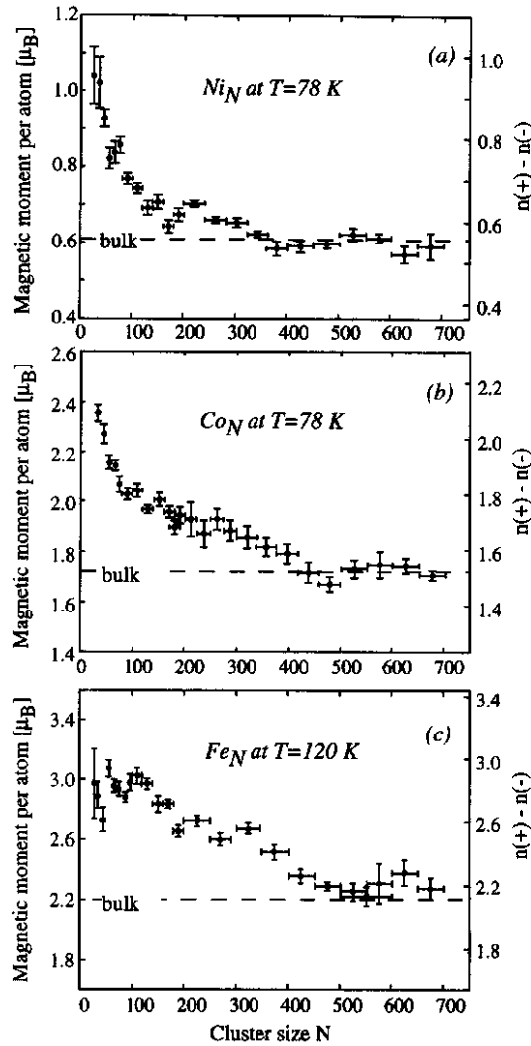


Figure 3.3 – Low temperature average magnetic moment per atom as a function of cluster size for nickel, cobalt and iron [Bill 95]. An enhancement with respect to the bulk value is observed. Size effects are also evident: the magnetic moment increases as the size is decreased and strong oscillations are observed in the small cluster region in which every atom gives a determinant contribution.

the fact that magnetism, as other cluster properties (cf. section 2.1), is very sensitive to the geometrical arrangement and as a consequence every atom will give, depending on the number and distance of its nearest neighbours, a different contribution to the total magnetic moment. The atomic magnetic moment is in fact determined by the spin orbit coupling and the contribution that each atom will give to the total moment will be determined by its coordination number.

Experiments in the gas phase also demonstrated that clusters display a *superparam-*

agnetic behaviour¹. This topic deserves to be discussed in more detail since superparamagnetism is the starting point for the interpretation of the magnetic behaviour of cluster assembled materials.

Superparamagnetism

In a cluster every atom has a magnetic moment of the order of μ_B and all atomic moments are aligned, giving rise to a total magnetic moment $\vec{\mu}$. Because of quantization, the projection of $\vec{\mu}$ along a fixed arbitrary direction, can assume only discrete values but, if μ is sufficiently big, these values can be considered continuous and a semiclassical treatment is justified. The cluster magnetic moment can, in this approximation, point in any direction of space. Let us now consider an ensemble of identical particles; the total magnetization of the system, \vec{M} , is given by the vectorial sum of all single magnetic moments. As it happens for the atomic magnetic moments in a paramagnet, the average magnetization will be zero in the absence of magnetic field since all magnetic moments are randomly directed in space. When a magnetic field \vec{H} is applied, they will orient and give rise to a net magnetization. The Hamiltonian of a single macrospin can then be written as:

$$\mathcal{H} = -\mu H \cos\theta$$

where θ is the angle between the magnetic moment and the axis of the magnetic field, that is assumed to be z .

The total magnetization can be found averaging over the ensemble:

$$\begin{aligned} \langle M_z \rangle &= \frac{\frac{1}{4\pi} \int_0^{2\pi} d\phi \int_0^\pi \sin\theta d\theta M \cos\theta e^{\mu H \cos\theta / k_B T}}{\frac{1}{4\pi} \int_0^{2\pi} d\phi \int_0^\pi \sin\theta d\theta e^{\mu H \cos\theta / k_B T}} \\ &= M_s \frac{\int_{-1}^1 x e^{xy} dx}{\int_{-1}^1 e^{xy} dx} \end{aligned}$$

where $y = \mu H / k_B T$ and $x = \cos\theta$. This leads to:

$$\frac{\langle M_z \rangle}{M_s} = \coth\left(\frac{\mu H}{k_B T}\right) - \frac{k_B T}{\mu H} = \mathcal{L}\left(\frac{\mu H}{k_B T}\right) \quad (3.3)$$

where $\mathcal{L}(y) = \coth(y) - \frac{1}{y}$ is the *Langevin function* and has the form shown in fig.3.4.a.

From the expression in 3.3 it can be remarked that the magnetic behaviour of a superparamagnetic system is determined by the the competing actions of the external field and of thermal agitation. As a consequence, magnetization scales as H/T .

¹This assertion is in fact extremely delicate since supermagnetism implies spin-relaxation in the presence of a thermal bath; in the case of supported and large clusters the bath is given by, respectively, the support or the vibrational and rotational excitations of the cluster itself. For small clusters no such spin-relaxation can take place. However, it was recently demonstrated by de Heer and co-workers [Xu 05] that even in this latter case a Langevin-like behaviour is observed due to coupling between spin and rotation.

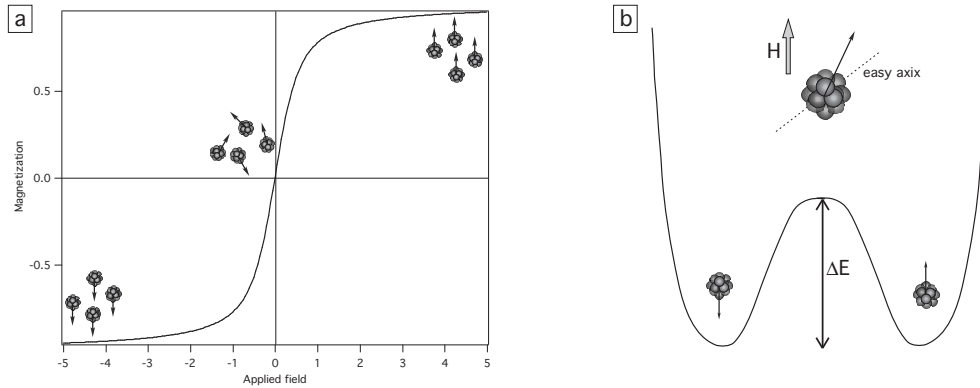


Figure 3.4 – a) Langevin function describing the magnetization of an ensemble of non interacting macrospins. b) Double well potential induced by the presence of an easy axis. If the thermal energy is not sufficient to overcome the energy barrier ΔE the particle is blocked.

Until now it was assumed that the macrospin is free to rotate in all directions of space. This is actually not true if the anisotropy energy is taken into account since in this case the coupling with the crystalline structure will force the magnetic moment to align in a preferential direction. For an easy comprehension let us consider the simplest scenario in which clusters have one easy axis that induces a double well potential, shown in fig.3.4.b, with an energy barrier defined by the anisotropy: $\Delta E = K_a V$, where V is the volume of the particle. Depending on the temperature, two different regimes will then be observed: if $k_B T \gg K_a V$ energy barrier can be easily overcome and a superparamagnetic behaviour is observed; if $k_B T \ll K_a V$ the magnetic moment is strongly coupled to the crystalline structure and the particle is said to be *blocked*. In the range of temperature in which the two energies are of comparable magnitude, a fluctuation of the macrospin is observed with a characteristic time:

$$\tau = \tau_0 e^{\frac{K_a V}{k_B T}}$$

where τ_0 is related to the natural frequency of gyromagnetic precession and lies in the range $10^9 - 10^{13} \text{ Hz}$. A consequence of these fluctuations is that the system will appear blocked or superparamagnetic depending on the characteristic observation time: the blocking temperature (T_B) below which the moment is coupled to the lattice is not unequivocally determined, but depends on the analysis technique used to make the measurement.

3.6 Cluster Assembled Materials

In section 3.5.1 we have shown that the average magnetization of clusters macrospins in a magnetic field depends on the interplay between magnetic field and thermal agitation. The result is the so-called superparamagnetic behaviour that is reflected, for what concerns magnetization, in the Langevin curve.

However, the subject of this study is the magnetic behaviour of clusters that are not free but embedded in a host material and are thus subject to interaction with the surrounding medium. Furthermore, inter-particle interactions may also arise since the average distance between clusters is sensibly smaller with respect to standard gas-phase experiments. These interactions strongly vary with cluster concentration and size, producing a complex phase diagram in which extremely different behaviours are represented. Additionally it should be remarked that some interactions can be mediated by the embedding matrix giving rise to effects that are not observed for free clusters and consequently it is more correct to talk about properties of cluster-assembled materials rather than of clusters embedded in a matrix. For the sake of simplicity, we will study the system as an ensemble of magnetic particles, including all matrix effects as corrections to the free-particle case.

We will follow the evolution of magnetic properties as a function of concentration, starting from the dilute system in which single magnetic moments are non interacting and superparamagnetic, then we will correct the superparamagnetic model in order to account for small interactions and finally we will consider the limiting case of strong interactions in which the magnetization is strongly influenced by correlation effects and the system actually behaves as a spin glass.

3.6.1 Dilute systems: the superparamagnetic limit

If the magnetic particles are kept well separated one from the other, they can be considered as independent and the only forces they will experience are due to the external magnetic field and temperature¹. Under the additional hypothesis that particles are sufficiently small to be considered as monodomain, the system can be treated with the same formalism that has been discussed for the free clusters case in the previous section: particles are superparamagnetic and the magnetization follows a Langevin curve.

This behaviour has actually been observed, for example, in the case of iron clusters embedded in silver by C. Binns and co-workers [Binn 02a]. In this experiment, iron clusters with an average diameter of $3nm$ were co-deposited with silver at different concentrations and magnetization was measured in a SQUID magnetometer (fig.3.5.a). At lowest concentration (0.8% atomic Fe) magnetization curves scale with the ratio H/T (fig.3.5.b) as it is expected in the case of superparamagnetism, since in this case the behaviour is fully determined by the interplay between Zeeman ($\vec{\mu} \cdot \vec{H}$) and thermal ($k_B T$) energies. An additional test that proves ideal superparamagnetism is the fact that the value of particles volume obtained by fitting magnetization with a Langevin function, does not depend on temperature, as shown in the inset of fig.3.5.b

¹Another force that influences the orientation of the magnetic moment is the anisotropy. Here I will not discuss the effect of anisotropy; some further results will be discussed in section 7.1.5 in the last part of this thesis.

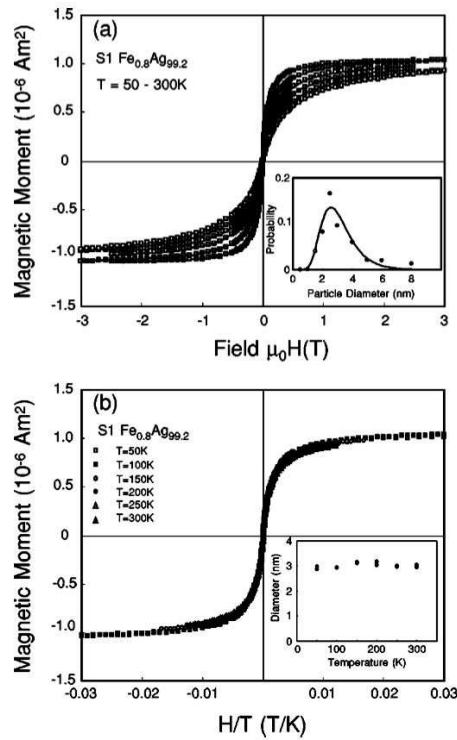


Figure 3.5 – Data of Binns and co-workers [Binn 02a] showing the normalized magnetization of iron clusters, with a broad mass distribution in the range of 0.5 – 8 nm, embedded in a silver matrix; Fe atomic concentration is 0.8%. In fig.b, magnetization is plotted versus H/T since, in the case of superparamagnetic behaviour, the curves are supposed to scale following this ratio. As an additional confirmation of the validity of this model, in the lower inset the average cluster size as obtained by fitting with a Langevin function is shown: the value stays constant as a function of temperature and is in good agreement with the value obtained by STM measurements.

3.6.2 Weak interactions: the interacting superparamagnet

In the same work cited in the previous section [Binn 02a] it was shown that, increasing the concentration of clusters to 10% and 20%, important deviations from the superparamagnetic behaviour are observed. First of all the magnetization does not scale as H/T . Furthermore, if the temperature is kept constant and the concentration is varied, an influence is observed on the shape of magnetization curves. Such effects are in contrast with the hypothesis of non-interacting particles. A consequence of this failure is that, fitting the curves with a Langevin function, a value of the macrospin is found that increases with temperature, as shown in fig.3.6.a. Similar results have been obtained by Allia and co-workers [Alli 01] on sample produced by melt spinning with a composition of $Co_{10}Cu_{90}$ and are presented in fig.3.6.b.

The increase of the *apparent* macrospin with temperature obviously does not reflect a real increment of the magnetic moment per cluster but it is rather an indication that

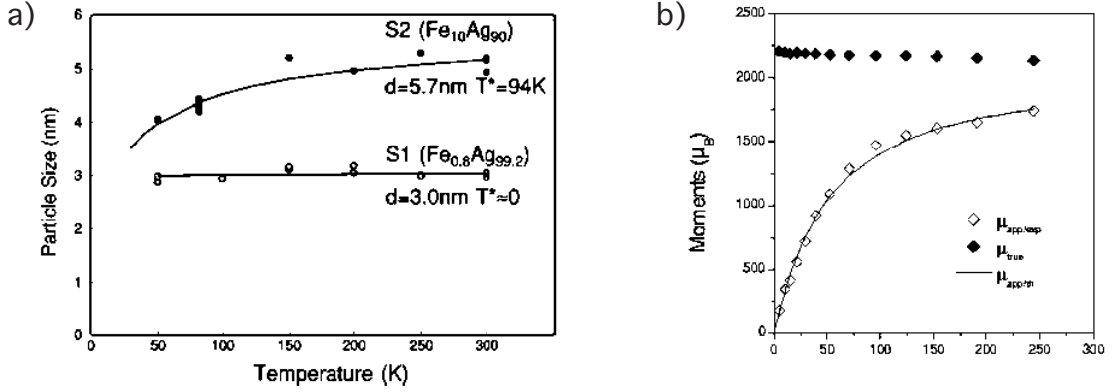


Figure 3.6 – Macrospin as a function of temperature, obtained by fitting with a Langevin function the magnetization curves. In a) ([Binn 02a]) two different samples are presented: one with 0.8% and the other with 10% atomic concentration of iron. In the first case, the macrospin stays constant with temperature meaning that the sample is fully superparamagnetic; in the second one, an increase of the apparent macrospin is observed. In b) a sample with a 10% atomic concentration of cobalt in copper is considered [Alli 01]. The macrospin is obtained using first a normal Langevin (empty symbols) and shows an apparent increase with temperature, and subsequently using a Langevin corrected taking account dipolar interactions (full symbols).

interactions occur between particles: when concentration is increased, the inter-particle distance becomes sufficiently low to allow dipole-dipole interactions to take place. These interactions act as a random field that opposes to the external field and hinders the moments to align. Since this effect is competing with the external field as temperature does, one can attempt to take account of it in the superparamagnet model, introducing a temperature correction to the Langevin function. The reason why the correction term is added to the temperature rather than to the field, is that its effect does not give any contribution to the ordering of macrospins, but goes rather in the opposite direction and enhances the disorder.

This model, presented by Allia and co-workers [Alli 01], and named *interacting superparamagnetism*, consists in introducing an extra term to the temperature:

$$kT^* = \epsilon_D = \alpha\mu^2/d^3$$

where μ is again the particle macrospin, d is the average inter-particle distance and α is a proportionality constant. As a result an apparent temperature will act on the clusters:

$$T_a = T + T^*$$

and the magnetization will be still expressed by a Langevin function:

$$M(H, T) = M_s \mathcal{L} \left(\frac{\mu H}{kT_a} \right) \quad (3.4)$$

in which μ is the real, temperature independent macrospin (fig.3.6.b).

3.6.3 Spin glasses

Spin glasses are magnetic systems in which the interactions between magnetic moments are in conflict with each other due to particular lattice structure (as in the case of the Kagomé lattice) or to fluctuations in sign of the interaction itself (as in RKKY-coupled systems) [Mydo 93, Bind 86].

As it was shown in section 3.3.1, if several identical magnetic moments are organized on a lattice, they will in most of the cases, experience all the same force due to interactions with surrounding moments and, below a critical temperature T_c , a long-range ordered state will form with a ferro- or antiferro-magnetic ordering depending on the type of interaction and on the inter-moment distance. However in some particular configurations, as the antiferromagnetically coupled triangular lattice, a magnetic moment can experience two opposite forces simultaneously and the system will present spin *frustration*.

Frustration inhibit the formation of a long-range ordered state, nevertheless a phase transition below T_f is observed from the disordered state to a frozen state with a short-range order with a characteristic length larger than the inter-moment distance but much shorter than the sample dimensions.

If the moments are not on a regular lattice and/or they are not identical it is still possible to observe the formation of a spin glass. In this case the key ingredient is the *randomness* of the system: because of the randomness of the coupling, each moment will feel a different force and frustration may be induced. This can be better understood in the case of *RKKY*-coupled macrospins: the coupling force changes in sign, as well as in magnitude, with the separation distance and, if the inter-moment distance is not constant, one moment might experience a different kind of coupling (ferro- or antiferro-magnetic) with two different neighbours and it will not know which one to “choose”. Consequently the random geometrical configuration can induce frustration and no long-range ordered state can be formed.

This subject will be discussed further in the last part of this work when the results will be presented and analysed.

Magneto Transport

In a perfect crystal electrons are described by Bloch states, $\psi_k(r)$, and, if an electric current is produced, it will flow forever. However in a real crystal deviations from the ideal periodicity are always present, due to impurities, finite size effects and thermal excitations. As a result the Bloch states are no longer the eigenstates of the system and a voltage needs to be applied in order to maintain a constant current.

For small perturbations of the equilibrium state, i.e. in linear response regime, the electrical current and the applied voltage are related by the electrical conductivity (or resistivity) via the well known relation:

$$I = \sigma \Delta V = \frac{1}{\rho} \Delta V \quad (4.1)$$

where the conductivity σ is defined by the scattering mechanisms the electrons experience when travelling through the material and it can be written, in the relaxation-time approximation, as:

$$\sigma = \frac{ne^2\tau}{m^*} \quad (4.2)$$

with n the density of charge carriers, m^* their effective mass and $\tau = \tau(\mathbf{r}, \mathbf{k})$ the relaxation time, i.e. the mean free time between two collisions for an electron located in \mathbf{r} with a momentum \mathbf{k} . Several scattering mechanisms with different relaxation times can take place and, as far as they are uncorrelated, Matthiessen's rule states that the total resistivity is given by the sum of partial resistivities:

$$\rho_{tot} = \sum_i \rho_i$$

In a non-magnetic metal, the main source of scattering is thermal excitations, i.e. phonons. The frequency of *phononic collisions* is proportional to the total number of activated thermal excitations and hence to the temperature. Consequently the phononic resistivity will be $\frac{1}{\rho_{ph}} \propto T$. Another source of scattering are *electron-electron collisions*. This effect gives a $\frac{1}{\rho_{el}} \propto T^2$ contribution to the total resistivity and it is much smaller than phononic scattering, being visible only at very low temperatures. Both these terms vanish

for $T = 0$, implying a zero resistivity at zero temperature. However, as remarked in the beginning of this chapter, this is true only in the case of a perfect crystal. If *impurities* or lattice defects are present, a further contribution, independent of temperature, needs to be added to the total resistivity:

$$\rho_{tot} = \rho_{ph} + \rho_{el} + \rho_i = aT + bT^2 + c \quad (4.3)$$

In the case of a magnetic material, another feature of the electrons will play an important role in defining the transport properties: their *spin*. If the scattering potential depends on the spin or if the density of state is different for the two spin channels, some electrons will experience a “lower resistance” in traversing the sample. We can then model the total current as the sum of two distinct currents one relative to spin-up and the other to spin-down electrons:

$$\vec{j}_{tot} = \vec{j}_{\uparrow} + \vec{j}_{\downarrow}$$

Consequently electrons can be used to probe the magnetic properties of a material, observing the evolution of transport properties as a function of an applied field.

The study of spin dependent transport reveals not only to be an important tool for analysing the magnetic behaviour, but also to be determinant for several technological applications. The best known spin-transport effect, for the discovery of which Peter Grünberg and Albert Fert have been awarded of the nobel prize in the present year, is *giant magneto resistance* (*GMR*). This discovery and its rapid application in electronics, drove great interest on the subject and lead to the birth of a new research field: *spintronics*. The goal of spintronics is to use the spin of electrons as an additional degree of freedom in order to conceive new devices with higher performances than the usual electronic ones [Ben 05]. Some examples of technologies that are already at an advanced stage are *GMR*-based reading heads and magnetic random-access memories (*MRAM*) based on the magnetic tunnel junction [Daug 97].

However, the great potential of spintronics is still not fully expressed. Future challenges include the use of magnetic semiconductors: this would allow a wealth of existing microelectronics techniques to be co-opted, as well as the development of devices based on the semiconductors optical, electrical and magnetic properties. Examples include the spin-polarized field-effect transistor (spin *FET*), proposed by S. Datta and B. Das in 1990 [Datt 90], that is much faster than electronic transistors and possesses an extra degree of freedom, the orientation of source and drain, allowing to change its functionality acting on its magnetic state.

4.1 Magneto Resistance

With the name of magneto resistance (*MR*) the dependence of the resistance on an applied magnetic field is indicated. Such an effect is present, to a certain extent, in all metals.

However the mechanisms giving rise to it, as well as the relative variation of ρ with the field, vary strongly depending on the magnetic structure of the material.

In particular, in 1988 Fert [Baib 88] and Grünberg [Bina 89] reported that a system of alternated magnetic and non-magnetic layers with thickness of the order of the electron mean free path (some nanometers) show a giant resistivity decrease when applying a magnetic field (fig. 4.1). In this section the phenomenology and the basic mechanisms giving rise to *MR* are reviewed.

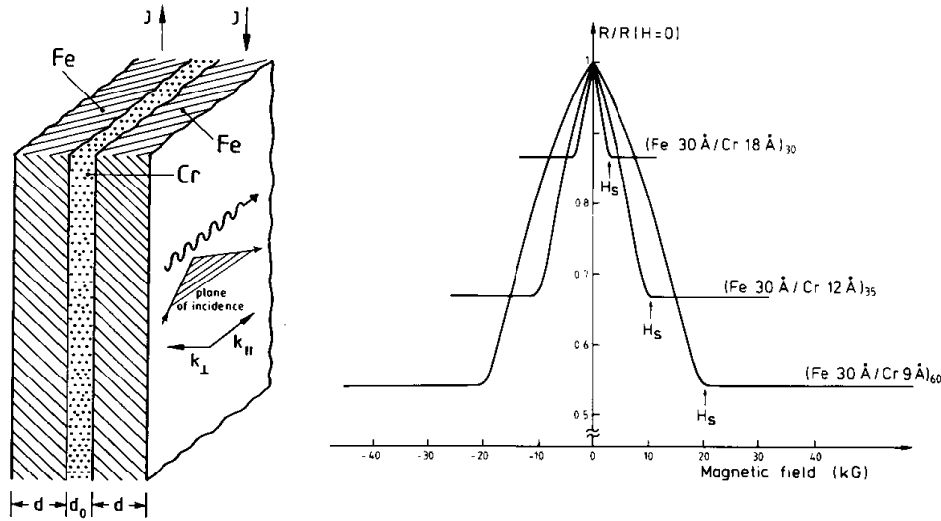


Figure 4.1 – *GMR* curves [Baib 88] for a system of *Fe* and *Cr* multilayers [Bina 89]. The systems on which the *GMR* effect was observed for the first time, were constituted of Iron ferromagnetic layers separated by a Chromium spacing layer. Depending on the thickness of the spacer, the *Fe* layers are coupled in a ferromagnetic or anti-ferromagnetic way. This spontaneous configuration can be broken with the action of an external magnetic field. The change in configuration is reflected in the transport properties of the system (as shown on the left) and a sharp decrease in resistivity is observed.

4.1.1 MR in normal metals

Non magnetic metals show an increase in resistivity when a magnetic field is applied. This effect is quite small and can be observed only at low temperatures and in samples with good crystallinity, i.e. when the impurity and phononic resistance are low.

A simple qualitative, although imprecise, explanation can be given in terms of the precession induced by the Lorentz force: since the trajectories are curved, and hence longer, the resistance is increased. A more rigorous argument, taking into account the form of the Fermi surface and the position of conduction electrons, can be found, for example, in [Zima 60].

4.1.2 MR in ferromagnets

Magnetoresistance in ferromagnets has been discovered by Lord Kelvin in 1857 [Thom 57] and it consists in the fact that, when the magnetic moments of the material are aligned, a strong difference between parallel and perpendicular resistivity appears. For this reason the effect is referred to as anisotropic magnetoresistance (*AMR*).

The explanation is related to the coupling of the magnetic moment to the spatial degrees of freedom due to the spin-orbit interaction [Gil 05]. This coupling introduces an anisotropic

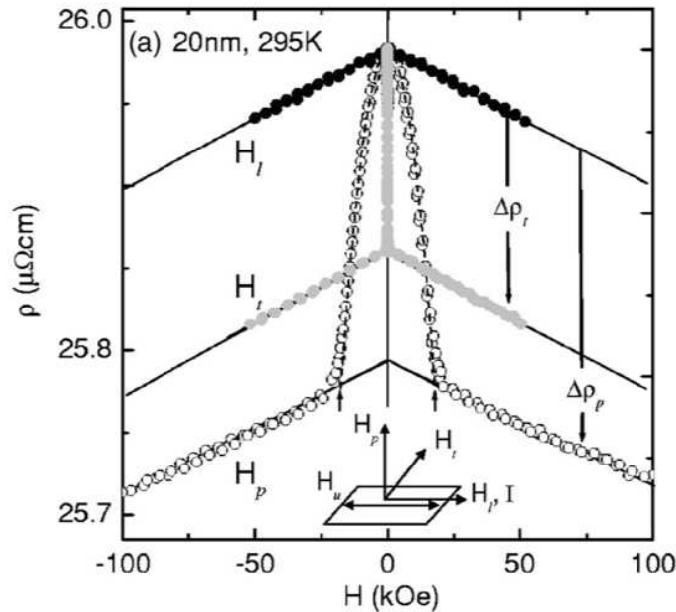


Figure 4.2 – MR curves [Gil 05] for a Co polycrystalline film at low temperatures measured for three directions of applied field in order to show the strong anisotropy effect.

shift of the 3d-levels (and a consequent anisotropic mixing with the s conduction band at the Fermi energy) resulting in different scattering rates for electrons travelling perpendicularly or parallel to the magnetic field.

4.1.3 MR in multilayers

As already stated, giant magneto resistance consists in a sharp decrease of the resistance of a magnetic multilayer system. In these systems the magnetic layers are coupled via a *RKKY* indirect exchange interaction mediated by the non-magnetic spacer. By tuning the thickness of the spacing layer, it is possible to obtain an antiferromagnetic alignment configuration with a spontaneous magnetization that averages to zero. With the application of an external field, the layers' magnetization are forced to align in a parallel configuration and the resistivity decreases by several tens of percent, as showed in fig. 4.1. Furthermore, the effect can be observed if the current is driven perpendicularly to the planes (*CPP*

configuration) or parallel to them (*CIP* configuration). We will discuss only the first case since it is more intuitive and also because it will be useful to understand *GMR* in granular systems.

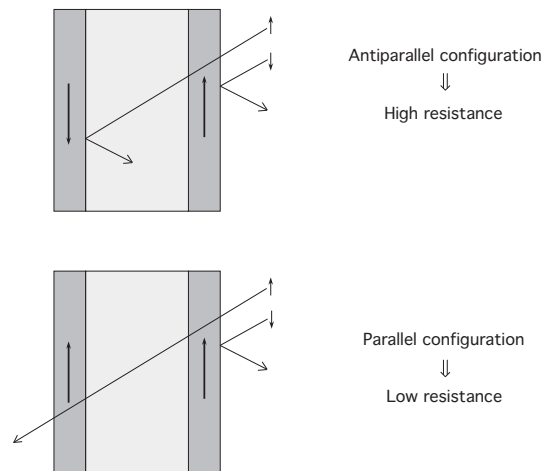


Figure 4.3 – Schematics of the mechanism giving rise to *GMR* in a multilayer system in the *CPP* configuration. The device represented in the figure is actually a spin valve since, depending on the relative orientation of the ferromagnetic layers magnetization, it does or does not allow the current flow.

Consider an electron travelling in a direction perpendicular to the planes. When it encounters an interface, it will have a certain probability of transmission t and of reflection r . These probabilities depend on the electronic structure of the two sides of the interface [Dien 92, Prat 91]. This is due to the fact that the conduction band of the magnetic layer splits and the majority spins will have energies close to the Fermi energy of the non-conducting layer, while the minority ones will be more distant. As a consequence, majority electrons will have a higher t than minority ones.

If we now consider a multilayer system at zero field (antiferromagnetic alignment), a spin-up electron will have a high transmission coefficient through the first layer, but will have a lower t at the subsequent interface; on the other hand, a spin-down electron will encounter a higher r at the first interface and pass easily through the second one. On the entire system, consequently, the two spin channels will have the same resistivity. If a magnetic field is applied, though, the situation changes because majority electrons will be transferred easily through all the interfaces (since they are all oriented in the same directions) while minority ones will have a much lower probability to be transmitted.

Since the two currents add in parallel, the decrease in the spin-up resistance is reflected in a decrease of the total resistance, giving rise to the observed *GMR* [Camp 70].

4.1.4 MR in granular materials

In 1992 A. Berkowitz and co-workers [Berk 92] and J. Xiao and co-workers [Xiao 92] reported *GMR* effect in granular systems constituted by annealed *Co/Cu* alloys (cf. fig.4.4).

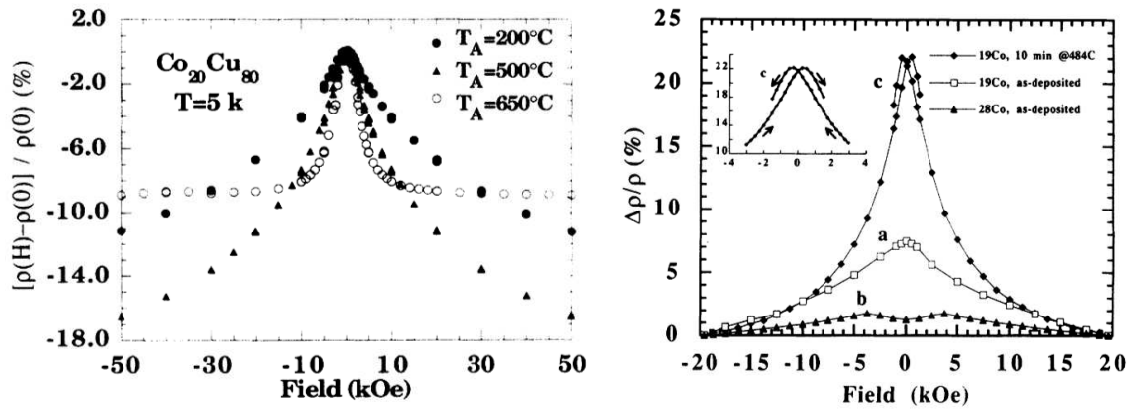


Figure 4.4 – *GMR* effect in *CoCu* alloys reported as a function of annealing temperature from Xiao [Xiao 92] on the left, and as a function of *Co* concentration from Berkowitz [Berk 92] on the right.

The effect in granular materials is lower than in multilayers and is based on a different microscopic mechanism. A qualitative explanation can be given in terms of spin-dependent scattering as it is represented in fig.4.5: let us assume that scattering probability of a conduction electron on a magnetic impurity depends on the relative spin orientation (fig. 4.4). In zero applied field, all magnetic moments are randomly distributed, consequently

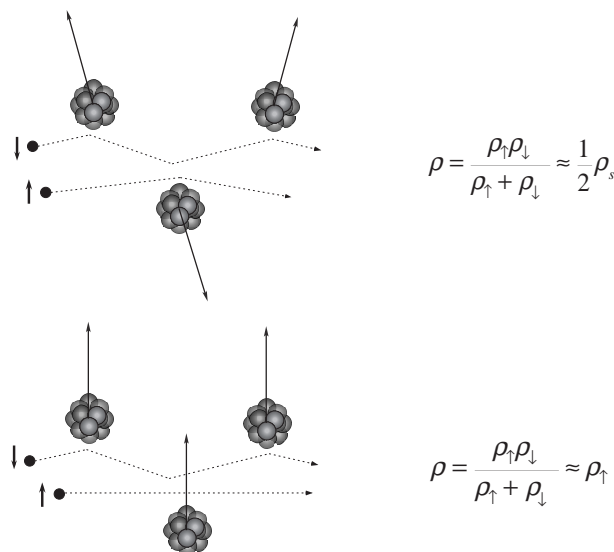


Figure 4.5 – Schematic representation of the mechanism giving rise to *MR* effect in granular materials.

majority and minority electrons will have the same scattering rate. If a magnetic field is applied and moments are thus oriented in the same direction, one of the spin channels will have a reduced probability of scattering and its resistivity will diminish, reducing as well the total resistance of the sample. A more accurate explanation of the magnetoresistance effect in cluster assembled materials will be given in the last part of the thesis.

We have assumed until now that, as clusters are embedded in a matrix, their magnetic moment survives and behaves as a free moment. This picture is however oversimplified and needs some further discussion. In the next section we want to give a qualitative understanding of the mechanisms that take place as a magnetic impurity is introduced in the sea of conduction electrons. These concepts will be useful in the last part of the thesis to interpret the experimental results.

4.2 The virtual-bound-state model

The easiest system we can think of, is an alloy of magnetic atoms in a non magnetic matrix. Although simple, this system presents several interesting behaviours that can be extended to the cluster case. We will discuss here only the case of transition metal impurities in a noble metal since it is the case of interest of this work.

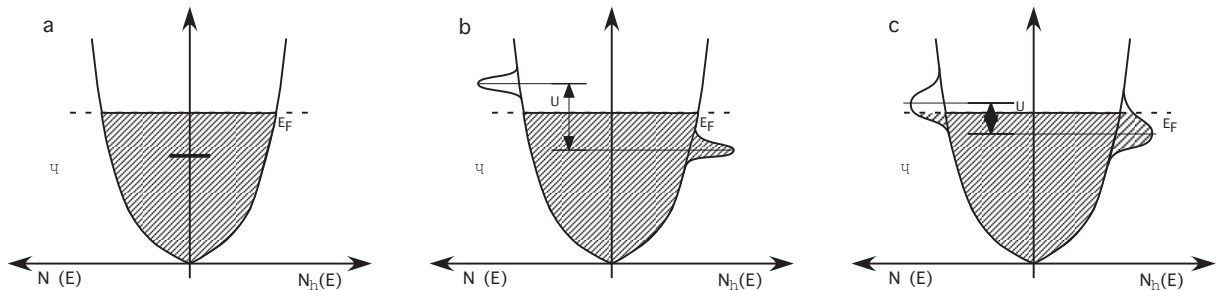


Figure 4.6 – a) Schematics of the density of states for the two spin channels for a normal non magnetic metal in the free electron approximation. b) An impurity is added to the sea of conduction electrons and two localized levels are sitting close to the Fermi energy. c) The impurity states mix with the conduction band of the host material and two valence bond hybrid states are formed.

The d electrons of the impurity occupy a localized energy level. If this level is close enough to the conduction band of the host metal, superposition of wave functions will take place and an hybrid spin-dependent state will be formed, as sketched in fig. 4.6. This mechanism has been described by Anderson and is called *s-d valence bond state model*. The formation of the valence bond states is due to the contribution of two effects: hybridization and intra-atomic Coulomb repulsion: the former causes the the level to be shifted and broadened and the latter causes an energy shift between spin-up and -down levels. The two effects have a strength characterized by V_{sd} (hybridization potential) and U (Coulomb

repulsion) respectively; depending on the ratio between these two quantities, different landscapes are possible as shown in fig. 4.6.

If $U \gg V_{sd}$, the levels are well separated and a strongly magnetic case is formed, in which only the impurity state lying below the Fermi energy will be occupied.

If $U \sim V_{sd}$, the levels can partially overlap with the Fermi energy and will be both be partially occupied. The difference in occupancy will give the net magnetic moment that could easily be, at this point, non-half-integer.

If $U \ll V_{sd}$, we arrive at a symmetric case in which the impurity has completely lost its magnetic character.

The importance of this model is to show how, when magnetic impurities are embedded in a sea of conduction electrons, the energy landscape is extremely sensitive on the parameters and several different situations can occur, ranging from a localized-like magnetic moment, to a completely ‘dissolved’ one.

This statement can be understood considering more in detail what happens in the spin up and down conduction bands (\uparrow and \downarrow CB) when the covalent mixing takes place. Some electrons will pass from the lower valence bond state to the \uparrow CB and some other will move from the \downarrow CB to the upper valence bond state. This displacement will cause a difference in Fermi energy in the two CB, i.e. a polarization of the electron sea that surrounds the magnetic impurity.

This polarization can have an opposed sign with respect to the magnetic moment of the cluster, resulting in a screening of the macrospin that takes the name of *Kondo effect*. In some particular systems as *PdFe*, it can happen that such polarization is ferromagnetically coupled to the impurity giving rise to an enhancement of magnetic moment rather than a screening effect. This polarization can extend over several Å allowing, even at low concentrations, the presence of interactions.

4.3 Hall effect

Another important transport effect that is used to study the magnetic properties of nano-structured materials is the Hall effect.

The Hall effect was discovered by E. Hall in 1879 and consists in the establishment of a potential difference in the transverse direction of a conductor through which a longitudinal current, I , flows and a magnetic field, H , perpendicular to the current is applied as shown in fig.4.7.

An intuitive explanation of this effect can be given on the basis of the Lorentz force

$$\vec{F}_L = -e(\vec{E} + \vec{v} \times \vec{B})$$

that deviates the electrons in the direction perpendicular to both the current and the field. The charge will accumulate at the border of the material until an equilibrium is achieved

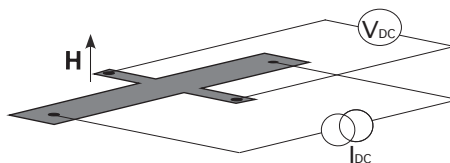


Figure 4.7 – Geometry of the Hall measurement protocol.

at a potential difference:

$$V_H = -\frac{IH}{ned} \quad (4.4)$$

Short after the discovery of the Hall effect, it was found that ferromagnets behave differently than paramagnetic and diamagnetic materials: in addition to the *ordinary* Hall voltage linear in the magnetic field, they show an *extraordinary* contribution proportional to the sample magnetization [Kund 93, Hurd 72], as can be seen in fig.4.8.

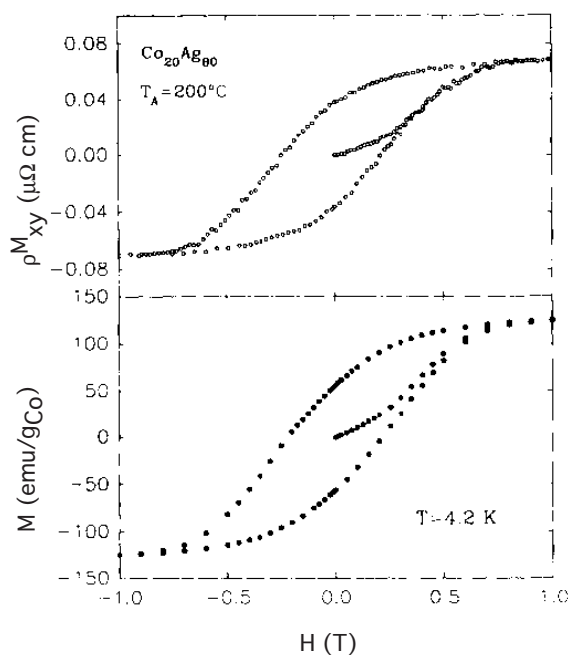


Figure 4.8 – Hysteresis loops at $T = 4.2K$ of the extraordinary Hall resistivity and of the magnetization for an annealed Co – Ag sample. A very good correspondence is observed for the two curves [Xion 92].

This effect originates from the asymmetric scattering of electrons due to spin-orbit interactions. Two different mechanisms have been proposed to explain such asymmetry: side jump [Berg 70] consisting in a lateral displacement of the wave packet and skew scattering [Lutt 58] in which the carriers are scattered at a constant spontaneous angle. Even if several studies have been performed in recent years on the subject, no unique answer has been

found and probably the effective mechanism depends on the structure of the sample.

Although a complete understanding of the extraordinary Hall voltage is missing, this effect is growing in importance as a means to study the magnetic behaviour of nanostructured materials. The main advantage of the technique being the higher sensitive to the magnetization with respect to other techniques such as standard or SQUID magnetometry, the Hall effect is well suited to the study of those systems that have a low total magnetization as, for example, granular films [Wang 94a, Gran 97, Tuai 04].

Part II

Experimental Methods

Sample Preparation

5.1 Concept and Overview of the Apparatus

The aim of this work is to grow and characterize cluster assembled materials. Since growth and characterization take place in different experimental set-ups, it is necessary to produce samples that are stable under ambient condition and can therefore be transferred out of vacuum. In order to specifically tailor the properties of those materials, it should be possible to control chemical composition, size and concentration of the clusters independently. Consequently a set-up has been built that allows to produce clusters within a very broad mass range, to characterize and to mass select them prior to deposition, and finally to deposit them under clean conditions simultaneously with the matrix [Hill 06].

The experimental setup is shown in fig. 5.1 and consists of four main parts: the cluster source, the transfer part, the Time-of-Flight mass spectrometer (TOF-MS) and the deposition chamber. Here a brief description of the apparatus is given, a more detailed discussion of the different parts can be found in the following chapters.

Clusters are grown in a magnetron-sputtering gas aggregation source that allows the production of a continuous and intense beam of cluster ions; furthermore an accurate tuning of the parameters gives access to a wide range of masses (between one atom to several tens of thousands). When leaving of the source the beam contains clusters that can be either charged (both negatively and positively) or neutral. Positively charged particles are guided, via electric fields, through a transfer part that is needed in order to pump away the residual source gases, and to block negative ions. The transfer part ends in an electrostatic bender that allows the deflection of the beam in two opposite directions, one leading to the TOF-MS and the other to the deposition chamber. Since both directions are perpendicular to the travelling axis of the beam, the deflector also allows to discard neutral clusters. The TOF-MS, thanks to its fast response, is extremely useful to get a real time picture of the beam composition and it allows to optimize the source and transfer conditions in order to get the desired mass spectrum and the maximum transmission efficiency. Afterwards the beam is deflected toward the deposition chamber. At the entrance of this chamber, the beam is guided with a quadrupole mass filter (Q-MF) and it is finally focused onto the

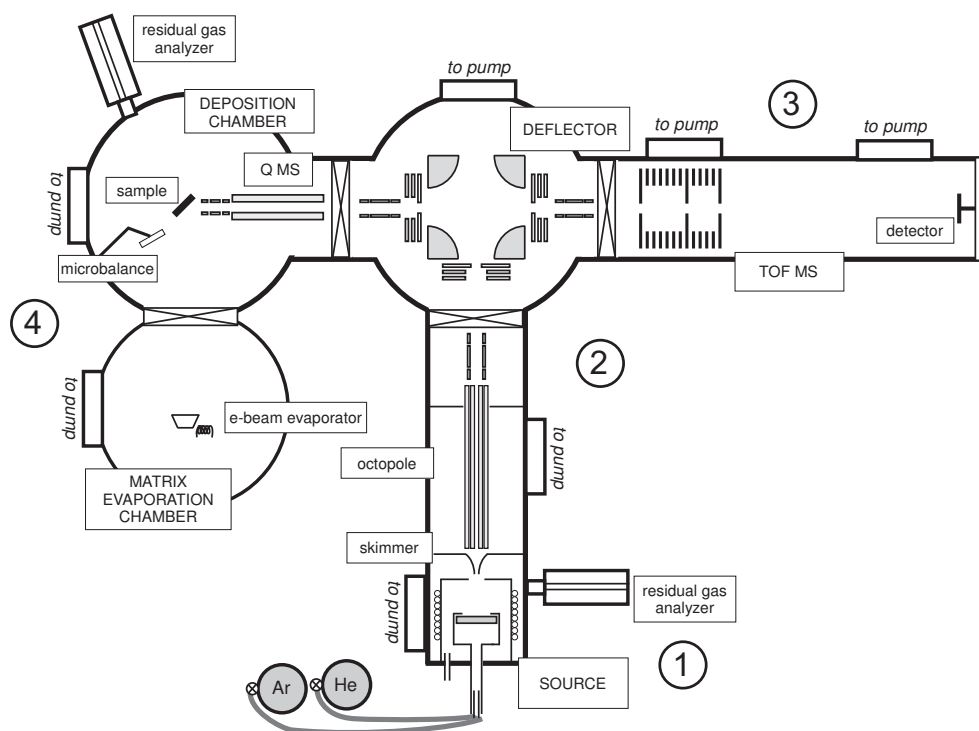


Figure 5.1 – Schematic overview of the experimental setup.

deposition surface in the sample holder. The sample holder contains a Faraday detector and four deposition surfaces that are mounted at 45° with respect to the beam travelling direction. This orientation allows to deposit simultaneously the clusters and the matrix that is evaporated from below. The matrix vapour is produced using an electron beam evaporator that is suited for most kinds of materials, both metallic and insulating. The evaporation rate is monitored through a microbalance and can be easily controlled over a wide range by varying the power of the electron beam.

In order to optimise the efficiency of the apparatus, it is extremely useful to monitor the cluster current at different points of the beam path. For this reason two Faraday detectors were placed inside the gate valves, one at the end of the transport part and the other after the deflector. Those detectors allow the measurement of the energy of the beam by means of a retarding field analysis (RFA).

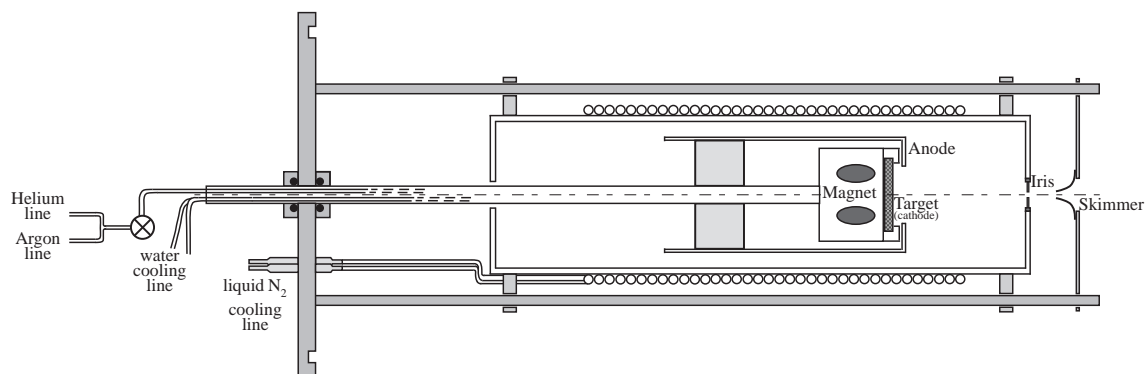
Great attention has also been given to vacuum conditions since the purity of the sample influences dramatically its properties. For this reason the residual atmosphere is continuously monitored with two residual gas analysers mounted in the source and in the deposition chamber, respectively. Typical values of pressure in different parts of the apparatus are listed in table 5.1 and a more detailed argumentation on the subject can be found at the end of the chapter.

Table 5.1 – Vacuum conditions in different parts of the apparatus.

	base pressure	during operation
aggregation chamber	$3 \cdot 10^{-7} \text{ mbar}$	$1 \cdot 10^{-1} \text{ mbar}$
source	$3 \cdot 10^{-7} \text{ mbar}$	$2 \cdot 10^{-3} \text{ mbar}$
transfer	$5 \cdot 10^{-8} \text{ mbar}$	$1 \cdot 10^{-4} \text{ mbar}$
deflector	$2 \cdot 10^{-8} \text{ mbar}$	$5 \cdot 10^{-7} \text{ mbar}$
TOF	$1 \cdot 10^{-7} \text{ mbar}$	$1 \cdot 10^{-7} \text{ mbar}$
deposition chamber	$1 \cdot 10^{-8} \text{ mbar}$	$1 \cdot 10^{-7} \text{ mbar}$
evaporator	$1 \cdot 10^{-8} \text{ mbar}$	$5 \cdot 10^{-7} \text{ mbar}$

5.2 The Cluster Source

The source was built in the institute following the setup of H. Haberland [Habe 94]. Cluster formation is based on vaporization through sputtering and further aggregation via collisions with a seeding gas. Due to the low temperature of the inert gas, cluster production proceeds primarily by successive single-atom addition. Since reevaporation is negligible, the cluster abundances are smooth functions of size (generally a LogNormal) determined by collision statistics.

**Figure 5.2** – Schematics of the source

Sputtering is performed with a commercial 2'' magnetron¹ that has been adapted to allow floating of the anode with respect to ground potential and a direct gas flow between the two electrodes. The sputtering process consists in accelerating Argon ions towards the target in order to extract materials out of it. In the process secondary electrons are also ejected and cause a further ionization of the gas, giving rise to a self sustaining glow discharge. This process can be optimized by introducing a ring magnet below the target (*magnetron sputtering*). The electrons are then trapped in cycloids and circulate for a

¹Kurt J. Lesker Ltd. Hastings, UK.

longer dwell time in the gas, causing a higher ionization probability. In these conditions it is possible to run the discharge at lower pressures so that the ions will experience a lower number of collisions and hit the surface with a higher energy. The advantages of this vaporization method are a high erosion rate and a high charged to neutral particles ratio due to the presence of metastable charged states of the sputtering gas. This latter characteristic is of a great importance since charged clusters can be guided and filtered using electric fields. The sputtering gas is a mixture of *He* and *Ar* and typical value of the discharge are between 1 *W* and 15 *W*.

Since the gas enters the chamber passing in between anode and cathode, a continuous adjustable flow of around 300 *sccm* is kept at the target surface. This ensures a sufficient number of collisions and allows the clustering process. At the same time the continuous flux drives the clusters to the exit of the aggregation chamber that is constituted by a diaphragm of variable diameter. The distance between the magnetron and the iris can also be adjusted since the head of the magnetron is mounted on a sliding system. All the parameters described above determine the average size of clusters. A complete understanding of the mechanisms governing the aggregation process is a complex problem to be solved, involving the hydrodynamics transition from a laminar to a molecular flow. For the aim of this work it is not necessary, however, to enter into the details of cluster formation and only a qualitative picture of the role played by each parameter is given here. First of all it is observed that

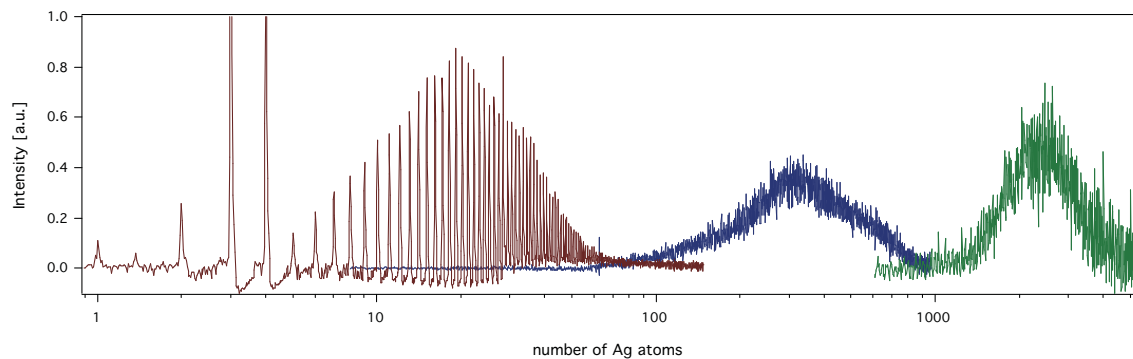


Figure 5.3 – Mass spectra of silver clusters as measured on the TOF-MS obtained with different source conditions. The spectra follow a LogNormal distribution and the average size can be varied over a wide range of masses. The intensity units are arbitrary.

an increase of gas pressure in the aggregation chamber, increases the number of collisions and consequently the average size of clusters; such increase can be obtained by varying the gas flow or by reducing the diameter of the diaphragm. A second parameter that acts on the size is the distance between the magnetron and the iris: a longer distance implies a longer dwelling time and a larger number of collisions, that will have as a consequence an increase in size. The parameter that proves determinant in order to control the intensity of the beam, is the power of the discharge. On the other hand, this parameter also acts on

the average size of the particles since a higher power is required to reach the larger sizes regime.

Another interesting characteristic of this source is its great versatility: clusters can be produced from all metallic materials and in a wide range of masses. In the figure, several mass spectra of Ag clusters are shown: by simple manipulation of the source conditions, the average size can be varied over several orders of magnitude. It is worth remarking that the size is referred to the number of atoms contained in the cluster and not to the diameter. This is important when considering the spread of the size distribution: typical values, for a LogNormal centered at 40 atoms¹, are of the order of 25%, as shown in fig.5.4; this spread in the number of atoms corresponds to a spread of about 6% in diameter. For larger clusters, smaller values of the spread are found.

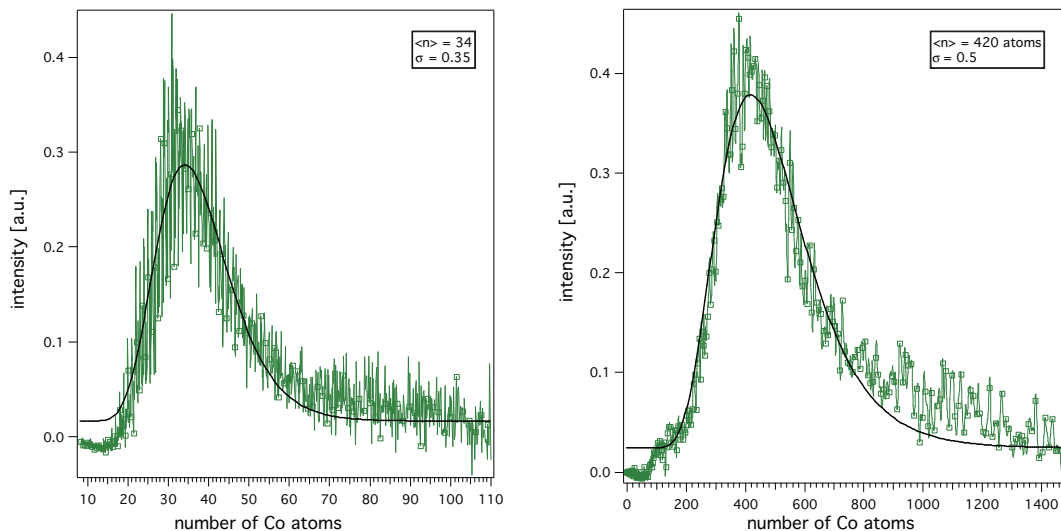


Figure 5.4 – Mass spectrum of clusters with an average size of 34 and 420 atoms respectively fitted with a LogNormal distribution. The spread of the LogNormal decreases with increasing size.

Kinetic energy of the beam

It is worth to discuss in more detail the kinetic energy distribution of the cluster beam. Clusters produced with this kind of source are cold: as already discussed in section 2.3 they are produced via successive collisions with the seeding gas, it is then expected that they will thermalize at the gas temperature. Helium and Argon are introduced in the apparatus at ambient temperature while the walls of the aggregation chamber are cooled with liquid nitrogen; the gas, colliding with the walls, will cool down at a temperature in between ambient and liquid nitrogen and so will do the clusters. Their thermal energy is then of the

¹As it will be discussed in part III most of the samples presented in this work were produced using clusters with an average size of 40 atoms and a size distribution comparable to the one described here.

order of 10 meV . The beam is cooled down further by the expansion stage that takes place at the exit of the aggregation chamber since the pressure in the transfer part is three order of magnitude lower than in the source.

On the other hand, clusters are created in a zone where the electrostatic potential is different from ground, and this potential gives another contribution to their energy. In practice, this is obtained by applying a voltage to the whole aggregation chamber whose typical values are between 30 and 60 V . As a consequence, the thermal energy of the beam is negligible with respect to their potential energy.

A third contribution to the total energy is given by the kinetic energy acquired in the expansion the beam undergoes at the exit of the source. Such kinetic energy is not the same for all the clusters, but depends on their mass: since they quit the aggregation chamber all with the same velocity, larger particles will have a higher energy and this difference results in a spread that, as shown in fig.5.5, is of the order of some eV .

As a result the total energy will be the sum of thermal, kinetic and potential terms, where the latter is dominant and easy to control. The actual energy of the beam can be measured by retarding field analysis (RFA) and the result, shown in fig.5.5 gives a gaussian distribution centered around an energy that is some eV lower than the chamber potential. This shift is due to the fact that clusters loose some energy in collisions when passing through the region between the iris and the skimmer. The energy spread, as already discussed above, is of the order of some eV .

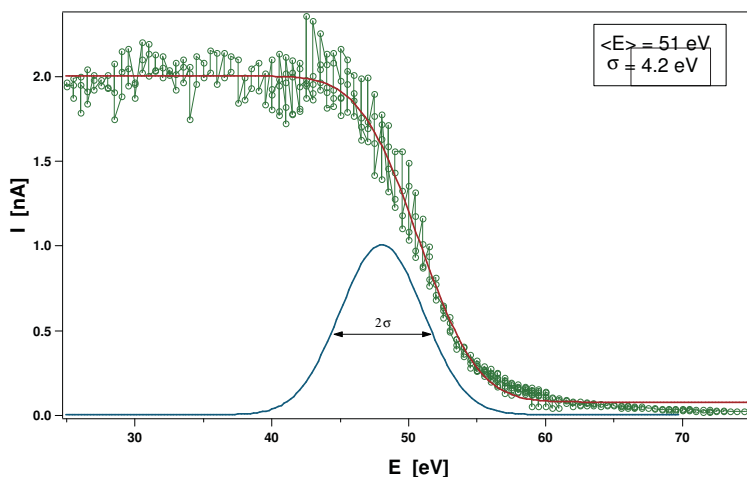


Figure 5.5 – Energy spectrum of clusters with average mass of 20 atoms, measured at the exit of the electrostatic bender. In this particular case the tube potential was fixed at 60V . The full circles are the experimental data and the solid line is a fit with a sigma function. The derivative of the fitting curve is also plotted for a better visualization the gaussian energy distribution.

The great advantage of producing a beam with these characteristics relies in the possibility of controlling the particle kinetic energy by applying an electrostatic potential, a

possibility that is of fundamental importance during deposition since it allows soft-landing of the clusters preserving them from fragmentation. Furthermore the reasonably low energy spread is useful to keep high the transmission efficiency of all the guiding elements, since focusing conditions depend on the energy of the particles.

The influence of several parameters, such as the voltage applied to the electrostatic guiding elements or the power of the discharge, on the energy and on its spread has been studied, but no particular effect of any of them could be observed.

5.3 Transfer and Deflector

The transfer part is mainly necessary in order to reduce the gas pressure that is very high at the exit of the source and should be several order of magnitude lower in the deposition chamber. This goal is achieved via differential pumping

In addition to that, this part is useful to screen out neutral and negatively charged particles and to collimate the beam. At the exit of the source, the first element is a skimmer, followed by an octupole that ends in a system of Einzel lenses that focuses the beam into the electrostatic deflector.

The **octopole** acts as an ion-guide: an RF potential is applied to the rods with alternating polarities, generating a well-like radial potential, proportional to r^6 , that confines the ions on the octopole axis. Additionally a DC-offset can be applied to the whole system in order to optimize field continuity with previous and following elements. By suitably choosing the DC-offset it is also possible to reduce the energy spread of the beam at the exit of the octopole, an effect that proves extremely useful in order to maximize the transmission efficiency of the subsequent element: the electrostatic deflector.

The **deflector** allows to direct the beam either to the *TOF* or to the deposition chamber. The bending field is produced by four hyperbolic electrodes and the beam is spatially collimated, at the entrance and at the exit by a three element Einzel lens followed by a three element slit lens that compensates for aberrations in the horizontal plane: since the deflector has a cylindrical symmetry, no focusing is needed in the vertical direction.

The trajectories of the ions in the deflector field were simulated with the help of the software SIMION¹ in order to estimate the optimal potentials to be applied. The software allows to draw 3D electrodes varying their potential and to simulate the trajectory of a beam of ions with adjustable initial energy, velocity and position. Such simulations reveal of fundamental importance since the complicated electric field structure induces strong aberration in the beam if the latter is not well collimated in space and velocity. It is then necessary to carefully determine all the potentials to be applied in order to optimize the deflector transmission.

¹Developed by D.A.Dahl at Scientific Instrument Services, Inc., Idaho National Engineering and Environmental Laboratory. www.simion.com

It should be remarked that ions trajectories in an electrostatic field do not depend on mass but are sensitive to energy, so that the deflector actually acts as an energy filter. The passing band was estimated from simulations to be of the order of 10 eV. It was already argued that typical energy spreads are of the order of a few eV and consequently the deflector will normally let all clusters through. However, since in this apparatus the energy spread of the beam is mainly produced by the fact that clusters come out of the source all with the same velocity, independently of their size, it may happen that, in case of a broad mass spectrum, the deflector acts as a mass filter [Alay 75]. This effect was actually observed in the case of bi-modal mass distribution¹ when it is often possible to observe only one at the time. Consequently the deflector acts as a mass filter with a passing window of the order of 5000 amu, and potentials need to be carefully adjusted depending on the beam characteristics.

A final remark concerns neutral clusters: these particles are not deflected and continue their straight trajectory. Hence the chosen geometry allows to collect neutrals for in-axis experiments simultaneously with the use of charged ions.

5.4 TOF Mass Spectrometer

The objective of a time-of-flight mass spectrometer (*TOF-MS*) is to determine the mass to charge ratio (m/z) of the particles contained in a beam. The basic operating principle consists in measuring the flight time through a drift tube after accelerating the charged particles with a pulsed electrostatic potential. Since all particles are accelerated by the same field, their velocities will depend only on the ratio m/z [Habe 95] and so will the flight time. Practically, a bunch of charged particles is extracted by a pulsed field and accelerated towards the detector where they are converted into an electric pulse. The signal is then collected by a pre-amplifier and visualized with an oscilloscope. For each pulse of the accelerator, a complete mass spectrum is obtained. This makes the *TOF-MS* a rapid tool for beam characterisation and, therefore, well suited for the optimization of parameters. Another advantage of this technique is the wide mass range, even if, as discussed in the following, mass resolution decreases with increasing times of flight (i.e. with increasing masses).

In the ideal case in which all particles have the same initial position and a negligible initial velocity (we assume $z = 1$), particles with equal mass will reach the detector at the same time:

$$t = \sqrt{\frac{L^2 m}{2eV}}$$

where L is the length of the flight and eV is the energy acquired in the acceleration stage.

¹Under particular source conditions, the mass spectrum can present two separated peaks.

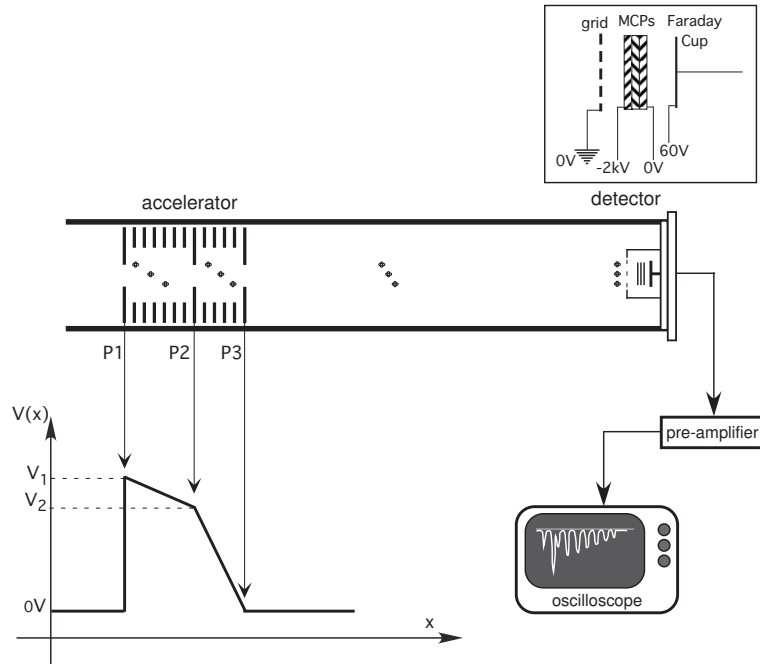


Figure 5.6 – Schematic illustration of the TOF-MS. Ions enter the accelerator in $P1$ with a spatial spread Δx and are then accelerated by a pulsed electric field. Since the potential decreases with x , clusters that are closer to $P1$ will receive a stronger acceleration, but at the same time they have to travel a longer distance to arrive at the detector.

Two different masses separated by Δm will reach the detector spaced by:

$$\Delta t = \frac{L}{2\sqrt{2eVm}} \Delta m$$

This means that the spacing is reduced for bigger masses so that the resolution decreases with increasing masses.

Up to now we supposed that the ions enter the accelerator all at the same time and with the same initial velocity. Obviously this is not true in our setup: particles enter the TOF-MS with both a position and a velocity spread, drastically reducing the resolution. In order to compensate for this problem, the acceleration can be divided in two stages and the potentials can be adjusted in such a way as to generate an electrostatic field that decreases with distance as showed in the figure 5.6. The double-field configuration, developed by Wiley and MacLaren[Wile 55], is based on the following steps: clusters ions are inserted between plates $P1$ and $P2$; the ions are accelerated by two different electric fields $E1$ and $E2$ by applying potentials to plates $P1$, $P2$, and $P3$; the cluster beam has a certain geometric width Δx , therefore ions starting nearer to plate $P1$ have a higher kinetic energy gain, but also a longer flight path than those starting near $P1$; the fast ions overtake the slow ones at the space focus that can be adjusted to correspond to the detector.

In this double-field configuration, both space focus and time resolution can be optimized

by adjusting the electric fields ratio $E1/E2$ and their values with respect to ground. Typical values of the accelerating potentials, of the pulse length and frequency are given in table 5.2.

Table 5.2 –

first acceleration stage	3.8 kV
second acceleration stage	2.6 kV
pulse length	20 μs
pulse frequency	10 Hz

The detector is constituted of three micro channel plates (MCP) mounted in a cascade configuration. The ions approaching the MCPs are accelerated at more than $2keV$ and, once they hit the surface, will produce a cascade of electrons that are collected on a Faraday plate as shown in the inset of fig.5.6. The signal is then amplified and sent to an oscilloscope where the flight times, triggered on the acceleration pulse, are displayed.

In this apparatus, the *TOF-MS* is required in order to optimize the beam. Once the desired mass distribution is obtained, the clusters are directed towards the deposition chamber.

5.5 Deposition

The final step of sample production, consists in the simultaneous deposition of the clusters and the matrix in order to produce the desired sample.

The samples studied in this thesis consist in thin films of about $50nm$ of copper or silver, containing cobalt clusters. Masses of clusters range between one and 6500 atoms but particular attention was directed toward smaller sizes of the order of some tens of atoms. Typical currents for this kind of beam are of a few nA that corresponds to $\sim 5 \cdot 10^{11}$ atoms per second. As a consequence, deposition times vary between 30 minutes and a few hours depending on the concentration to be achieved.

Clusters enter the deposition chamber passing through a **quadrupole mass filter**¹ (*Q-MF*) consisting in four cylindrical rods to which an *AC* voltage superposed to a *DC* component is applied (fig.5.7). The potential in the *Q-MF* has the form (assuming an ideal field):

$$\Phi(r, t) = \Phi_0(t) \frac{x^2 + y^2}{r_0^2}$$

where

$$\Phi_0(t) = U + V \cos(\omega t)$$

¹Extrel 9.5 mm , maximum mass 4000 amu , *RF* frequency 0.88 MHz .

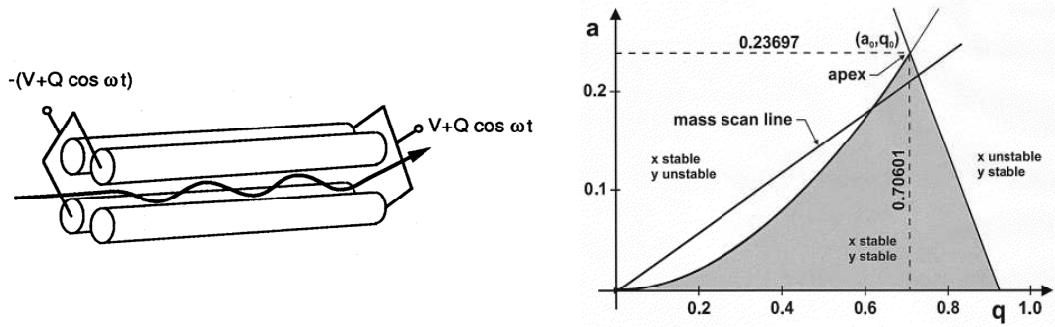


Figure 5.7 – Schematic representation of a quadrupole showing the applied AC and DC potential, and stability graph in the $(a - q)$ plane: stability and instability regions are labelled and a typical mass scan line is also plotted.

The trajectory of an ion in the quadrupole is the solution of Mathieu's equations

$$\frac{d^2u}{d\chi^2} + [a_u - 2q_u \cos(2\chi)]u = 0$$

where $\chi = \omega t/2$, u represents x or y , and the two parameters

$$a_u = a_x = -a_y = \frac{8eU}{mr_0^2\omega^2}; \quad q_u = q_x = -q_y = \frac{4eV}{mr_0^2\omega^2}$$

where introduced. Depending on the mass of the ion (m), the solutions of these equations contain either a strictly growing exponential factor (unstable solution) or an oscillatory term (stable solution). The stability of the solution can be represented in a (a, q) plane, as shown in fig.5.7. In normal operation, the amplitudes of U and V are simultaneously varied along a mass scan line of fixed ratio U/V , where this ratio defines the mass resolution (more detailed informations of the working principle of a quadrupole mass filter can be found, for example, in [Blau 98, Doug 05]).

The Q - MF can operate as an ion guide, or as an effective filter with resolution up to $1amu$. Consequently it is possible, varying the resolution, to chose a window of deposited masses between the complete distribution and a precisely selected single mass. The Q - MF is followed by a three-elements Einzel lens that focuses the ions to the deposition surface. The potentials of the surface and of the whole sample holder can also be adjusted and the ion current can be monitored on line during deposition. The control on the electrostatic field in the deposition region is extremely important in order to achieve soft-landing conditions: when reaching the surface, clusters have a kinetic energy that is converted into internal energy during the impact. This results in an overwarming of the cluster that might lead to the loss of one or more atoms. In order to avoid this effect, that would limit the control on the sample characterization, it is necessary to slow down the ions to energies lower than $1eV$ per atom[Brom 96]. This condition is satisfied by adapting the potential of the deposition region. As previously discussed (cf. section 5.2), clusters produced in this source

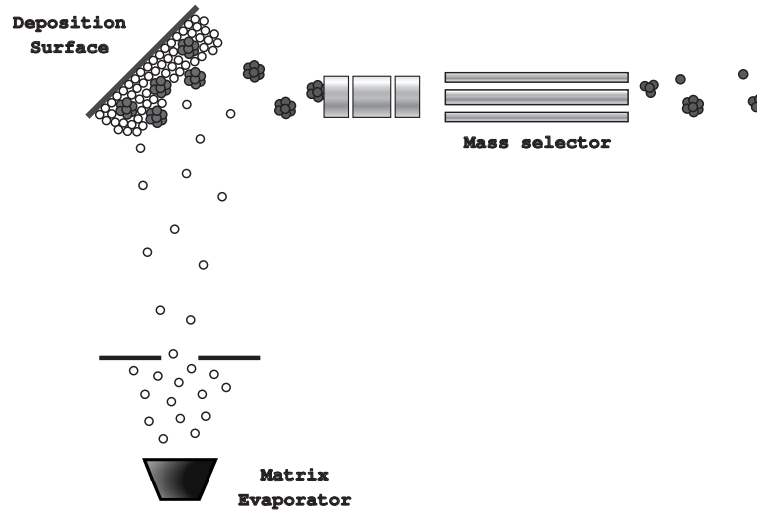


Figure 5.8 – Schematics of the deposition process: clusters coming from the deflector are mass filtered and focused onto the deposition surface: the matrix is evaporated simultaneously from below.

have an energy of a few tens of eV with a small spread so that applying a potential to the deposition surface it is already sufficient in order to guarantee a deposition energy of the order of $0.5eV$ per atom.

While directing the clusters to the substrate, the matrix is simultaneously deposited using an electron beam evaporator situated in another chamber. The matrix deposition rate can be varied to control the concentration of clusters in the sample and the flux is monitored with a microbalance.

The two chambers are separated by a diaphragm cooled with liquid nitrogen that acts as a cryo-pump for H_2O , CO_2 and CO vapour produced by the warming of the evaporator.

All samples described here have been produced at room temperature, but the sample holder design provides the possibility to heat or cool down the deposition surface.

A final remark concerns the neutralization of the sample: when reaching the deposition surface, the clusters are charged. To prevent an accumulation of charge, a conductive substrate¹ has been chosen. However, when an insulating matrix is used, a tungsten filament, located below the sample holder, can be switched on to produce an electron cloud that neutralizes the clusters once they have reached the surface.

Once the cluster deposition is accomplished, a protecting layer about 5 nm thick, is deposited on top in order to prevent from oxidation when the sample is taken out of vacuum. This layer is of the same material as the matrix and it was measured [Gan 03] that a time of the order of 100 hours is necessary for oxygen in standard room conditions to penetrate through it and start oxidizing the underlying clusters.

¹Slightly conductive polyimide: Kapton XC, Goodfellow, $40\text{ }\mu\text{m}$ thickness, $370\text{ }\Omega/\text{cm}^2$.

5.6 Residual gas analysis

As already underlined in previous sections, great attention has been devoted to the quality of the residual gas inside the apparatus in order to prevent cluster oxidation.

The composition of the residual gas showed to be particularly critical in the source, where clusters spend a considerable amount of time and undergo a large number of collisions, and in the deposition region, where they rest exposed to the atmosphere for a time of the order of one minute. In the aggregation chamber the main risk is to produce oxidized

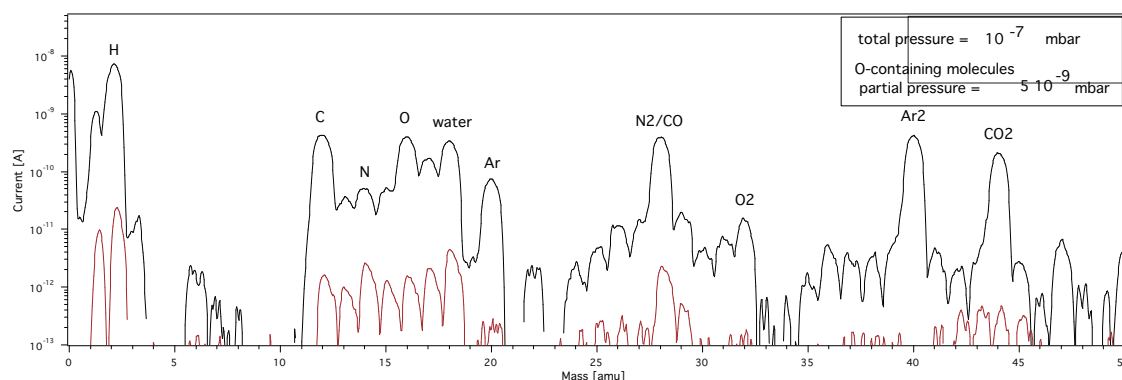


Figure 5.9 – Mass spectra of the residual gas taken in the deposition chamber during operation and with evaporator switched off. Principal peaks are identified. In this case, the worst condition are considered, the total pressure being 10^{-7} mbar. The partial pressure of oxygen-containing molecules can still be evaluated to be less than 10^{-8} mbar.

clusters or to have aggregation with the residual water. The base pressure in this region is normally of the order of 10^{-7} mbar and a liquid nitrogen cryo-pumping assures a low amount of water. Anyway, it should be considered that during operation the pressure is greatly enhanced by the introduction of the seeding and sputtering gases (*He* and *Ar* respectively), so that the purity of the atmosphere is completely determined by the quality of those gases and by possible leaks in the gas lines.

Concerning the deposition chamber, the risk comes from the residual oxygen that can oxidize the clusters before they are completely covered, and hence protected, by the matrix. Typical matrix deposition rates are of the order of $5 \cdot 10^{-2}$ monolayers per second. A comparable residual gas condensation rate, assuming a sticking coefficient of 1, is achieved for pressures of the order of $1 \cdot 10^{-8}$ mbar. This pressure is comparable to the value measured during deposition, but it should be kept in mind that the atmosphere is mostly composed by inert gases (as *He* and *Ar* coming from the source) and *H₂* produced by in the matrix evaporation process. The residual gas mass spectrum is continuously monitored during deposition and, as shown in fig.5.9, the oxygen-containing molecules are just a small fraction of the total atmosphere and their partial pressure can be evaluated to be below $1 \cdot 10^{-8}$ mbar, one order of magnitude lower than the matrix deposition rate.

5.7 Conclusions

The sample production technique was described and analysed in this chapter. The process can be summarized in the following steps:

- cluster ions with an adjustable size distribution are produced in a magnetron sputtering source;
- the beam is characterized via a time of flight mass spectrometer and then deflected to the deposition chamber;
- clusters are mass selected with a quadrupole mass filter and focused on the deposition surface;
- the matrix is evaporated with an electron beam and co-deposited with clusters;
- the sample is removed from vacuum to perform the desired measurement.

The advantages of this production methods are:

- the control of cluster size and concentration independently;
- a wide range of cluster sizes (from two to several tens of thousands of atoms);
- the possibility of using different types of matrices (both metallic and dielectric) and of cluster material.

Measurements

6.1 Sample characterization

In order to test the performance of the apparatus and check the quality of the produced samples, several analysis, both chemical and physical, are performed on a regular basis. Main features that need to be tested are the chemical status of clusters to exclude oxidation and their integrity after deposition.

6.1.1 X-Ray Photoelectron Spectroscopy

X-ray Photoelectron Spectroscopy (XPS) is performed in order to check the oxidation state of clusters and to measure their concentration in order to compare it with the value estimated during the deposition. XPS was performed by Nicolas Xanthopoulos in the laboratory

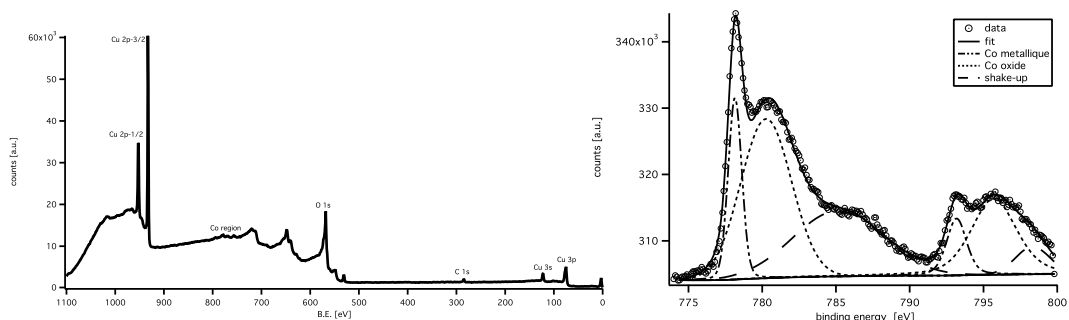


Figure 6.1 — XPS spectrum of a copper sample containing cobalt clusters of avg size 600 atoms. On the left a complete survey shows the different elements composing the film: Cu, Co, O and C; they high quantity of oxygen is due to the long exposure to air. On the right a zoom on Co 2p peak is showed. Clear proof of oxidation is observed: 50% of cobalt is in a oxide-state.

of Metallurgical Chemistry¹ at EPFL. In fig.6.1 the XPS spectrum for an oxidized sample is shown. After careful amelioration of the vacuum conditions, a substantial decrease of the percentage of oxidized cobalt was obtained. It should though be remarked that XPS

¹Laboratoire de métallurgie chimique - Institut de Matériaux - Sciences et Techniques de l'ingénieur.

analysis is a surface technique and the first layers of the sample are the most exposed to degradation.

Nevertheless the risk of oxidation is very high for this kind of nanostructures and it is enhanced when they are extracted from vacuum in order to perform an experimental analysis. Consequently it is necessary to regularly check the quality of the sample. Since XPS is a time-consuming and sample-destructive technique (as pre-sputtering is necessary to clean the surface from atmospheric pollution), other strategies need to be found. A good solution is to monitor the conductive properties: it was observed that a sample in good condition has the typical metallic resistivity with a plateau at low temperatures, while a semiconductor-like behaviour appears when degradation occurs since the formation of oxide insulating regions reduces the conductivity. For this reason a resistivity versus temperature measurement was always performed as a reliability test before every measurement session.

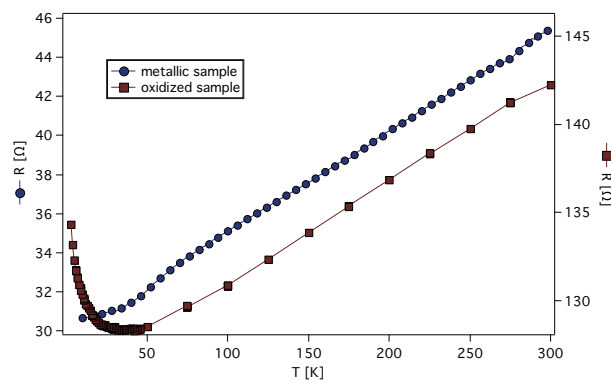


Figure 6.2 – Resistivity curves for two different samples: the square symbols follow a semiconducting behaviour at low temperatures, meaning the sample underwent oxidation.

6.1.2 High Resolution Transmission Electron Microscopy

High Resolution Transmission Electron Microscopy was used to verify the integrity of clusters after collision with the deposition surface and to exclude coalescence or formation of an alloy with the matrix. Images of large clusters allow to affirm that particles stay separated and intact after deposition. It is furthermore possible to observe a spherical shape and the crystallinity of the big cluster shown in fig.6.3.a.

Small clusters are shown in the image in fig.6.3.c. In this case it is not possible to resolve the single particles. It is nevertheless possible to exclude the formation of larger clusters due to coalescence. In certain regions of the image, it is also possible to observe the crystalline planes of the matrix, this proves that the metal is polycrystalline.

These images allowed us to exclude the formation of an alloy between the matrix and cluster material and, in the case of big clusters, to observe that no significant fragmentation occurs during deposition and that a spherical shape is conserved. Actually the images being

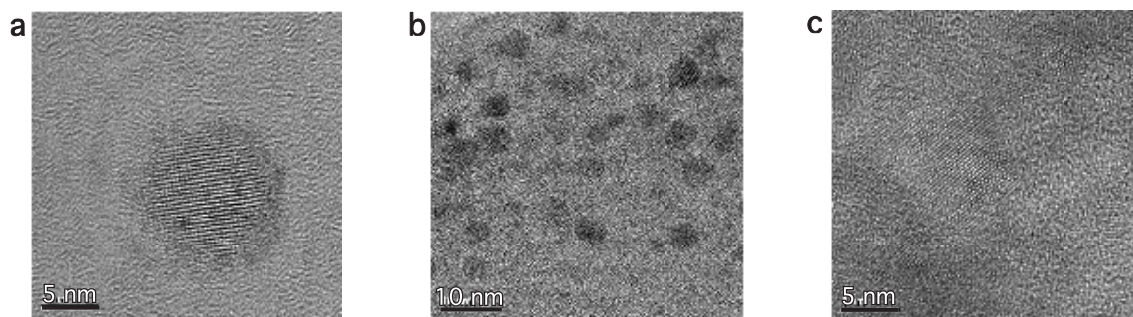


Figure 6.3 – a) Image of a large cobalt cluster of about 10000 atoms b) Image of a copper/cobalt sample containing clusters of avg size 6500 atoms with 8% Co atomic concentration. Clusters are well separated and their size is comparable with the one inferred from the TOF mass spectrum. c) Image of a copper/cobalt with same 8% concentration of Co, but with clusters of 15 atoms.

a 2D projection of the sample, a deformation of the cluster during the impact cannot be excluded. Anyway the directional isotropy was confirmed by other results as the absence of a global easy axis in magnetization measurements. This subject will be further discussed in the following. For what concerns small clusters, it was not possible to determine their size from the images, coalescence can still be excluded since a granular inhomogeneous structure is observed.

HRTEM images were taken by J-P. and M. Abid at the CIME facility of the EPFL.

6.2 SQUID magnetometry

A standard technique to measure the magnetic character of a material, is the use of a Superconducting Quantum Interference Device (SQUID)¹. The basic principle is to make the sample oscillate in a coil and to detect the variation of flux of magnetic field, measuring the induced current, through that coil. What makes this technique more sensitive with respect to standard magnetometry is the use of a Josephson junction based detector to measure the induced current.

This instrument allows the detection of very low signals, the resolution being of $10^{-8}emu$, and for this reason it is suited to characterize samples containing low quantities of magnetic material. However it should be kept in mind that magnetic pollutants contained in the atmosphere might deposit on the sample holder or in the instrument chamber and produce a signal of $\sim 10^{-5}emu$, i.e. of the same order of magnitude than the signal produced by our samples², therefore data must be analysed carefully. Because of this limitation, the SQUID

¹The instrument used for this purpose is a *Quantum Design MPMS* (San Diego, USA) equipped with a superconducting magnet that can reach $5T$.

²Typical samples considered in this work contain 10^{15} magnetic atoms, assuming a magnetic moment of one Bohr magneton per atom, the total magnetization can be estimated to be of the order of $10^{-5}emu$.

has been mainly used to compare and confirm the results obtained with other techniques.

6.3 Transport measurements

Electrical and thermal transport properties are governed by the interaction of conduction electrons with the microscopic medium they have to cross. Inversely, transport properties can be studied to get an insight on the nature of the scattering events electrons are submitted to. In other words, the electrons are used to probe the microscopic nature of the sample. In particular, the fact that electrons possess an intrinsic magnetic moment allows them to be used to test the magnetic behaviour of a material. In addition to that, transport properties are sensitive to concentration of magnetic material rather than to its total amount, and consequently such technique is particularly suited to study magnetic nanostructures and granular systems in which the total amount of magnetic material is very small.

Experiments were performed using a technique developed in collaboration with the group of Prof. Ansermet¹. The set-up allows to perform several different measurement protocols. In the present case the properties that have been tested are magnetoresistance (*MR*), Hall voltage and magneto-differential-resistance (*MDR*). A typical set of measurement is showed in figure 6.4.

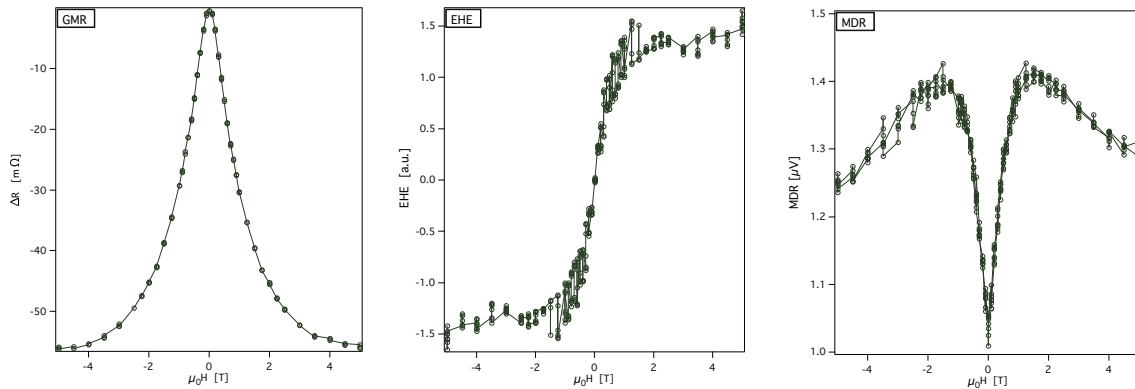


Figure 6.4 – Typical results of the three measurement protocols.

All these measurements were performed in a cryostat that allows temperature control between 3 and 350K and that is equipped with a superconducting magnet generating a maximum field of $\pm 5T$. A special sample holder was conceived to perform simultaneously a complete set of measurements. The sample has a rectangular shape ($5 \times 1mm^2$) and has two perpendicular Hall contacts at half-length. It is mounted at the end of a rod, that can be fitted in the cavity of the cryostat, in such a way as to be oriented perpendicularly to the magnetic field. Electric connections are realized by pressure contacts and silver

¹Laboratoire de Physique des Matériaux Nanostructurés - Institut de Physique des Nanostructures - EPFL

paste is added in order to guarantee stability under temperature variations. All cables are connected to the exterior by BNC feedthroughs. An optical fibre is also fixed to the rod and brought very close to the sample surface in order to perform *MDR* measurements.

In the following, a description of each measurement protocol is presented together with the basic physical mechanisms giving rise to the observed effects. These basic concepts are introduced with the purpose of motivating the experimental work and a more complete discussion can be found in parts I and III.

6.3.1 Magneto Resistance

Resistivity is the intrinsic parameter of a material that describes its current response to an electric field:

$$\vec{j} = \frac{1}{\rho} \vec{E}$$

The response would be infinite (and hence ρ would be zero) if electrons could travel through the medium conserving their momentum, as it would be the case in a perfect metal at $T = 0$. However in a real material electrons experience continuous interactions with the lattice and the response is limited to finite values [Ashc 76].

The most important source of scattering at room temperatures are phonons. Since their number increases linearly with temperature, the effect of phononic scattering is a linear increase of resistivity and it becomes dominant at high temperatures. Since phonons do not possess a magnetic moment, they do not act on the electronic spin. At low temperatures, on the other hand, the contribution of impurities and, to a lower extent, of electron-electron scattering become important and the resistivity stops to decrease and stays constant. Obviously the electrons interact differently with different kinds of impurities and in particular, because of their spin, they are sensitive to a magnetic scattering potential. An external magnetic field acts on these magnetic scattering centers and breaks the symmetry of the material, producing a consequent change in electronic conduction properties. As a result, the resistivity will depend on the magnetization of the material, and such effect is called magneto-resistance¹.

The magneto resistance measurement is performed by a conventional two point technique: a DC current is driven through the sample and the DC voltage response is detected (V_{xx}). The magnetic field is applied following the orthogonal geometry as shown in the diagram. Typical currents are of the order of $1mA$ and, in the case of our samples, measured voltage drops are in the $10mV$ range, the resistance being of tens of Ohms.

The experimental results are often reported normalized between 0 and 1. This choice is justified by the fact that the analysis performed in this study refers to the shape of the curve rather than to the intensity of the effect. In fact the values of the intensity is often not reproducible in our measurements (since the process of sample preparation as well as

¹Other kinds of magnetic interactions, as electron-magnon scattering, are not discussed here.

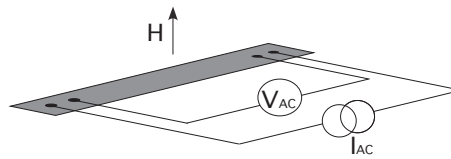


Figure 6.5 – Geometry of the GMR measurement protocol.

the measurement technique itself have been refined during the work) and can be thus taken into account only on a qualitative basis.

6.3.2 Hall voltage

The Hall effect is the result of deflection of charges under the action of an external electromagnetic field: if a current is driven through a sample and a magnetic field is applied perpendicularly, the conduction charges will experience a Lorentz force resulting in charge accumulation, and thus in a potential difference in the direction perpendicular to both the current and the magnetic field. The recorded voltage is linear in magnetic field and depends on the density and charge of carriers:

$$V_{xy} = -\frac{IH}{ned}.$$

In the presence of magnetic impurities, an additional effect is observed: the local moments produce a spin-dependent scattering potential that breaks the left-right symmetry, consequently an additional transverse displacement is produced and the resulting voltage drop is proportional to the sample magnetization. These two effects, called normal and extraordinary respectively, add up in the measured signal resulting in a curve as the one shown in fig.6.6. If a sufficiently high field is applied to as to reach saturation, it is possible to

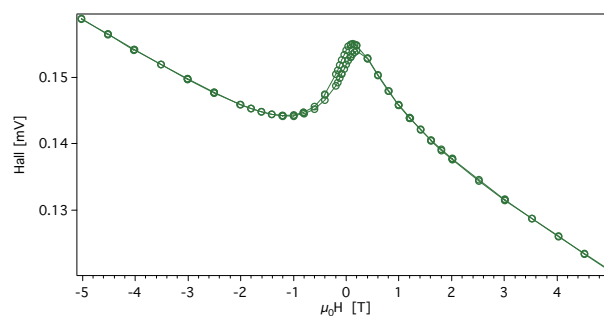


Figure 6.6 – Hall effect measured on a sample containing Co clusters. The ordinary (linear) effect as well as the extraordinary (sigmoidal) one can be observed.

separate the linear and hysteretic part and this protocol can be used to directly measure the magnetization of the sample.

To measure V_{xy} a standard Hall geometry was used: a steady current is driven through the sample and a magnetic field is applied in a perpendicular direction; the voltage drop is detected in the direction perpendicular to both current and magnetic field (V_{xy}). Also in

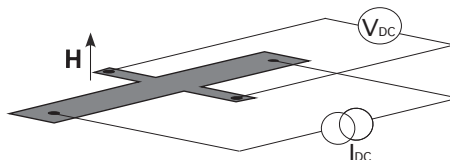


Figure 6.7 – Geometry of the Hall measurement protocol.

this case typical currents are of the order of $1mA$ but the detected voltage is around $5\mu V$. It should be considered that the alignment between the two perpendicular contacts is never perfect and a spurious longitudinal component is always superposed to the Hall signal.

Hall signal analysis procedure

It is worthwhile discussing in more detail the procedure followed to analyse Hall data, since the signal results from the superposition of several components that have to be discerned carefully. As already stated, the ideal Hall signal is composed of two parts: the first is linear in the magnetic field (normal) and the second is proportional to the magnetization (extraordinary). In addition to that, an extra contribution can come from longitudinal resistivity since it is experimentally impossible not to have a slight misalignment between the two points of measure. In the case of a magnetic material, the latter contribution will also be field-dependent as it will follow the standard MR behaviour. Hence we can write the total measured effect as:

$$R_{xy}(H, T) = C_1 \cdot H + C_2 \cdot m(H) + C_3 \cdot MR$$

The way that was adopted to eliminate the MR contribution consists in extracting from the total signal the even part: since the Hall effect is odd in the field while the MR is even, the following is verified:

$$\frac{1}{2} (Total(H) - Total(-H)) = \frac{1}{2} (MR(H) - MR(-H) + Hall(H) - Hall(-H)) = Hall(H)$$

It should be taken in mind that such procedure, eliminating all the even contributions to the total signal, eliminates also any eventual hysteresis. However, as it will be discussed in detail in section 7.1.2 most of our samples show an anhysteretic behaviour at every temperature and when this does not happen, it is still possible to study separately the two components of the signal (hysteretic and anhysteretic).

6.3.3 Magneto Differential Resistance

This measurement protocol was developed in the laboratory of prof. Ansermet [Grav 05] and consists in detecting the AC voltage response locked to a periodic temperature variation of a sample that is traversed by a constant current.

The temperature oscillation is achieved by illuminating the sample with a laser emitted by a $30mW$ diode of wavelength $680nm$ with a frequency of $22Hz$. For these energy values, no photoelectric effect takes place and the effect of the laser is a temperature variation of less than $1K$. At the same time a constant current is driven through the sample and the voltage variation produced by the temperature oscillation is detected. The behaviour as a function of applied magnetic field¹ and average temperature was studied. In some of

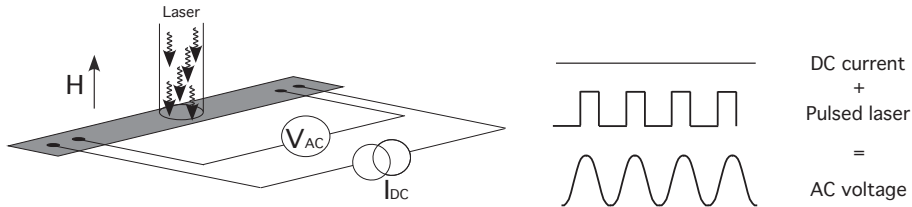


Figure 6.8 – Geometry of the MDR measurement protocol.

our published works, this measurements has been presented under the name of *MTGV*: Magneto-Thermo-Galvanic Voltage. This name comes from the fact that the protocol was developed to study the relation between heat, charge and spin currents in multilayered magnetic systems. In such case, the geometry of the sample allowed to establish a temperature gradient between the magnetic and non-magnetic layer and to observe the dependence of the Thermo-Galvanic effect on the magnetization [Grav 05]. In the case of cluster assembled samples, the nature of the sample and its geometry produce a completely different signal and the name *MDR* is more correct than *MTGV*.

As a matter of fact, this measurement detects a variation of resistivity ΔR produced by a variation of temperature ΔT , hence it can be interpreted as a derivative of the resistance with respect to temperature. The process of derivation allows to drop all scattering terms that are not temperature dependent, in particular all the effects due to non-magnetic impurities. By consequence, the voltage drop that is detected is mainly due to the temperature dependent part of the magnetic scattering and several effects that are normally masked by the phononic part of the resistivity, can be highlighted with this protocol. In fact this measurement shows to be extremely sensitive to variation of magnetic field or, more correctly, of local magnetization and it also furnishes greater details on the conduction mechanism. In fig.6.9 a comparison between *MDR* and the derivative of resistivity obtained by resistance measurement is shown. It can be observed that the curves are compatible but the quality

¹The magnetic field was applied perpendicularly to the film surface in order to avoid spurious Hall or Nerst effect.

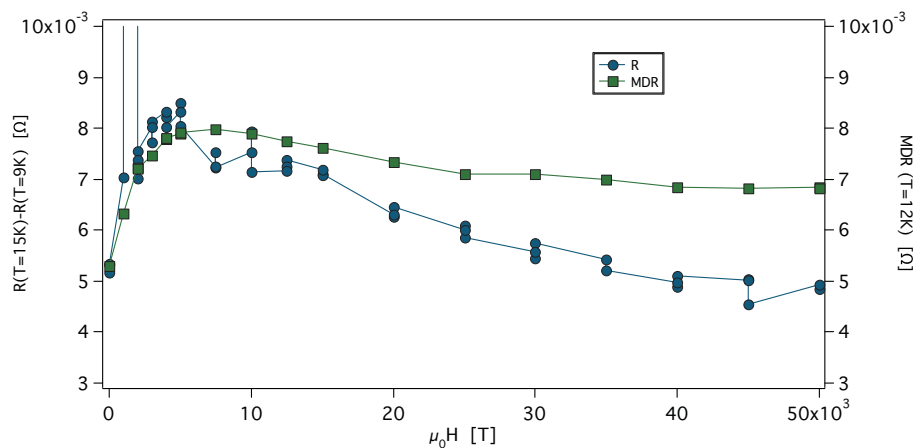


Figure 6.9 – Comparison between $\Delta R/\Delta T$ obtained with a resistance and an MDR measurement. The MDR signal was taken at $T = 12K$ while resistance was measured at 15 and 12K.

of the MDR is higher. Furthermore it is not always possible to operate the derivative on the resistance data because the extraction of such a small signal is often corrupted by the noise level.

The MDR effect must not be confused with magnetic thermoelectric power ($MTEP$): in the latter, there is no applied current and a temperature gradient is established at the extremities of the sample. $MTEP$ measurements have been performed in order to exclude any contribution to the MDR signal, and no response was ever observed. Any spurious contamination coming from Hall or Nernst effect can also be excluded since the observed signal does not have the correct parity in magnetic field: Hall and Nernst potentials are both odd function of B while the observed MDR is even.

Part III

Results and Discussion

Outline

As discussed in the previous chapter, the magnetic behaviour of cluster assembled materials has been tested via their transport properties. The goal is to be able to determine single cluster magnetic characteristics (the magnetic moment per cluster as a function of size, in primis but also their anisotropy) as well as their collective behaviours. Several samples

sample name	avg # of atoms	at. <i>Co</i> conc.	matrix
CoCu5	15	8%	copper
CoCu9	600	8%	copper
CoCu11	6500	8%	copper
CoCu12	2300	8%	copper
CoAg3	23	1.7 %	silver
CoAg13	1	1.4 %	silver
CoAg12	250	1%	silver
CoAg14	500	6%	silver
CoAg15	40	0.3%	silver
CoAg16	42	0.8%	silver
CoAg17	350	3%	silver
HCoAg1	40	30%	silver
HCoAg3	40	2.4%	silver
HCoAg4	40	1.3%	silver
HCoAg5	40	3.8%	silver

Table 6.1 –

containing cobalt clusters with different average size and concentration have been produced (Table 6.1) and For all samples *MR* and *MDR* have been measured at different temperatures ranging from 3 to 300K, in magnetic field up to 5T. In the case of the *H*-series, the Hall voltage has also been recorded. The measurement protocols used to obtain these signals, as well as the procedures to extrapolate the information from raw data, has already been discussed in section 6.3. In the two following chapters the experimental results will be presented and interpreted following different models.

In chapter 7 the experimental results relative to *MR* and Hall voltage will be interpreted in the framework of the Mott hypothesis of two parallel currents. Several models will be used in order to describe the magnetization, expressed by the Hall voltage, and to understand the relation between it and magnetoresistance. It will be shown how those models explain the observed behaviour, at least in a qualitative way. It will also be pointed out that for a more detailed description of *MR* interactions between clusters as well as some conduction mechanisms that are not included in Mott description, have to be considered.

In chapter 8, these effects due to interactions and mixing between spin channels, will be used to interpret the *MDR* behaviour. In particular it will be shown how this measurement protocol underlines the failure of models based on independent particles and separate spin currents. A possible mechanism for spin mixing in granular systems is also presented.

Magnetotransport in the Mott model

7.1 Results: MR and Hall voltage

One of the main advantages of the particular sample preparation technique is the possibility of varying independently several parameters as cluster concentration, size and composition. Furthermore such parameters can be controlled with great accuracy, as in the case of the average size for which an extremely narrow mass distribution can be obtained. In what follows a comprehensive overview of the experimental results as a function of these parameters is given.

7.1.1 Magnetic Field and Temperature

The two external parameters that have been varied are temperature and magnetic field. The samples under study can be assumed to be, at least for a qualitative description, superparamagnetic. As discussed in section 3.5.1, in such case the magnetization is defined by the interplay of H and T , reason why for each sample several $M(H)$ and $MR(H)$, with H ranging between -5 and $5 T$, have been measured at different temperatures from 3 to $300K$. A typical set of measurements as a function of temperature, is shown in fig.7.1. Both raw and normalized data are plotted for MR in order to underline the difference in amplitude and in form respectively.

For what concerns the Hall voltage, it can be seen that the curve reaches saturation more slowly as the temperature is increased. Furthermore, the low-field susceptibility, as obtained from the slope of the magnetization curve at low fields, is higher at low temperatures, as predicted by the Curie's law. Such behaviour is reflected in the MR where, additionally, a decrease in magnitude is observed.

An intuitive reasoning can easily explain this trend: when no external field is applied, the magnetic moments are randomly oriented and no net magnetization exists. As the field is added, the moments will tend to align in its direction; on the other hand the thermal

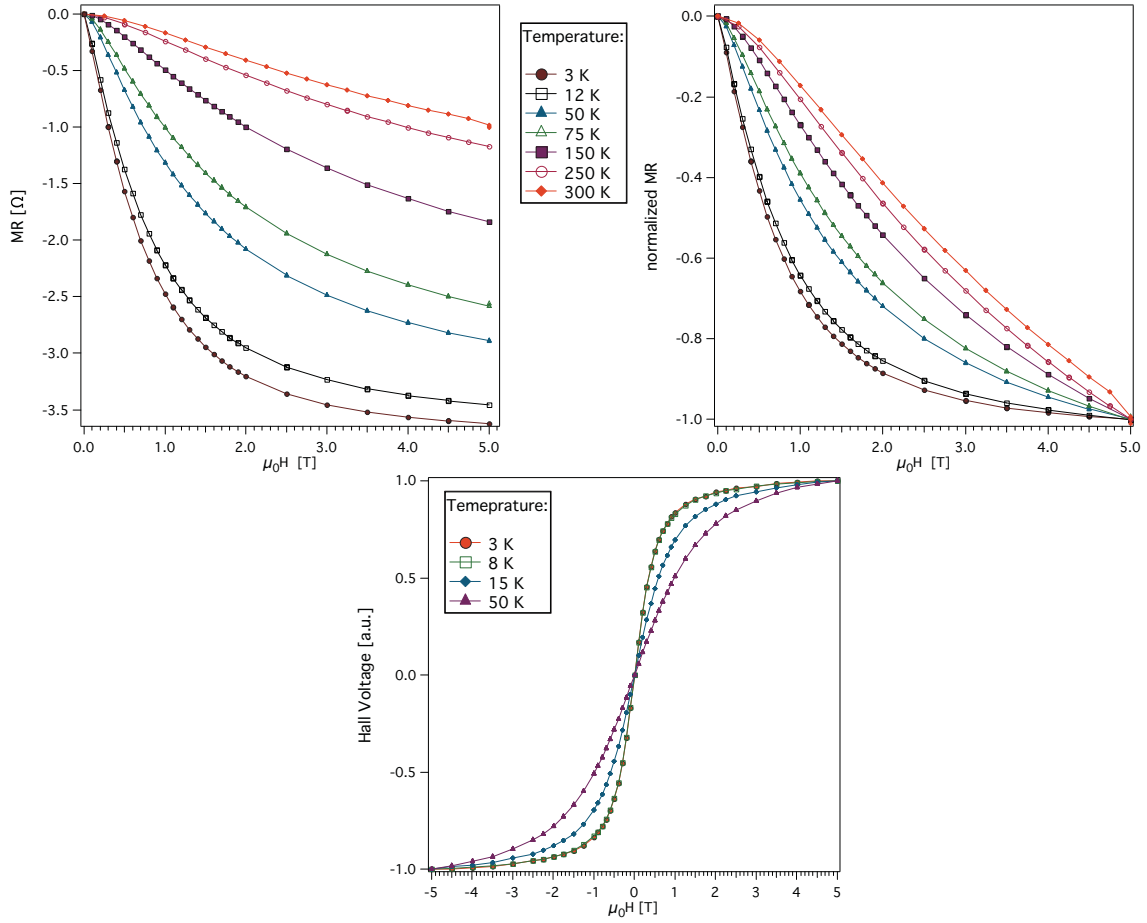


Figure 7.1 – *MR of sample CoAg16 (40 atoms; 0.8%) at different temperatures; on the right the same curves normalized between 0 and -1 are shown. On the bottom: normalized Hall Voltage of sample HCoAg4 (40 atoms; 1.3%) at different temperatures. As T is increased, a slower approach to saturation is observed in both magnetization and MR curves.*

agitation will disorient them and lower the total magnetization. As a consequence it will be harder to reach saturation as the temperature is increased.

7.1.2 Hysteresis

In the curves shown in fig. 7.1, no coercivity is visible and the same can be stated for most of the samples. However in more concentrated samples (as the *Cu* series and *HCoAg1*) the opening of a hysteresis with a coercive field of the order of $5 \cdot 10^{-2} T$ was observed below a critical blocking temperature T_B at which blocking occurs.

In fig. 7.3 *MR* curves of samples containing clusters with different sizes at the same atomic concentration (8%) are reported. All the samples show hysteretic behaviour even if the number of atoms per cluster is varied from 15 to 2300 and in the small size regime no blocking is expected at the considered temperature (13 K). It is interesting to observe how

the blocking temperature varies as a function of size, since information can be withdrawn on the nature of the blocking mechanism.

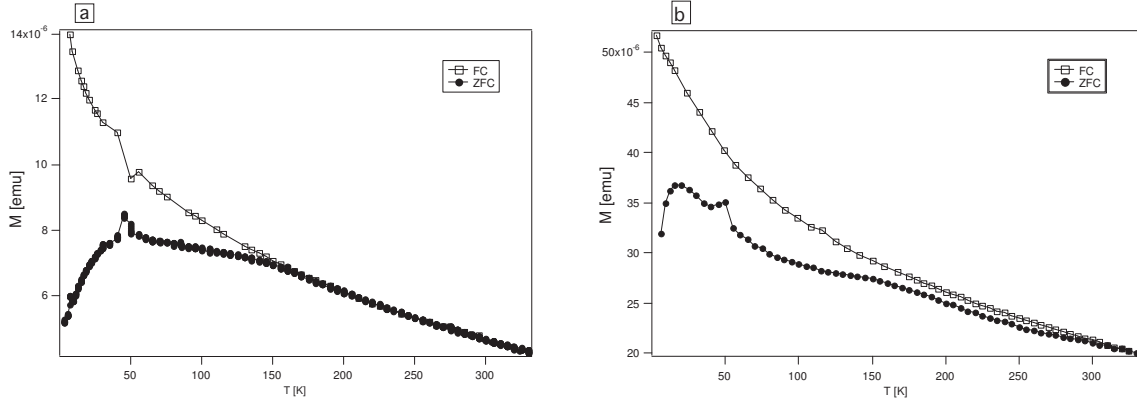


Figure 7.2 – Zero-field-cooled and field-cooled magnetization curves for samples a:CoCu5 and b:CoCu9 (8% at. conc.; 15 and 600 avg atoms respectively). The blocking temperature can be estimated as the maximum in the ZFC curve. In this case the T_B is greater ($\sim 50K$) for smaller clusters than for the larger ones ($\sim 25K$) revealing that the blocking is due to interactions in the first case. The shoulder that is observed at $175K$ for both samples, is probably due to the blocking temperature of the oxide layer [Gang 93, Vere 99] that the clusters under study in this specific case, present. The peak at $50 K$ is a systematic error due to the measurement protocol and does not have any physical meaning.

T_B temperature can be determined by measuring the magnetization as a function of temperature in a zero-field cooled procedure that consists in cooling the sample in zero field, applying a small magnetic field in order to be able to measure the magnetization and then raising the temperature while continuously measuring $M(T)$. At low T the magnetic moments are frozen in random directions the total magnetization averages to zero; as T is increased, the thermal energy might become sufficient to overcome the energy barrier and the magnetic moments will orient with the external magnetic field, with a consequent increase of M ; as T is increased further, the thermal agitation will produce again a random orientation of the magnetic moments and M will decrease again. The blocking temperature is defined as the temperature for which the magnetization is maximized.

As shown in fig. 7.2, a T_B is observed for both samples and it is greater for the sample containing smaller clusters, revealing a different origin in the two cases: in the case of bigger particles it is due mainly to the cluster internal anisotropy, while in the second case the major cause are interactions. This conclusion is justified by the fact that the anisotropy energy scales with size, hence the activation temperature necessary to overcome the potential barrier should be smaller in the case of smaller clusters. In the present case, however, the smaller the clusters the shorter will be their inter distance, as shown in the simulated representations of the clusters distribution in fig. 7.3, and the stronger the interaction. This explains the greater T_B , in agreement with reported simulations [Garc 00].

We have in this result a first indication of the importance of interactions and of the fact that, in the case of small clusters, also the average size and not only the concentration is a determinant parameter for what concerns their strength.

However, since this study is centered on the analysis of diluted systems of small particles that are supposed to be non interacting and unblocked, those hysteresis are normally smaller than $250mT$ and they have not been studied in detail. In some cases, where coercivity appeared only at very low temperature, the hysteresis has been eliminated in the data treatment; this choice is justified by the fact that the anhysteretic parts of MR and magnetization represent the superparamagnetic component of the system [Alli 99].

7.1.3 The effect of size

The effect of size can be easily observed in fig. 7.3 showing the $CoCu$ series¹ in which the concentration was kept constant at 8%. Both the shape and the amplitude of the MR are strongly affected by the variation of size.

Concerning the shape, it is observed that for smaller clusters no saturation is attained, while the onset of saturation is already observable in the case of 600 atoms and a complete saturation is obtained for larger clusters. The different approach to saturation can be explained qualitatively considering that larger clusters possess a larger magnetic moment and can be though saturated by applying a weaker magnetic field. Furthermore the coercivity, observable for all these samples because of the high concentration (as discussed in section 7.1.2), becomes more important as the size is increased.

For what concerns the amplitude, a maximum is observed in the case of clusters containing 600 atoms. An optimal size for MR is obtained by several theoretical works and observed experimentally on samples prepared with annealing procedures. Zhang and Levy [Zhan 93, Shen 03] argued that the amplitude of the signal is increased as the cluster size decreases because of the increase of the surface to volume ratio [Levy 90]; however, being smaller clusters harder to align and, for a fixed magnetic field, a maximum in MR is observed for an optimal size.

Gu and co-workers [Gu 96], on the other hand, pointed out that two opposite effects coexist: from one side MR is increased with decreasing size because of the increase of the surface contribution; from the other, below a critical size, the cluster interface resistivity becomes much greater than that of the non-magnetic matrix and the probability of scattering with the cluster is diminished thus reducing the MR .

In the present case, MR seems to be maximised for clusters of 600 atoms, confirming the existence of an optimal size. However, since saturation is not reached in the case of this sample and of the one containing smaller clusters, it is not possible to establish which

¹These samples were produced in the earlier period of this work and at the time the experimental apparatus used for transport measurements was limited to $0.8 T$ and $13 K$.

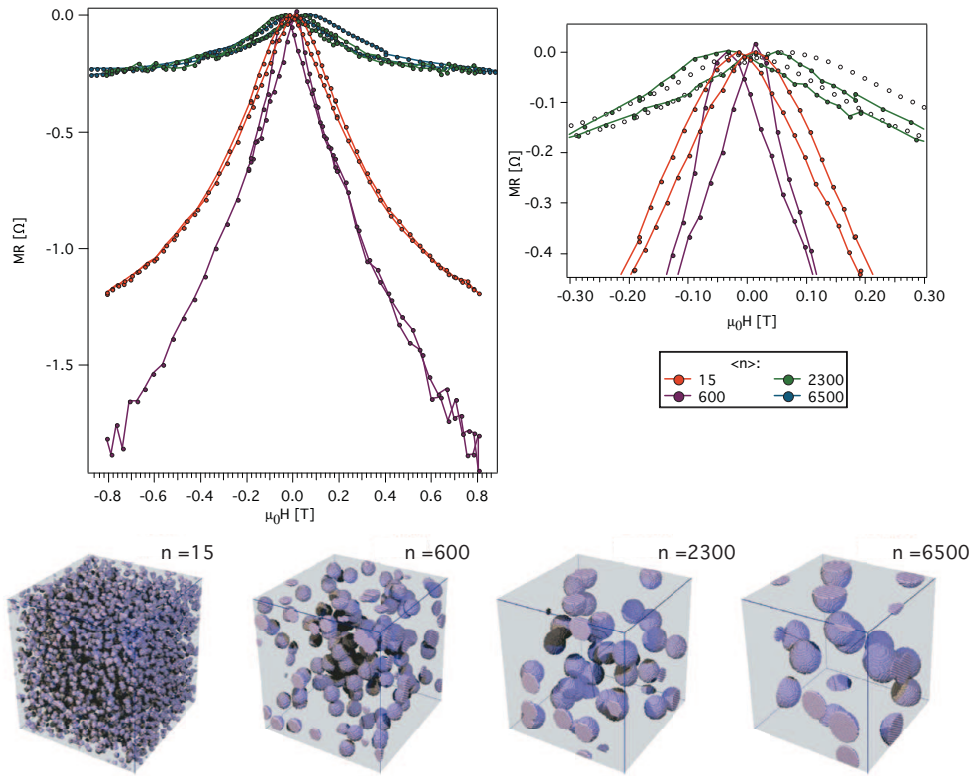


Figure 7.3 – *MR of samples $CoCu_5$, $CoCu_9$, $CoCu_{12}$ and $CoCu_{11}$ at 13K. In the in-set the low field region is shown in more detail to underline the hysteretic behaviour. Simulated random distributions of clusters of the corresponding sizes on a fcc lattice are also shown. The hysteresis is observed for all samples, independently on the cluster size. This fact can be justified observing the typical geometrical distribution as obtained from the simulations: while for big clusters the hysteretic behaviour is induced by the blocking of each single cluster, in the smaller size regime the blocking is due to inter-cluster interactions.*

mechanism, between the two described above, determines the observed behaviour¹

7.1.4 The effect of concentration

As shown in fig.7.4, no drastic variation of the form of *MR* and Hall voltage are observed at low temperature when the concentration is changed. This can be understood with the fact that, in most of the samples, concentration was kept very low (less than a few percent) in order to avoid coalescence as well as interactions between the clusters. This explanation

¹It should be pointed out that the experimental determination of the *MR* absolute value, is not unambiguous in the measurement configuration that has been used: such determination requires the exact knowledge of the sample resistance that cannot be obtained with a two point measurement in which the contacts resistances add in series. Moreover the way the electrical contacts are realized is not reproducible and consequently their resistivity will change from case to case. As a consequence the values of *MR* in percent have to be considered as an indication and will not be taken into account in the following.

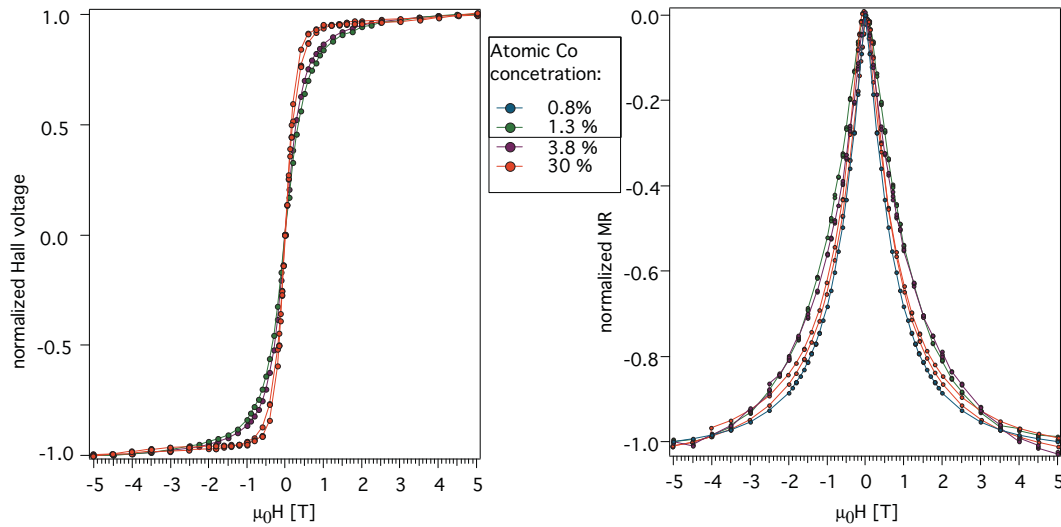


Figure 7.4 – Hall and MR voltage of samples containing clusters of 40 atoms at different concentrations. All measurement are performed at $T = 3K$

is confirmed by the fact that the Hall voltage curve for $HCoAg_1$, that has a concentration (30%) remarkably higher than the other samples, is steeper at low fields and saturates faster.

However, concentration effect become more evident when the temperature behaviours are compared. In fig 7.5 MR curves for two samples with slightly different concentration (0.8% and 0.3%) of cobalt are shown for different temperatures. For the more concentrated

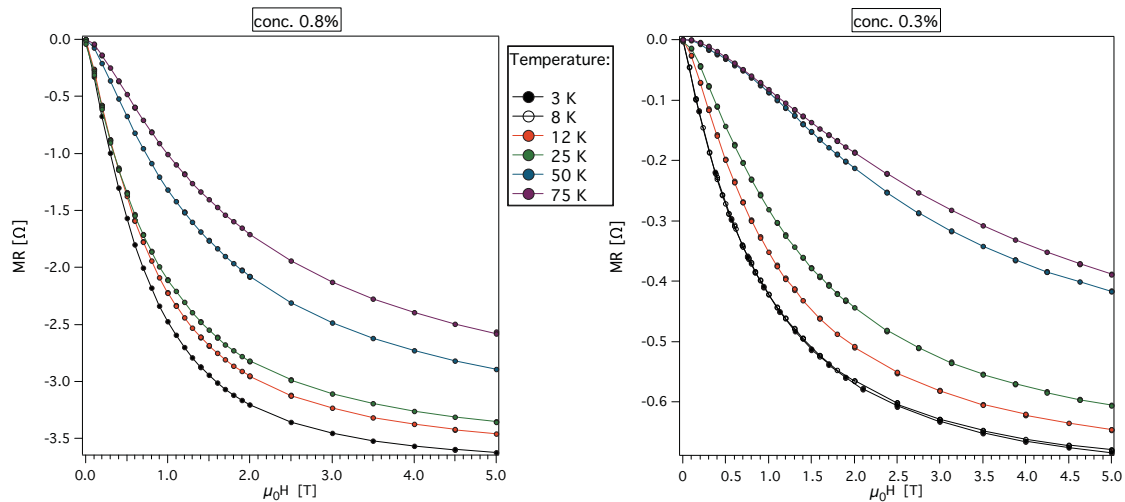


Figure 7.5 – MR measured at different temperatures for two samples, both containing clusters of average 40 atoms but at different concentration (0.8% and 0.3%). Temperature behaviour is affected by the concentration and the more concentrated sample (on the left) shows less pronounced changes, especially at high T .

sample, the changes in the form of MR are less pronounced than for the dilute one. Focusing on the curve at $75K$, for example, it can be remarked that the onset of saturation is not even observable for the sample at 0.3%, while a change of slope is quite evident for the second one.

This subject will be discussed in detail in the following section where the effect of interactions will be analysed.

7.1.5 Anisotropy

It was questioned in the previous chapter whether any anisotropy, global or local is present in the samples.

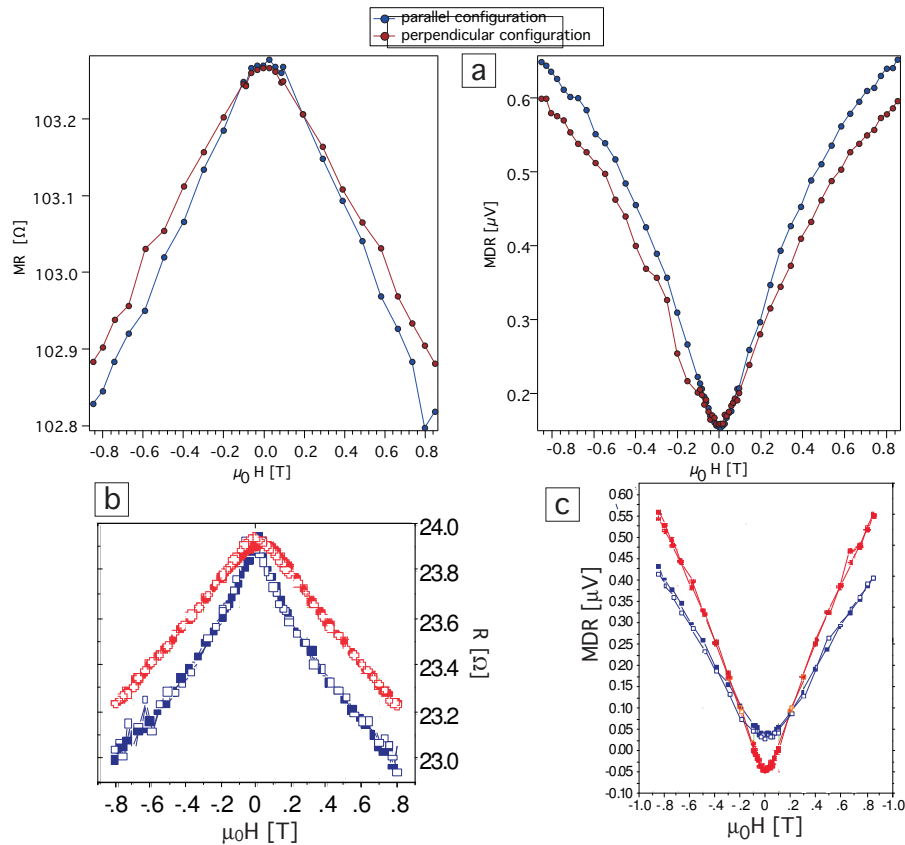


Figure 7.6 – MR and MDR curves at $13K$ for sample $CoAg_3$ (23 atoms; 1.7%). Measurements have been performed both with the magnetic field parallel and perpendicular to the electric current. It is shown here how different behaviour can be encountered. This aspect requires a further study that has not been performed here.

As shown in fig.7.6 several situations are observed experimentally. In some cases no substantial difference is observed if the measurements are performed in a parallel or perpendicular configuration, while in other samples the anisotropic behaviour is more evident.

Even if a systematic study has not been performed on this subject, the most reasonable scenario is that clusters have both an internal and a sample geometry induced anisotropy.

The internal anisotropy is due to the fact that each cluster has an easy axis¹ induced by the internal crystallinity and by the interface with the matrix [Jame 01a]. However, since the clusters are deposited in a random direction, such local anisotropy averages to zero on a global scale and it is not visible when comparing measurement taken in different configurations.

On the other hand, the 2D nature of the sample, induces an additional shape anisotropy that is reflected in *MR* as well as in *MDR* experiments². A confirmation of the fact that the observed anisotropy is induced by the particular shape of the sample, can be found in fig.7.6.c, in which the curve refers to a sample containing cobalt atoms, thus no internal anisotropy exists.

7.1.6 The effect of the matrix

Another aspect that has been considered is the influence of the matrix: since the magnetic properties of those systems are defined by the interplay of the non-magnetic conduction band of the matrix and the localized d-type electrons of the magnetic clusters, it is expected that the details of the Fermi surface play an important role. A complete study on the influence of the matrix has not been performed, but a comparison can be made between the *Cu* and the *Ag* series. In particular, in fig.7.7, it is observed that the form of the *MR* curves is indeed influenced by the surrounding matrix.

A similar comparison has been made for *MDR*³ curves [Hill 07b] and is reported in fig.7.8. In this case it is possible to remark that, even if some differences are present, the form of the signal is equivalent from a qualitative point of view.

We can conclude that the matrix does have an effect on the magnetic behaviour acting, probably, on both the properties of the isolated clusters and on the inter-cluster interaction mechanisms. Such an influence is expected since the energy separation between the d-band of the cluster and the Fermi energy of the matrix is determinant in the formation of the macrospin, as discussed in section 4.2. However magnetism survives when clusters are embedded in both *Cu* and *Ag* matrices. In the following the discussion will concern mainly *Ag*-samples.

¹More generally a biaxial case should be considered, however the phenomenology of magnetization curves does not change substantially and hence I will consider the simpler case.

²In this section some *MDR* measurements are discussed together with magnetoresistance since anisotropy will not be treated in the next chapter, in which magneto differential resistance is presented.

³As done for the anisotropy effect, *MDR* curves are reported here since this topic will not be discussed further in the following chapters.

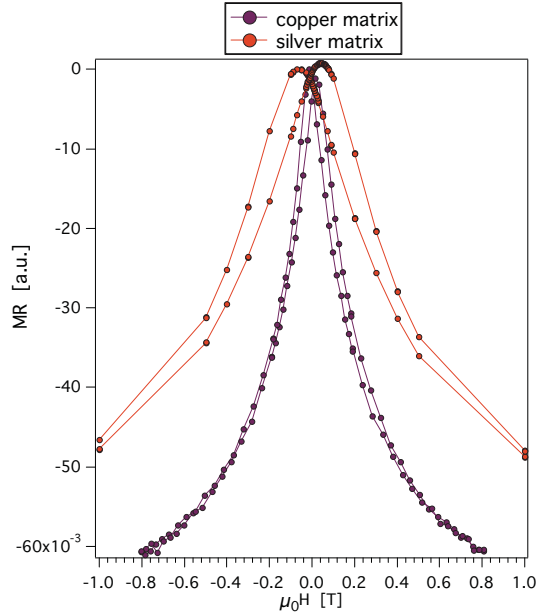


Figure 7.7 – *MR curves at 15K for samples $CoCu9$ (600 atoms; 8%) and $CoAg14$ (600 atoms; 6%) that have both comparable size and concentration. It can be observed that the shape of the signal is different in the two cases.*

7.2 Magnetotransport in the two current approximation

As described in the previous section, a set of measurements, exploring the effects of several fundamental parameters, has been recorded. In this section these results will be interpreted in the frame of the Mott model. This model relies on the hypothesis that the conduction can be described considering two separated spin sub-bands that do not exchange electrons one with the other and that add in parallel. In terms of conductivity this reads:

$$\sigma_{tot} = \sigma_{\uparrow} + \sigma_{\downarrow}$$

I will show how magnetotransport in granular solids is a domain that is far from being fully understood and how the possibility of preparing well characterized samples via cluster assembling demonstrates the limits of the models that are commonly used. Such limits are more evident when the *MDR* curves, that have not been presented up to here, are considered and I will discuss these as well as the novel perspectives that this technique presents in the next chapter.

In fact it is well known since a long time that the models traditionally employed to interpret magnetotransport in granular materials, even furnishing a good qualitative explanation of *MR* and magnetization curves, do have strong limitations that have been attributed to the presence of interactions [Greg 94, Dupu 97, Alli 99, Binn 02a], to the broad mass distribution of magnetic particles [Ferr 97, Hama 00], or to the formation of oxide anti-ferromagnetic shells [Koch 05, Zhan 05]. Because of the interplay of all these

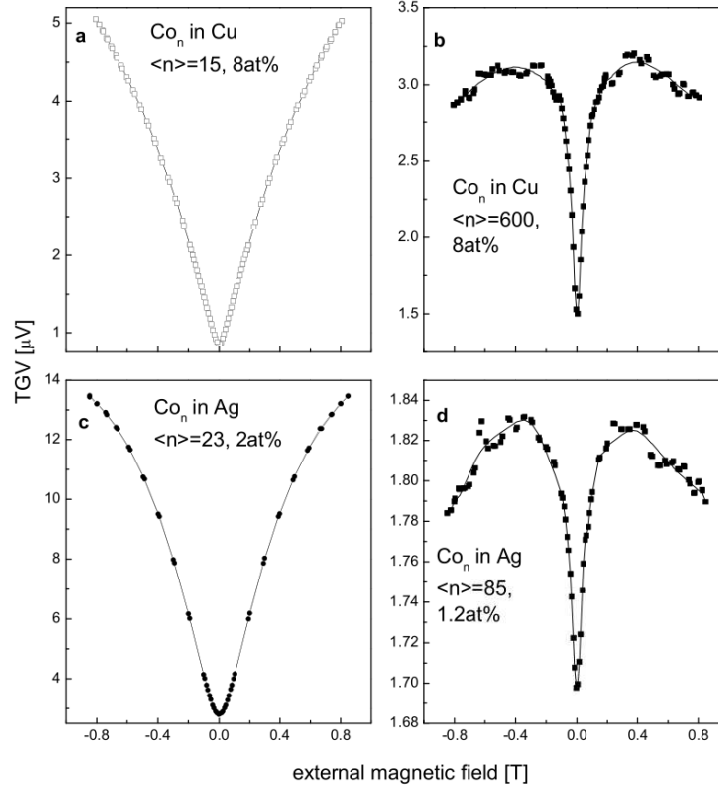


Figure 7.8 – *MDR curves for two sets of samples containing clusters of comparable sizes embedded in Cu and Ag respectively. Although the shape of the signal is similar in the two cases, a significant influence on the matrix can be observed.* [Hill 07b]

factors it has not been possible up to now to separate their different contributions. In this work, both the mass distribution and the anti-ferromagnetic shell structure can be ruled out as causes of models failure. It is then possible to underline the effects of interactions and to determine their origins.

For the sake of clarity the interpretation of experimental results will be presented starting from models that give only a qualitative description and all the ingredients necessary for a full understanding will be subsequently added.

First of all it should be remarked that the problem of interpreting transport properties of granular materials is twofold: on one side it is necessary to model the relation between *MR* and magnetic configuration and, on the other, magnetization itself has to be determined. The most important theories on magnetization of cluster-assembled materials have already been reviewed in section 3.5 and here I will address the first problem.

The system under study consists of a non magnetic medium in which are randomly dispersed magnetic impurities with a concentration c and a magnetic moment $\vec{\mu} = \mu_B \vec{S}$,

that we assume to be equal for all the particles¹. The macrospin \vec{S} is the cluster magnetic moment expressed in unities of Bohr magneton; since the clusters are monodomains (all the atomic moments are aligned) $S = N s$ where N is the number of atoms and s is the magnetic moment per atom expressed again in units of μ_B .

I have already discussed in section 3.6.1 that, if the concentration is low enough, the system behaves as a superparamagnet and its total magnetization follows a Langevin function, \mathcal{L} , the argument of which is given by $\frac{\mu H}{k_B T}$.

In the beginning I will restrict the discussion to this hypothesis while at the end of the chapter the effects of interactions will be introduced.

7.2.1 The origin of magneto-resistance

When a current I is driven through the sample, the conduction electrons scatter from the impurities and, because of their spin, they are sensitive to the presence of a spin-dependent potential.

The carriers that take in charge the conduction process are in the present case the valence electron of the matrix and, as the matrix is a noble metal (*Ag* or *Cu*), they belong to an *s*-type band.

On the other hand the clusters under study are made of *Co* and, as discussed in sections 2.2 and 4.2, their valence electrons will occupy *d*-levels that, as the number of atoms per cluster increases, will form a narrow *d*-band. Such bands are energetically close to the *s*-band of the matrix so that hybridization may occur.

Their conductivity is normally described in the frame of the Boltzmann formalism² within the *two current model* that implies the introduction of two coupled equations related to the \uparrow and \downarrow spin channels. Here we restrict ourselves to the case of two separated conduction bands. This theory was first developed by Mott and it assumes that electrons belong to either s_\uparrow or s_\downarrow sub-band without having the possibility of changing their spin state. These two conduction channels add in parallel [Mott 64] giving for the resistivity the following expression[Fert 69]:

$$\rho = \frac{\rho_\uparrow \rho_\downarrow}{\rho_\uparrow + \rho_\downarrow} \quad (7.1)$$

where:

$$\rho_\uparrow = \frac{m^*}{e^2 n \tau_\uparrow} \quad \rho_\downarrow = \frac{m^*}{e^2 n \tau_\downarrow}$$

The magneto-resistance results from a difference, induced by the sample magnetization, between relaxation times τ_\uparrow and τ_\downarrow that reflects in a decrease in resistivity of one of the two channels and hence of the total resistance. The fact that the collision probability depends on the spin has been explained in two different ways, represented schematically in fig.7.9.

¹This assumption, introduced now for practical reasons, will be justified in section 7.2.2

²In appendix B, the Boltzmann formalism is presented for the general case of two non separated currents. The restriction to the Mott model is straightforward.

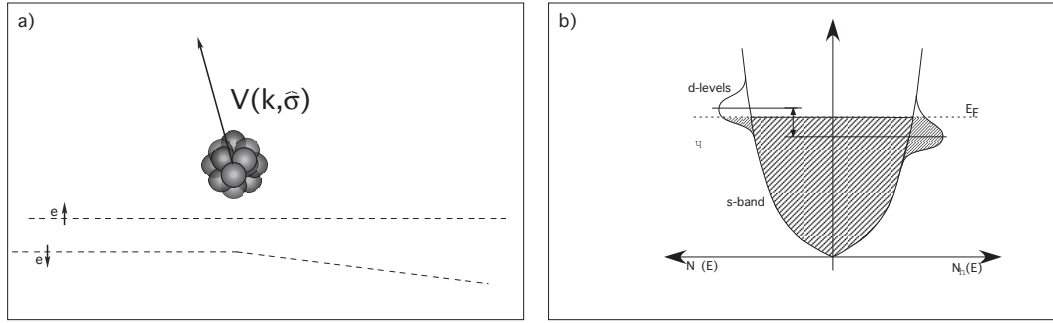


Figure 7.9 – Schematic representation of the two different mechanism hypothesized to explain *MR*. In a) it is assumed that the scattering potential depends on the spin orientation of the conduction electron, while in b) a different *DOS* at the Fermi energy is assumed for the two spin conduction sub-bands. Even if the underlying mechanism is different, in both cases the result is a different scattering probability for spin-up and spin-down electrons.

The first model, proposed by Zhang and Levy [Zhan 93, Zhan 95] and Wang and Xiao [Wang 94a, Wang 94b], assumes that the asymmetry originates from a spin dependent scattering potential at the interface between magnetic impurities and non-magnetic matrix, while the density of states (*DOS*) at the Fermi energy is considered to be the same for the two conduction channels.

The second model, introduced by Xing and co-workers [Xing 93, Shi 93], attributes the difference in conductivity to a splitting of the *DOS* at E_F without the need of a spin-dependent potential. In this case, it is assumed that hybridization arises between the *s*-band of the matrix and the *d*-levels of the clusters, the Fermi level being close in the two materials. When a magnetic field is applied, the *d*-levels split, inducing a difference in population between \uparrow and \downarrow bands.

Even if the microscopic mechanism generating the difference in resistivity between the two channels is different, both models obtain for the *MR* a quadratic dependence on the magnetization. In the following this result is presented in the frame of the Zhang and Levy model.

7.2.2 Zhang and Levy model

This model is based on the *two parallels currents* hypothesis and on the assumption that *clusters do not interact*. The first hypothesis implies that the electrical conductivity can be written as:

$$\sigma = \frac{ne^2}{2m} \sum_{\sigma} \frac{1}{\Delta(\sigma)} \quad (7.2)$$

In a first approximation, once the scattering potential V is known the imaginary part of the self energy, $\Delta(\sigma)$, can be evaluated with Fermi's golden rule. In the model, the total V is given by the sum of contributions coming from non-magnetic impurities scattering

(nm), scattering at the surface of magnetic impurities (s) and scattering in the interior of magnetic impurities (m). The last two terms are still divided into two contributions: spin-dependent and spin-independent. The general form of the potential is then:

$$\begin{aligned}
V(\vec{r}, \sigma) &= \sum_i V_i^{nm} \delta(\vec{r} - \vec{R}_i) + \\
&+ \sum_\alpha \sum_{s \in \alpha} V^s (1 + p_s \hat{\sigma} \cdot \vec{\mu}_s) \delta(\vec{r} - \vec{R}_s^\alpha) + \\
&+ \sum_\alpha \sum_{i \in \alpha} V_i^m (1 + p_b \hat{\sigma} \cdot \vec{\mu}_i) \delta(\vec{r} - \vec{R}_i)
\end{aligned} \tag{7.3}$$

where i is the lattice site at which the scattering event occurs, α is the index of the magnetic impurity, μ_s and μ_i are atomic magnetic moments at the surface and in the interior respectively, p_s and p_b are the ratios between spin-dependent and spin-independent part of the potential, again for surface and interior of the clusters.

The conduction electrons can be assumed to be described by plane waves so that the scattering matrix, via Fermi's golden rule in the hypothesis that only elastic collisions take place, has the form:

$$\Delta(\sigma) = \pi \sum_{k'} |V_{k,k'}^\sigma|^2 \delta(\epsilon_{k'} - \epsilon_k)$$

At this point, we introduce two further approximations:

- since in the case of our interest, the magnetic particles are extremely small, the fraction of interior atoms is negligible with respect to those on the surface, as a consequence we can neglect the third term in eq. 7.4, and consider that conduction electrons scatter only at the interface between granules and matrix; furthermore, even in bigger clusters, the scattering at the interface has proven to be the dominant mechanism giving rise to MR [Rubi 98, Dupu 97];
- we also assume that particles are monodispersed: they all contain the same amount of atoms; this hypothesis will be justified at the end of this section.

Under these hypothesis and summing over k , we obtain:

$$\Delta(\sigma) = \frac{\pi}{N} \left[\sum_i |V_i^{nm}|^2 + \sum_\alpha \sum_{s \in \alpha} |V^s|^2 (1 + p_s^2 + 2p_s \hat{\sigma} \cdot \widehat{\mu}_\alpha) \right] DOS(\epsilon_F)$$

We now introduce two characteristic length: the non-magnetic and the surface mean free paths:

$$\begin{aligned}
\lambda_{nm} &= \frac{\epsilon_F/k_F}{\frac{\pi}{N_{nm}} \sum_i |V_i^{nm}|^2 DOS(\epsilon_F)} \\
\lambda_s &= \frac{\epsilon_F/k_F}{\frac{\pi}{N_s} \sum_\alpha \sum_{s \in \alpha} |V^s|^2 DOS(\epsilon_F)}
\end{aligned}$$

where N_{nm} and N_s are the total number of non-magnetic and magnetic impurities, respectively and consequently we can express them in terms of granules concentration as $\frac{N_{nm}}{N} = 1 - c$, $\frac{N_s}{N} = c$. In terms of λ_{nm} and λ_s , the scattering matrix is:

$$\begin{aligned} \Delta(\sigma) &= (1 - c) \frac{\epsilon_F/k_F}{\lambda_{nm}DOS(\epsilon_F)} + c(1 + p_s^2 + 2p_s \widehat{\sigma} \cdot \widehat{\mu}_\alpha) \frac{\epsilon_F/k_F}{\lambda_s DOS(\epsilon_F)} = \\ &= \left[(1 - c) \frac{\epsilon_F/k_F}{\lambda_{nm}DOS(\epsilon_F)} + c(1 + p_s^2) \frac{\epsilon_F/k_F}{\lambda_s DOS(\epsilon_F)} \right] + 2cp_s \frac{\epsilon_F/k_F}{\lambda_s DOS(\epsilon_F)} \widehat{\sigma} \cdot \widehat{\mu}_\alpha \end{aligned}$$

In the last line the first term represents the non magnetic contribution (both from normal and magnetic impurities) and the second one accounts for the spin-dependent scattering. For the sake of simplicity we introduce two quantities:

$$\begin{aligned} \xi_0 &= \frac{(1 - c)}{\lambda_{nm}DOS(\epsilon_F)} + \frac{c(1 - p_s^2)}{\lambda_s DOS(\epsilon_F)} \\ \xi_1 &= \frac{2cp_s \langle m \rangle}{\lambda_s DOS(\epsilon_F)} \end{aligned}$$

that allows to express $\Delta(\sigma)$ as¹:

$$\Delta(\sigma) = \frac{\epsilon_F}{k_F} [\xi_0 + \xi_1 \sigma]$$

Coming back to the conductivity, we have:

$$\begin{aligned} \sigma &= \frac{ne^2}{2m} \left[\frac{1}{\Delta(\uparrow)} + \frac{1}{\Delta(\downarrow)} \right] \\ &= \frac{ne^2}{2m} \frac{\epsilon_F}{k_F} \left[\frac{1}{\xi_0 + \xi_1} + \frac{1}{\xi_0 - \xi_1} \right] \\ &= \frac{ne^2}{2m} \frac{\epsilon_F}{k_F} \frac{\xi_0}{\xi_0^2 - \xi_1^2} \end{aligned} \tag{7.4}$$

and the resistivity reads:

$$\rho = \frac{2m\epsilon_F}{ne^2 k_F} \frac{\xi_0^2 - \xi_1^2}{\xi_0} \tag{7.5}$$

This allows us to write MR as a function of magnetic field as:

$$MR(H) = \frac{\rho(H) - \rho(\infty)}{\rho(\infty)} = -\frac{\xi_1^2}{\xi_0^2} \tag{7.6}$$

The importance of this result relies in the quadratic dependence of GMR on the magnetization,

$$MR \propto (1 - m^2) \tag{7.7}$$

as this is the starting point for most interpretation of transport results.

¹We introduced the average magnetization m as the sum on all particles of the projection of μ on the tensor σ .

The effect of size distribution

In the model presented in the previous paragraph, clusters have been assumed to have all the same mass. In most of the samples presented here, however, clusters are not mass selected, but only mass filtered: masses follow a LogNormal distribution with widths of the order of 25% or smaller¹. Zhang and Levy developed their model also in the case of non monodispersed particles and pointed out that mass distribution plays an important role: since smaller granules contribute strongly to MR but need greater fields to be aligned, they will give an important contribution at higher fields while bigger clusters will dominate at lower fields [Alli 95].

In order to justify the restriction of using a single mass in the model, MR in the two cases of a single mass and of a distribution of masses comparable with those used in experiments have been simulated. As shown in fig.7.10, it is observed that the form of the curve is essentially unchanged in the case in which a distribution comparable to those used in our samples, is used in place of a single mass. However in the following, only the form of the signal is analyzed and therefore it is a reasonable approximation to consider masses to be monodispersed.

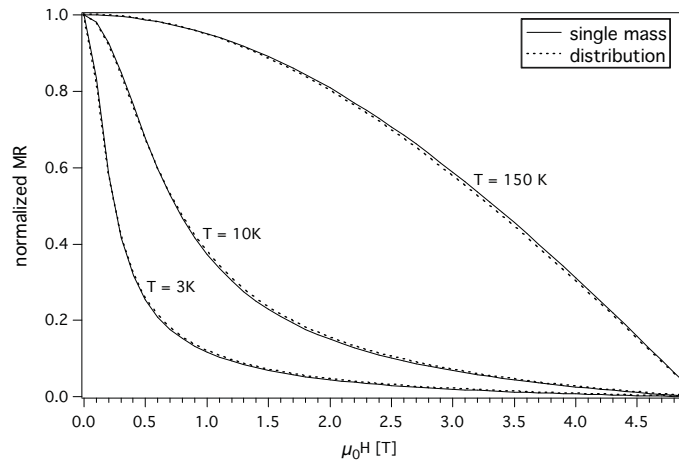


Figure 7.10 – Simulation of MR curves obtained in the frame of ZL model assuming a Langevin-type magnetization. The full-line curves are obtained assuming that all clusters have the same mass of 40 atoms, while the dashed curves correspond to a mass distribution following a LogNormal statistics with average value of 40 atoms and a sigma of 0.25. Even if the sigma is over-estimated with respect to real values found in our samples, the effect of having a size distribution instead of a single mass, is negligible.

¹Even if a mass spread of 25% might seem large and it is comparable to values found in other works in which the effects of distribution are not negligible, it should be remarked that the samples under study contain very small clusters and a distribution width of 0.25 on clusters containing in average 40 atoms, means that 90% of them posses between 35 and 45 atoms.

7.2.3 MR in the superparamagnetic limit

In the case of dilute, independent mono-domain particles with a macrospin S , the magnetization follows a Langevin curve (as discussed in par.3.5) and the normalized MR can be written as:

$$MR(H, T) = \mathcal{R} \left(1 - \mathcal{L}^2 \left(\frac{\mu_B S H}{k_B T} \right) \right) = \mathcal{R} \left(1 - \left(\tanh \left(\frac{\mu_B S H}{k_B T} \right) - \frac{k_B T}{\mu_B S H} \right)^2 \right) \quad (7.8)$$

The expected behaviour for the magnetization and the MR is reported in fig.7.11.

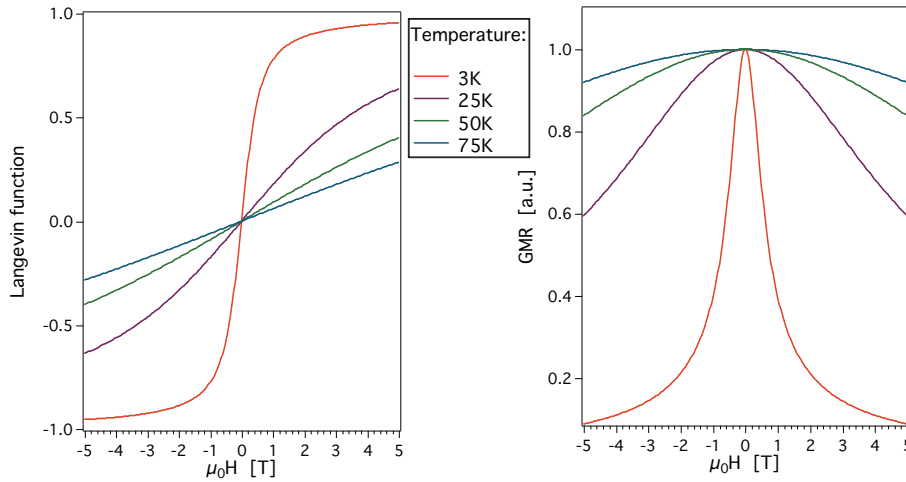


Figure 7.11 – Simulations of the magnetization (on the left) and of MR (on the right) in the superparamagnetic model for different temperatures assuming a magnetic moment per cluster of $20\mu_B$.

By fitting the data with this function, it is possible to extract the macrospin value [Pare 97] $\mu = \mu_B S$ and consequently this technique can be used to study the evolution of the magnetic moment with cluster size as it has been done with Stern-Gerlach experiments for clusters in the gas phase [Bill 93, Bill 94, Bill 95].

This strategy has been successfully used in the case samples containing large clusters (of the order of several nanometers in diameter) in order to find a relation between the clusters average size and the macrospin [Binn 02b, Resp 98, Gras 71]. However, up to now, the same result has not been achieved for small clusters in the sub-nanometric regime because samples studied via transport properties are often not well characterized, containing particles of unknown size or with a broad mass distribution.

With the sample preparation technique used in this work, we have the possibility to finely tune the size and the concentration of clusters, and hence to make a direct comparison of our data with the expression given in 7.8. In fig.7.12 magnetization and MR are fitted with a Langevin function and eq.7.8 respectively. The accordance of the fit with the experimental data is good and the values obtained for the macrospin are comparable (both of the order of $20\mu_B$) and in good agreement with the expected value: since the

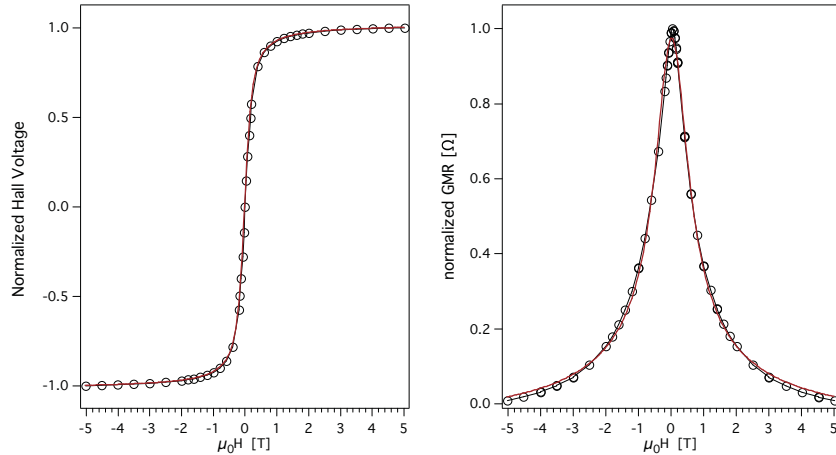


Figure 7.12 – Fit of magnetization (as obtained from Hall measurements) and MR , based on the superparamagnetic model. Data refer to a sample containing clusters of 40 atoms with a concentration of 30% ($HCoAg_1$). Both measurements were taken at $T = 3 K$.

sample under study contains clusters of 40 atoms, such value of the macrospin corresponds to a magnetic moment of $0.5\mu_B$ per atom that is reasonable if compared with the value of $2.2\mu_B$ found in the gas phase, taking into account possible quenching effects due to the surrounding matrix [East 97].

However, as the dependence on T is taken into account, the agreement shows to fail. In particular, the model implies that the magnetization, and consequently the MR , scales with the argument of the Langevin function $\frac{\mu H}{k_B T}$. The value of μ being constant with temperature, this implies that a plot of Hall voltage or MR as a function of $\frac{H}{T}$, should scale on the same curve.

Figure 7.13 shows the result of such a test, and it can easily be observed that the scaling condition is not satisfied: at low temperatures the superparamagnetic model does not adequately describe the system under study; however, starting from $\sim 25K$ the curves scale with H/T . This behaviour is an indication of blocking below a critical temperature T_B that might be due to intra- or inter-cluster interactions.

Furthermore if the fit is performed for several temperatures and for different samples, as shown in fig.7.14, the macrospin value shows a strong temperature dependence that is not compatible with the superparamagnetic hypothesis. So that, even if it is true that for each temperature the curves can be fitted with a Langevin-based function, the evolution with T is not consistent. This behaviour is observed for all the samples even at very low concentrations. Moreover the values found at high temperatures are of the order of several tens of μ_B per atom¹, a value that is unphysical in the superparamagnetic model picture.

¹This value is obtained dividing the macrospin by the number of atoms per cluster, hence assuming valid the superparamagnetic model.

The evidences found for the failure of the superparamagnetic model prove that the hypothesis on which it is based, are not fulfilled. In particular they show that clusters are not uncorrelated and that the effects of interactions have to be taken into account.

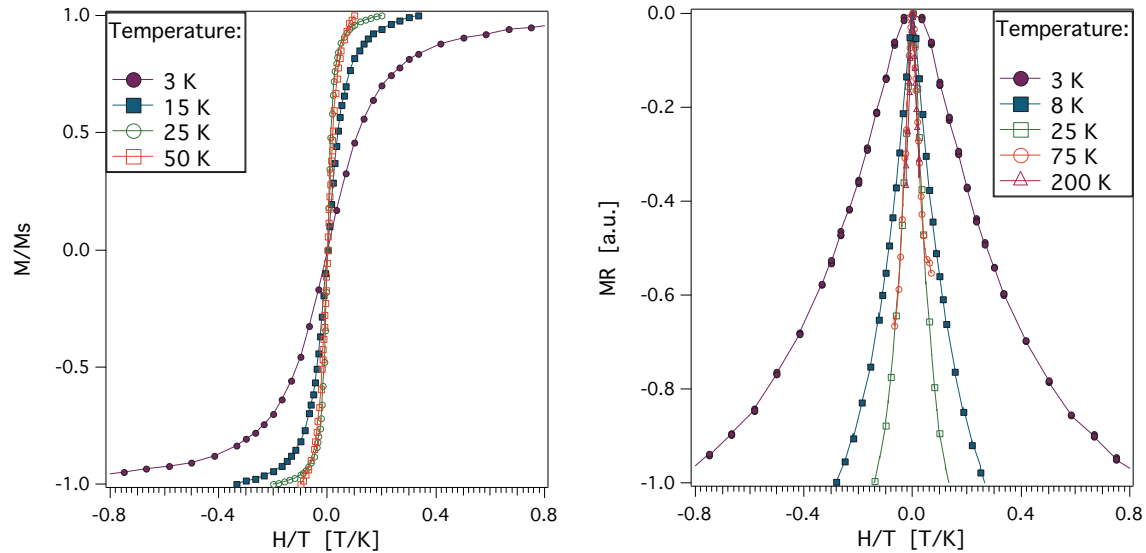


Figure 7.13 – MR and reduced magnetization of sample $HCoAg_4$ (40 atoms; 1.3%) plotted vs H/T . In both sets of measurements, the curves scale as H/T for temperatures greater than $\sim 25K$ while the scaling fails at lower temperatures.

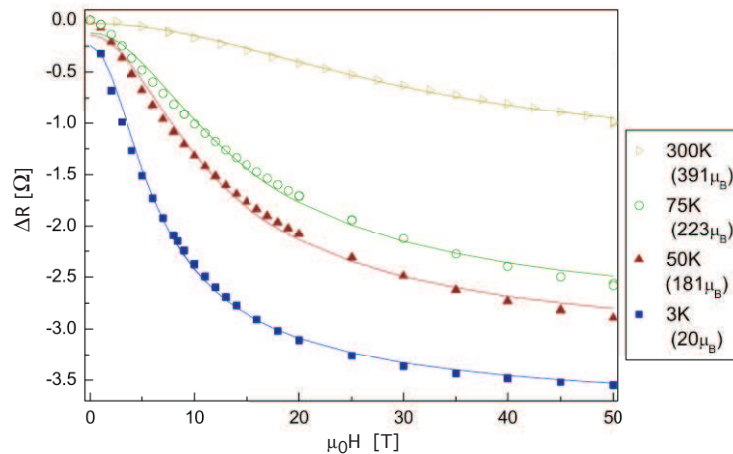


Figure 7.14 – MR of sample $CoAg_{16}$ (40 atoms; 0.8%) fitted with a Langevin based curve for different temperatures. On the right the values of the apparent macrospin as obtained from the fit, are displayed. It can be observed how those values increase as T is increased.

7.2.4 Interaction Mechanisms

In the preceding sections it was claimed that interactions occur between particles, even at very low cluster concentration. However the origin of such interactions has not yet been discussed.

In section 3.4 several mechanisms giving rise to coupling between magnetic moments were presented. Here we review again these mechanisms and their effects are evaluated in the specific case of the samples under study.

Anisotropy

The internal anisotropy produces an intra-cluster interaction between each particle magnetic moment and its magnetic easy axis. In case of small clusters, it was observed in micro-SQUID measurements [Jame 01b, Dupu 04] that the major contribution to the anisotropy energy is given by the atoms located at the surface. This was explained by their lower coordination. XMCD measurements [Luis 06] reveal that capping with a noble metal further increases the surface anisotropy of *Co* clusters, reaching values of the order of $1mJ/m^2$. Such an anisotropy might be responsible for the small changes of magnetization and *MR* observed at low temperatures, where the thermal energy is not enough to overcome the anisotropy energy barrier. The blocking temperature T_B can be evaluated as:

$$T_B = \frac{E_A}{k_B \ln(\tau_{exp}/\tau_0)} \quad (7.9)$$

where E_A is the anisotropy energy, τ_{exp} is the experimental probing time, of the order of 10 s in the present case, and τ_0 is a characteristic trial time of the order of $10^{-10} \div 10^{-13}\text{ s}$. As discussed above, the anisotropy energy can be attributed to the surface atoms. Giving a rough estimate of the surface as being of the order of $1nm^2$, a value can be found of about:

$$E_A = K_s \times surface = 1[mJ/m^2] \times 1 \cdot 10^{-18}m^2 = 10^{-22}J$$

This gives a blocking temperature lower than 1 K .

Dipolar interactions

The characteristic energy of the dipolar interaction can be obtained using the expression:

$$E_{dip} = \frac{\mu_0}{4\pi r^3} \left[\vec{\mu}_i \cdot \vec{\mu}_j - \frac{3}{r^2} (\vec{\mu}_i \cdot \vec{r})(\vec{\mu}_j \cdot \vec{r}) \right]$$

where μ_i and μ_j are two magnetic moments and r is the distance between them.

For a sample containing clusters of 40 atoms with an atomic *Co* concentration of about 1%¹, $r \sim 5nm$ and $\mu \sim 70\mu_B$; this translates into a characteristic temperature of $\sim 20mK$, in agreement with the value found in [Altb 96].

¹The values of sample *CoAg16* have been considered here.

Indirect exchange

In this case the exchange interaction, $J_{RKKY}(r)$, is indirect and mediated by the conduction electrons of the matrix, as described by the Ruderman, Kittel, Kasuya and Yoshida mechanism. For large inter-cluster distances r , the $RKKY$ interactions can be approximated to:

$$J_{RKKY}(r) \propto \frac{\cos(2k_F r)}{r^3}$$

In ref. [Altb 96] the $RKKY$ interactions between two Co clusters of 43 atoms in a silver matrix have been calculated as a function of r . In a crystalline lattice they oscillate with an amplitude in the range of μeV over a distance of several nm , i.e. of the same order as the dipolar interactions. In a disordered structure, as the one considered here, the average coupling strength is estimated to be lower but, however, still present.

The consequence that can be deduced from these estimations is that, even in very dilute samples, interactions are present due to the fact that the clusters considered here are small and thus their average distance is short enough to allow a certain degree of correlation between moments. The importance of considering both cluster size and concentration in

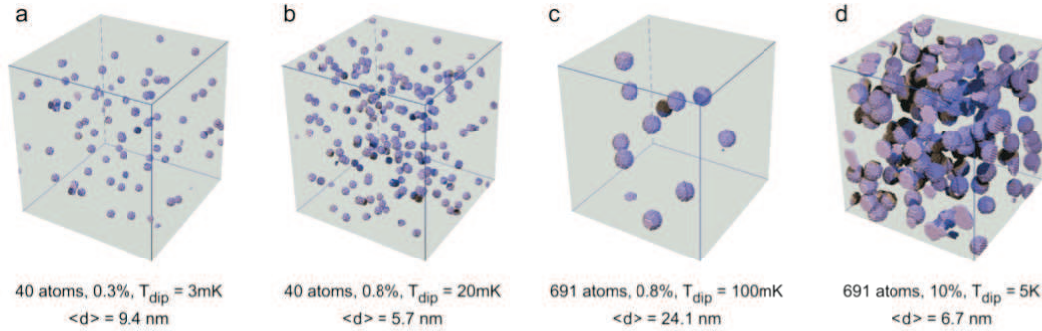


Figure 7.15 – Simulated images of monodisperse Co clusters distributed randomly in a fcc lattice with 10^6 sites. Different cluster sizes and concentrations are represented for comparison.

evaluating the strength of interactions is well visualized in fig.7.15. In the figure a random distribution of monodispersed clusters is simulated. It is easily remarked that for two identical concentrations (0.8 %) the average inter-particle distance is much larger if bigger clusters are considered: $\langle d \rangle = 24nm$ in the case of clusters containing 691 atoms and only $5.7nm$ in the case of 40 atoms. As a consequence the effects of interactions will be stronger in samples containing smaller particles.

7.2.5 MR for interacting superparamagnets

Both the superparamagnetic and the Zhang-Levy model are based on the hypothesis that no interactions occur between particles. However this condition is often not satisfied in

granular systems. As it was discussed in the previous section, a first consequence is that fitting the MR with a Langevin function, the value of the macrospin is not constant in temperature but shows an increase and eventually reaches saturation as shown in fig.7.16 and 7.17. In this case an apparent value of the macrospin, S^* , is obtained from a Langevin fit at each temperature.

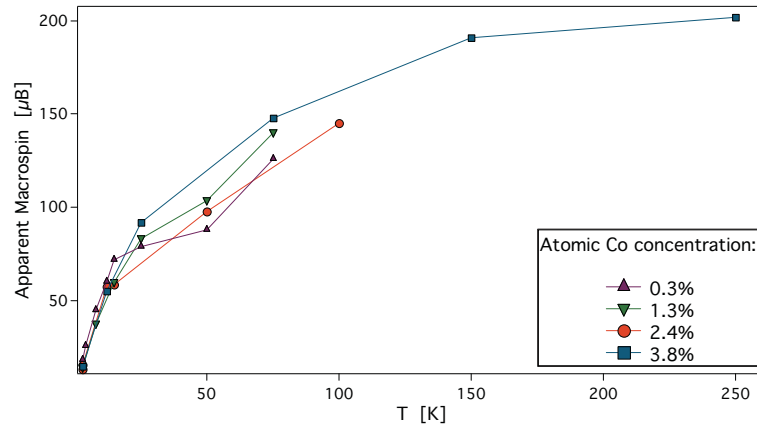


Figure 7.16 – Apparent macrospin as a function of temperature for samples containing clusters of 40 atoms at different concentrations. On the bottom line, the average inter-cluster distance for each size and concentration is reported. All curves superpose in first approximation.

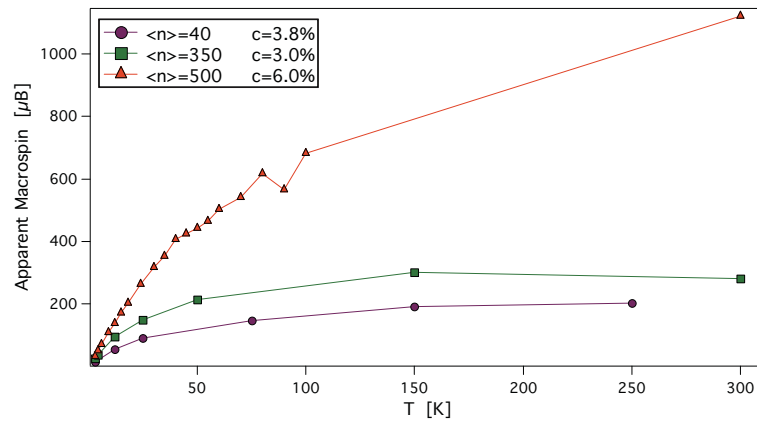


Figure 7.17 – Apparent macrospin as a function of temperature for different cluster sizes, for samples at high concentration.

As discussed in section 3.6.2, for low particle concentration, the superparamagnetic model can be corrected in order to take into account the effect of interactions, as far as they are small enough. This adapted model, called *interacting superparamagnet* model, consists of keeping for the MR in its non-interacting $(1 - m^2)$ form and in introducing a correction term in the argument of the Langevin function.

The interacting superparamagnet was introduced by Allia and co-workers [Alli 01] and

assumes that the clusters magnetic moments fluctuate with frequencies of the order of GHz exerting a disordering random torque on each other which opposes to the ordering effect of the external field¹. The effect of these fluctuations is similar to that of thermal agitation and can hence be taken into account introducing an effective temperature T^* in the argument of the Langevin function. Recalling eq.3.4, one obtains

$$MR(H, T) = \mathcal{R} \left(1 - \mathcal{L}^2 \left(\frac{\mu_B \mu H}{k_B T_a} \right) \right)$$

with $T_a = T + T^*$. This model has proven successful in describing systems with concentration up to 10% [Alli 01, Binn 02a], much higher than those of the samples considered here.

In order to derive T^* , MR curves have been fitted with a Langevin function and the values of the apparent moment S^* plotted as a function of temperature. Since the relation

$$S^* = S \frac{1}{1 + \frac{T^*}{T}}$$

exists, it is then possible to extract a value for T^* and for the real macrospin S . However, the values found for S are much bigger than expected from the size of clusters. Binns and co-workers [?] observed a similar behaviour on a sample containing iron clusters of $\sim 2.5nm$ diameter at 10% atomic Fe concentration. In their case, the effect was attributed to a rigid coupling between several clusters due to dipolar interactions. In our diluted samples a similar mechanism is not plausible since the average size and intercluster distance imply a characteristic temperature for dipolar rigid coupling well below $1K$.

Furthermore, it is interesting to remark that no particular change is observed varying the concentration, as long as it is kept lower than a few percent. On the other hand, the sample with 6% of Co shows a much higher apparent macrospin that is not fully justified by the larger size of clusters (when compared to the smaller difference observed between the 40 and the 350 atoms sample).

As a consequence it can be asserted that two different interaction mechanisms exist: a first one that strongly depends on intercluster distance and that is probably of magnetostatic dipolar origin, and a second one that survives at very low concentration and that seems to be related to matrix-mediated correlation mechanisms.

7.2.6 Beyond the superparamagnetic model

It was shown in the preceding sections that one of the basic hypothesis of superparamagnetism as well as of the ZL model, i.e. the hypothesis of absence of interactions, is not fulfilled in samples containing small magnetic clusters, even at low concentrations.

It is still questionable whether these models fail only in describing magnetization or if also the quadratic relation between magnetization and MR is wrong. An answer can

¹Refer to section 3.6.2 for more details on the model.

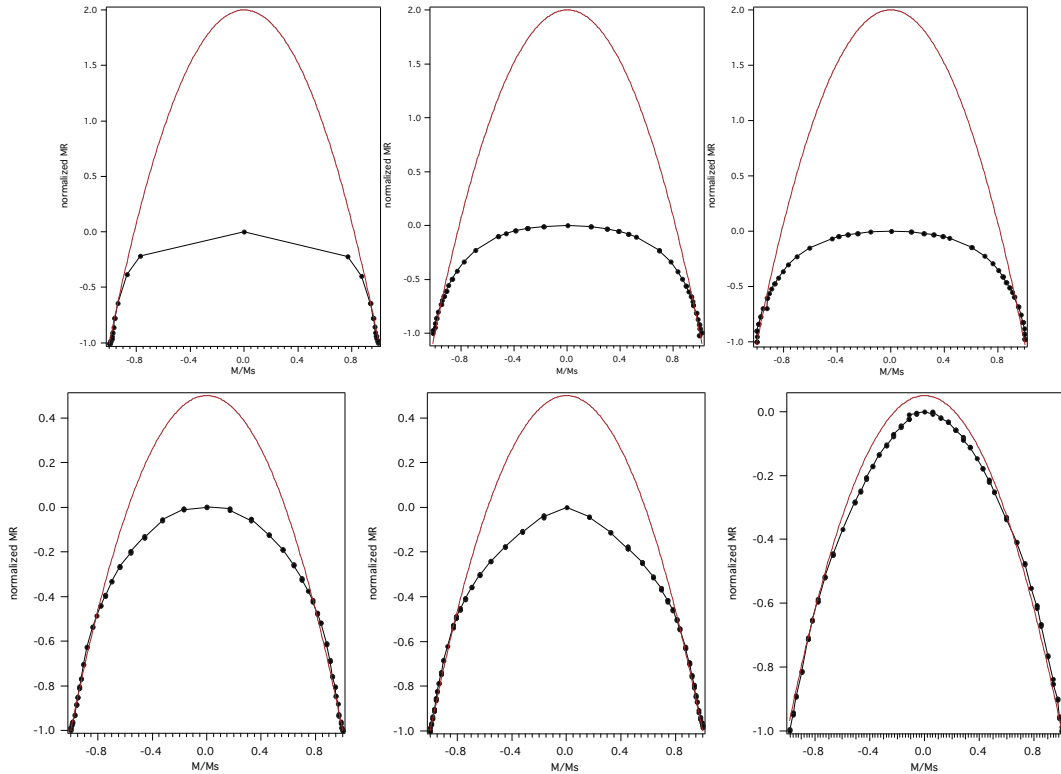


Figure 7.18 – MR plotted versus reduced magnetization (obtained by the Hall voltage) for sample $HCoAg_1$ (40 atoms; 30%) at $T = 3, 50, 150K$ and $HCoAg_4$ (40 atoms; 1.3%) at $T = 3, 8, 50K$. A parabola is also plotted for comparison. While in the most concentrated sample (on top) no changes are observed with increasing temperature, the diluted sample (on the bottom) shows how the MR curve approaches a parabola at high T when correlations are destroyed and the quadratic formula is valid.

be given by plotting the magneto-resistance data versus the square of the normalized Hall voltage. This test has been performed for different concentrations on those samples where the reduced magnetization (M/M_s) has been determined via the Hall effect measurement.

In the upper part of fig.7.18 the result for a highly concentrated sample (30% at. Co) is shown and no remarkable changes are observed for increasing temperature. The pronounced flat top of the experimental parabola confirms the presence of strong interactions that are not affected by a temperature variation.

On the other hand, in the bottom part of fig.7.18, a more diluted sample is presented (1.3% at. Co). In this case the flat top is very pronounced at low temperatures but the behaviour becomes parabolic above 25 K .

In the majority of the cases presented here, the cluster concentration is sufficiently low to consider valid the parabolic behaviour at least in first approximation and at high enough temperatures. However as the interactions grow stronger, the hypothesis of GMR being parabolic in the magnetization needs to be abandoned. In order to better understand this fact, let us find eq.7.7 with another argumentation.

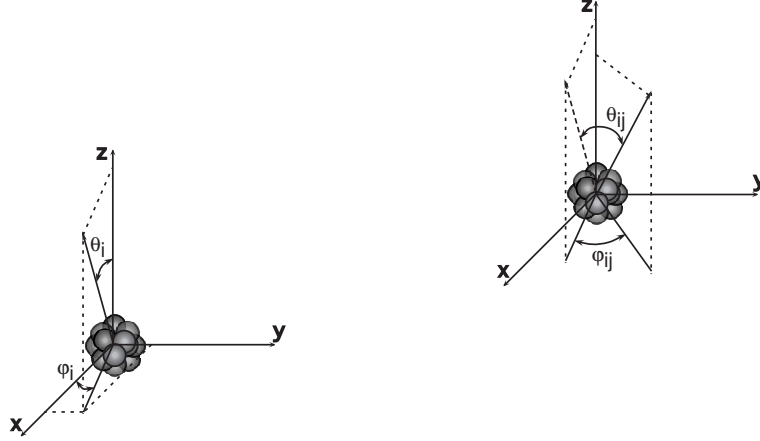


Figure 7.19 – Magnetic clusters at position i and j on a conduction electron path. The two magnetic moment vectors are represented as well as their twist and tilting angles.

Assume that two magnetic moments $\vec{\mu}_i$ and $\vec{\mu}_j$ are situated on an electron trajectory. The probability that the electron will scatter on both of them is proportional to the angle $\cos \theta_{ij}$ between them. We can generalize this statement asserting that

$$R = R_0 - k \langle \vec{\mu}_i \cdot \vec{\mu}_j \rangle = R_0 - k \langle \cos \theta_{ij} \rangle$$

where the average is performed on all the magnetic moments in the sample. The problem now reduces to evaluating $\langle \cos \theta_{ij} \rangle$. If we introduce a preferential axis (the one along which we are going to apply the magnetic field) as showed in fig.7.19, we will have:

$$\begin{aligned} \langle \cos \theta_{ij} \rangle &= \frac{1}{\mu^2} \langle \vec{\mu}_i \cdot \vec{\mu}_j \rangle = & (7.10) \\ &= (\langle \cos \theta_i \cos \theta_j \rangle + \langle \sin \theta_i \sin \theta_j (\cos \phi_i \cos \phi_j + \sin \phi_i \sin \phi_j) \rangle) \end{aligned}$$

The first term gives the reduced magnetization, \bar{u} , while the second one describes the correlation between $\vec{\mu}_i$ and $\vec{\mu}_j$.

If the effect of interactions is negligible, this correlation term is zero and eq.7.7 is obtained again. Otherwise an extra contribution to the MR has to be considered. A treatment of the effect of correlation can be found in [Alli 95] and [Lope 02] here I will revise their argumentation to estimate the effects of correlation in the case of our interest.

The authors assume that correlation of both tilt and twist angle has an exponential decay:

$$\sim e^{r_{ij}/r_\alpha(H)}$$

where $\alpha = \theta, \phi$ and the characteristic length depends on the applied magnetic field. Furthermore they evaluate the averages in eq.7.10 using an Hamiltonian containing an internal interaction field that acts on each site i as:

$$H_i = \mu \sum_k \lambda_{ik} \bar{u}_k$$

where λ_{ik} is the coupling between moment and can be positive or negative depending on the interaction mechanism, and \bar{u}_k is the local reduced magnetization of a moment located in k as it acts on the site i . The complete Hamiltonian takes the form:

$$\mathcal{H} = -\mu H_{ext} - \mu H_{int} = -\mu H_{ext} - \mu^2 \sum_k \lambda_{ik} \bar{u}_k \quad (7.11)$$

and allows to find a self consistent equation for reduced magnetization \bar{u}_k , in analogy with the calculation for a superparamagnetic system:

$$\bar{u}_i = \mathcal{L} \left(\frac{\mu H + \mu^2 \sum_k \lambda_{ik} \bar{u}_k}{k_B T} \right) \quad (7.12)$$

Assuming that interactions produce a negligible correction to the total magnetization, the following expression can be found for $\langle \cos \theta_{ij} \rangle$ and hence for the *MR*:

$$\langle \cos \theta_{ij} \rangle = \bar{u}^2 + (\langle u^2 \rangle - \bar{u}^2) e^{\lambda/r_\theta(H)} + \left(1 - \bar{u}^2 - \frac{\langle u^2 \rangle - \bar{u}^2}{1 + \bar{u}^2} (1 - \bar{u}^2 e^{\lambda/r_\theta(H)}) \right) e^{\lambda/r_\phi(H)} \quad (7.13)$$

the important parameter of the model being the characteristic correlation length in the two angular directions.

Calculations of the effect of correlation on *GMR* have been performed, in the case of dipolar interaction, by Lopes and co-workers [Lope 02] and their results are shown in fig.7.20. It can be observed that in the correlated case a sharper decrease is observed at low fields and that this effect diminishes with temperature. These results can be understood in terms of the extra contribution given to the total magnetic field by the internal interaction field. When $H = 0$ a correlated state forms: although the system is magnetically disordered

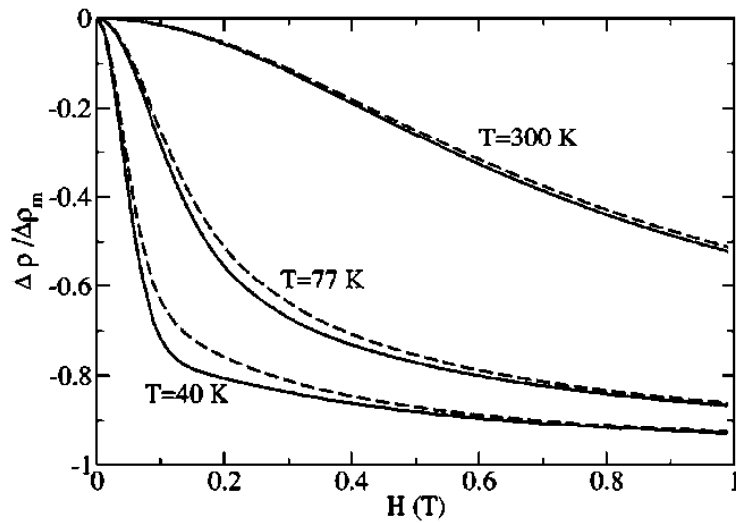


Figure 7.20 – Simulated *GMR* for particles with a magnetic moment of $1492\mu_B$ in the absence of correlation (dashed lines) and for a correlated system (full lines) for several temperatures [Lope 02].

and no blocking occurs, a correlation among moment fluctuations is present and its effect can be imagined as a viscous force acting on each magnetic moment. When an external field is applied, the correlation will at first facilitate the alignment since all moments will orient with a collective rotation. However, as the field is increased, the correlated state is destroyed and the MR curve will eventually superpose to the non-interacting one.

As a consequence the susceptibility will be governed by the correlation and will be high at low fields and decrease as the field is increased.

These features induced by correlation seem to well describe the observed experimental behaviour. In the following section the subject will be discussed in further detail in the framework of spin glasses.

7.2.7 Correlated Spin Glasses

A possible interpretation of the results presented here might be the formation of a correlated spin glass [Chud 95, Mydo 93]. This model assumes that the macrospins are weakly coupled and, because of their random geometrical distribution, strongly frustrated.

The image that can be drawn is that, the clusters being extremely small, even at low concentration they are close enough to interact via dipolar or RKKY interactions. The sign of the coupling depends on the relative orientation (for what concerns the dipolar interaction) and on the distance (in the case of RKKY) giving rise to a random local field that defines on each magnetic site a local anisotropy axis. The system will thus experience a *weak random anisotropy* [Albe 78, Harr 73]. The result is a frustration of the macrospins. The Imry and Ma theorem [Imry 75] states that such a random anisotropy forbids the formation of a long range order state and consequently the macrospins are not coupled rigidly but rather correlated on a length scale much larger than the pairwise ferromagnetic exchange range. Consequently the magnetization undergoes smooth stochastic rotations over the sample, in contrast with the ferromagnetic domain structure with defined boundaries [Fish 88, Chud 88].

Such a correlated spin glass is known to be a soft magnet at low fields while at high fields it slowly reaches saturation. The origin of this behaviour relies in the fact that at $H = 0$, even if the total magnetization averages to zero, the system is not disordered, but rather undergoes a smooth random rotation. As a small field is applied, the macrospins will orient coherently giving rise to a faster response than in a non-interacting system. However this orientation is not complete: since the spin glass system does not possess a long range order, the magnetization will still present fluctuations on the scale of the correlation length. In order to reach saturation it is necessary to destroy the correlated state and this requires an extra energy giving rise to a slower approach to saturation.

As a result to regimes can be recognised: at low fields the magnetization curve shows a $H^{-1/2}$ behaviour, followed at high field by a H^{-2} [Chud 89, Teja 91]. Magnetization

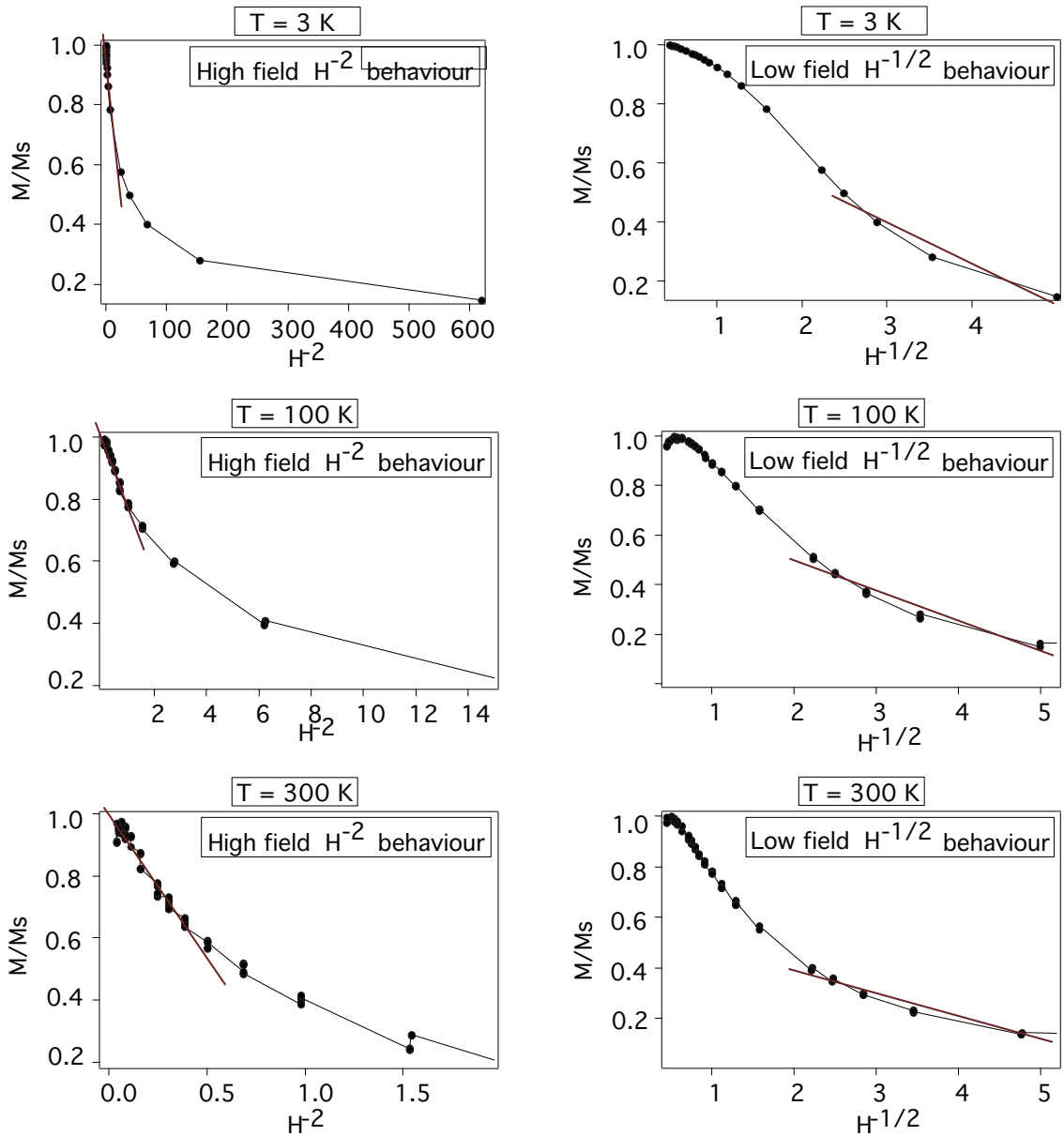


Figure 7.21 – Magnetization curves, obtained from the Hall voltage, of sample $HCoAg_4$ (40 atoms; 1.3%) plotted as a function of $H^{-1/2}$ and H^{-2} for several temperatures. The lines are guides to the eye.

of a diluted sample has been plotted versus $H^{-1/2}$ and H^{-2} at different temperatures, as shown in fig.7.21, in order to verify the theoretical behaviour. At high fields a reasonable agreement is observed, while at low fields no linear behaviour can be recognized. However, not enough data were available to perform this test in a more systematic way and the result presented here cannot be considered as a proof of the failure of the model. Further experiments are necessary in order to better characterize the nature of the correlated state.

7.3 Conclusions

MR and Hall-effect measurement have been interpreted in the frame of the two parallel currents model of transport in granular materials. The results have proven to be in qualitative agreement with similar experiments reported in literature and with standard models used to interpret them.

However such agreement is far from being satisfactory: the superparamagnetic model showed to fail even in very diluted samples (concentration lower than 1%) and the correction apported in the frame of the interacting superparamagnet model in order to include weak interactions, are not sufficient neither.

The failure of the models has been attributed to the presence of correlations mediated by the matrix which are responsible for the formation of a correlated spin glass. Furthermore, the presence of correlation is confirmed by the impossibility of describing MR with a quadratic dependence on the magnetization.

If the presence of interactions is surely a major cause for the impossibility of describing magnetotransport in the frame of the superparamagnetic model, another origin of contrast between experiments and the theories presented here, might be the presence of spin mixing. In fact in the Mott picture, the two spin channel are assumed to be parallel and the possibility of spin flipping events is not considered. This hypothesis, while being realistic in magnetic systems, is not necessarily fulfilled in the case of cluster assembled materials. In the following chapter it will be relaxed and the importance of spin mixing mechanisms will be underlined with the further help of the MDR measurement protocol.

Beyond the Mott hypothesis

We saw in the previous chapter that the Mott picture of electronic transport, is not sufficient to explain all the details of spin-transport in cluster-assembled systems. In fact the model traditionally used to describe MR and magnetization describes only in first approximation the experimental behaviour. If part of the failure can be attributed to the presence of interactions between clusters, we want to show here that it is also necessary to abandon the hypothesis of parallel currents and to consider the effects of intermixing between the two spin channels.

We claim that the failure of the models shown in the preceding chapter might be due not only to the presence of interactions, but also to the importance of the spin-mixing effects.

Furthermore it will be pointed out how the novel measurement of differential resistivity (MDR) can underline the limits of Mott picture and be used to study the effects of spin-mixing.

8.1 Experimental

As done in the previous chapter for MR and Hall effect, the experimental results as a function of the different parameters are presented here for MDR . Their interpretation will follow in next section.

8.1.1 Magnetic Field and Temperature

The typical MDR curve, as can be seen in fig.8.1 shows a rapid increase with magnetic field, followed by a slower decrease at higher fields. No saturation was observed in our samples up to $5T$.

The effect of temperature is twofold: on one side the signal amplitude is strongly suppressed as the temperature is increased, furthermore, the steepness of both the upward and downward parts is reduced at higher temperature, inducing also a displacement of the maximum towards higher fields.

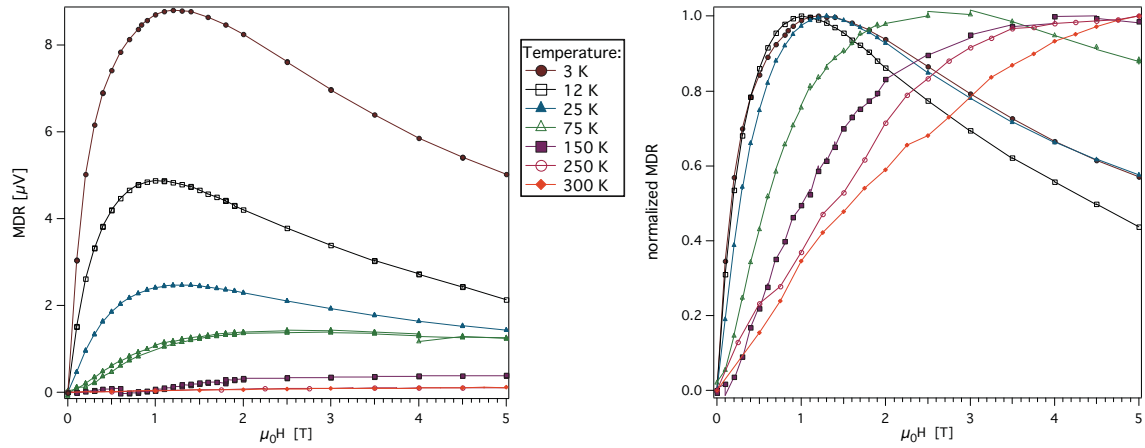


Figure 8.1 – *MDR* (left) and *normalized MDR* (right) as a function of temperature for sample *CoAg16* (40 atoms; 0.8%).

8.1.2 Concentration

In fig.8.2 and 8.3 data for samples containing clusters of the same average size at different concentration are reported. While in the case of *MR* no significant difference is observed at low temperature ($T = 3\text{ K}$) for concentration up to 30%, differences in the *MDR* are visible. The sample at higher concentration reaches the maximum faster than the others and shows a sharper decrease at high fields. This fact is interesting since it indicates that the *MDR* measurement is more sensitive to the details of local magnetization with respect

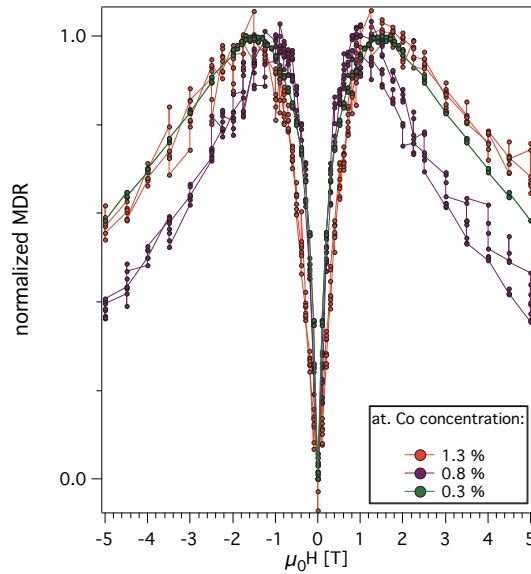


Figure 8.2 – *MDR* of samples containing clusters of 40 atoms at different concentrations. All measurements are performed at $T = 3\text{ K}$.

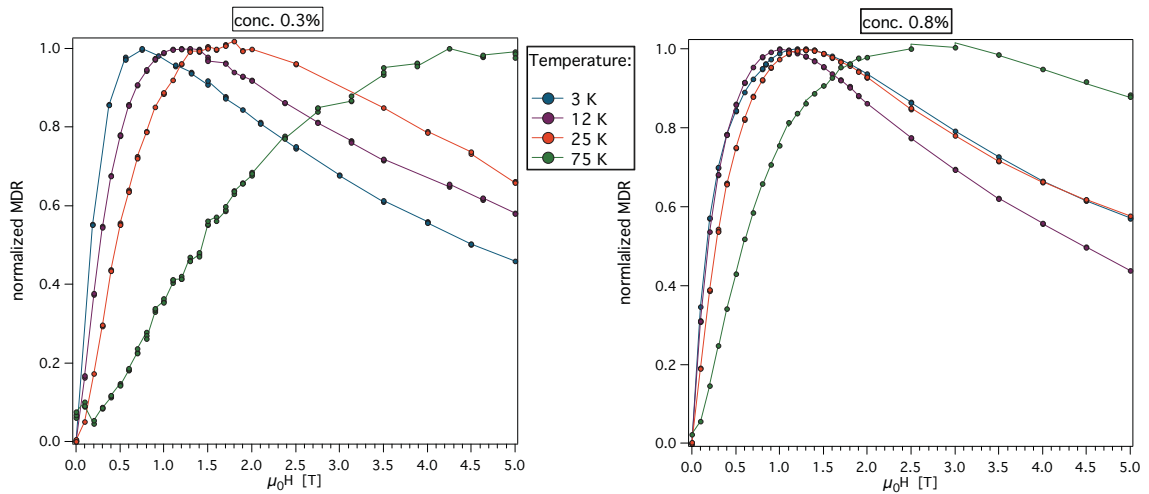


Figure 8.3 – *MDR* of samples containing clusters of 40 atoms at two concentrations. Curves at different temperatures between 3 and 75 K are plotted to underline the changes in temperature behaviour.

to *MR*.

When the temperature dependence is considered, the differences become more important: the higher concentration sample shows a blocking at low temperature that is not observed for the dilute one. This different temperature behaviour is particularly evident when considering the curve at 75 K: on the left the maximum is eventually reached at $H = 5 T$ while on the right it is clearly attained at about 3 T.

8.1.3 Size

The effect of size on *MDR* is displayed in fig.8.4 for the *CoCu* series. An evident reduction of the signal intensity is observed as the size is increased. Such a sharp decrease is due in part to the fact that, the atomic *Co* concentration being constant in the four considered samples, the cluster concentration decreases, reducing the number of scattering events. It is however interesting to remark that no analogous decrease was observed in *MR* curves, proving that the *MDR* measure is sensitive to different effects than those determining magnetoresistance.

Furthermore a size effect is observed in the form of the signal, as showed in fig.8.5. The maximum that characterizes the *MDR* is shifted to lower fields as larger clusters are considered. This can be explained with a faster saturation in the case of larger values of the macrospin, in analogy with what is observed for *MR*.

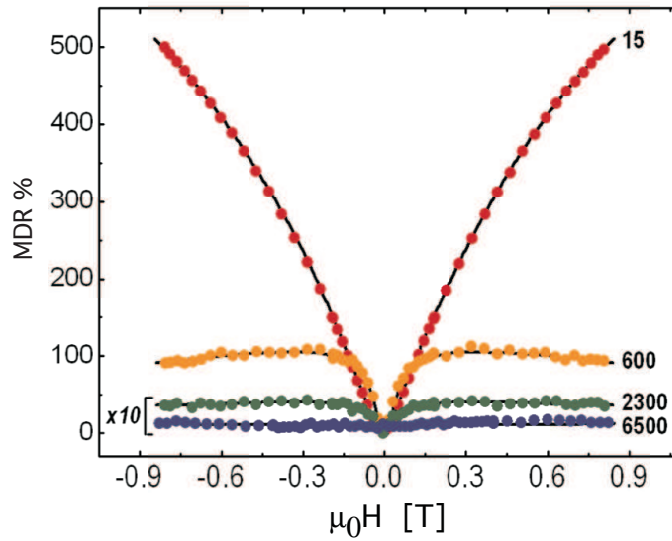


Figure 8.4 – MDR of samples $CoCu_5$, $CoCu_9$, $CoCu_{12}$ and $CoCu_{11}$. All samples contain the same atomic Co concentration (8%) while the average cluster size is marked next to each curve. Curves referring to samples $CoCu_{12}$ and $CoCu_{11}$ are multiplied by a factor 10 for a better visualization. All measurement are performed at $T = 14K$.

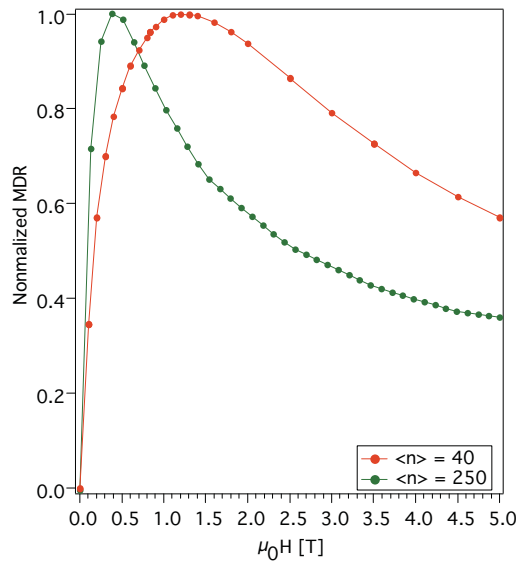


Figure 8.5 – Normalized MDR curves for samples $CoAg_{12}$ (250 atoms; 1.0%) and $CoAg_{16}$ (40 atoms; 0.8%) at $T = 3K$. The effect of size on the shape of the signal is clearly observed and is much more evident than the size effect on MR curves.

8.2 *MDR* in the superparamagnetic model

In presenting the results, it was already underlined how this measurement protocol reveals some details that are not visible in the *MR* data. In particular it was remarked that *MDR* is more sensitive to concentration and size effects. This greater sensitivity to the conduction details can be underlined comparing the experimental results with the superparamagnetic model.

As discussed in section 6.3.3 this measurement consists in a differential resistance measurement $\frac{dR}{dT}$. In the superparamagnetic hypothesis an expression can though be found deriving the *MR* formula given in eq.7.8 with respect to temperature:

$$MDR(T, H) = \frac{dMR}{dT} = \frac{d}{dT} \mathcal{L} \left(\frac{\mu_B S H}{k_B T} \right)$$

The expected temperature behaviour of *MDR* in the superparamagnetic model for a sample containing clusters with a macrospin of $20\mu_B$ is reported in fig.8.6, while in fig.8.7 simulations for different sizes are reported. It can be observed that both the size and temperature

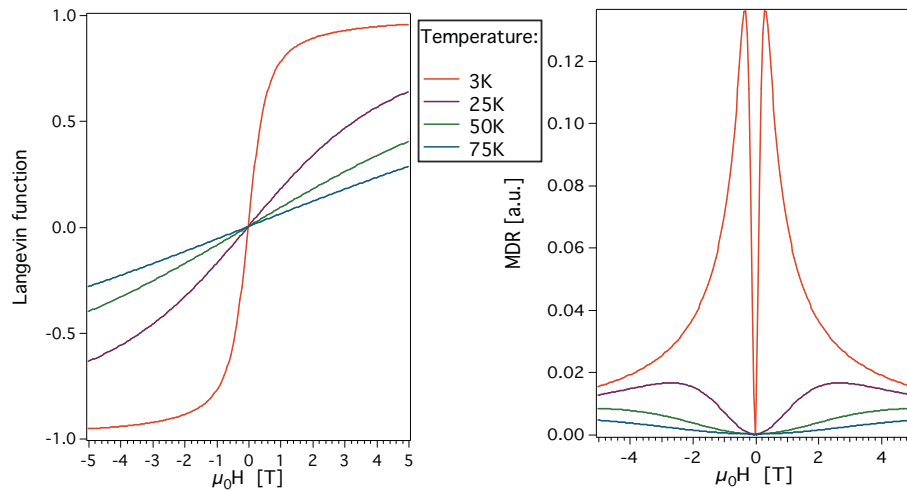


Figure 8.6 – Simulations of *MDR* in the superparamagnetic model for different temperatures assuming a magnetic moment per cluster of $20\mu_B$. On the right the same curves have been normalized to better show their shape.

effect are qualitatively reproduced by the model.

However, when the given expression is used to fit the experimental data, the agreement is far from being good. It is again interesting to compare the result with the one obtained for *MR*: while in the latter case (as for the Hall measurement) it was always possible, for a given temperature, to fit the data with a Langevin-based curve, this is not the case for *MDR* results. In fact it is not possible in the frame of the Langevin model to simultaneously reproduce the fast raise at low fields and the slow saturation. This failure is obviously more evident as the temperature dependence is taken into account.

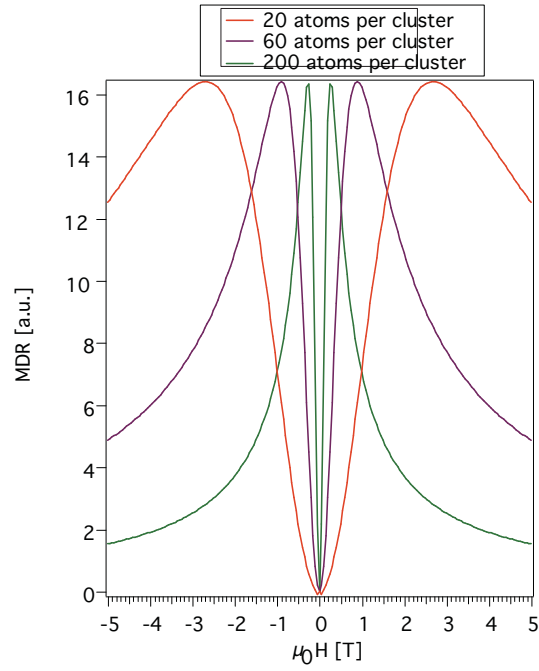


Figure 8.7 – Simulations of MDR in the superparamagnetic model for different cluster sizes. Temperature was fixed at 25K, and a value of $1\mu_B$ per atom was assumed.

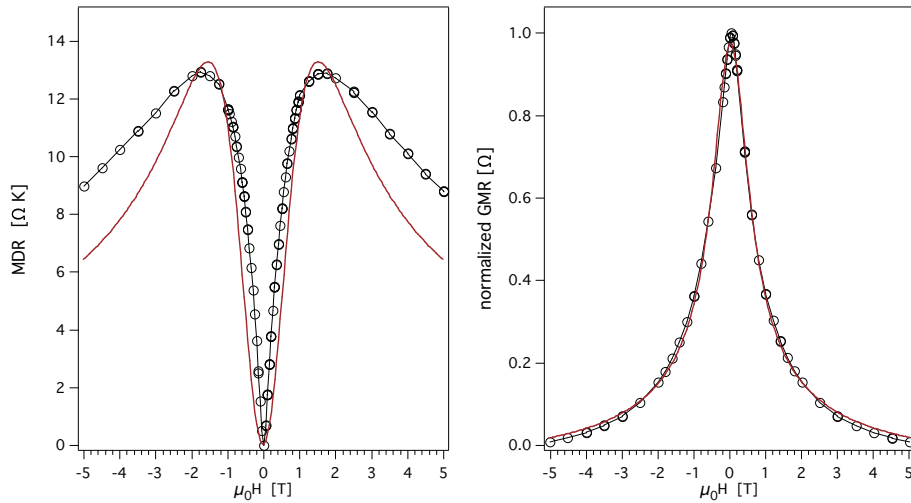


Figure 8.8 – Fit based on the superparamagnetic model for MDR data; MR is also reported for comparison. Data refer to a sample containing clusters of 40 atoms with a concentration of 0.8% (CoAg16). Both measurements were taken at $T = 3$ K.

8.2.1 The importance of MDR

On the basis of what is observed, it can be affirmed that this measurement protocol is more sensitive to the details of the mechanisms defining magnetotransport properties. Up to

now, however, no explication was given for such greater sensitivity nor for the mechanisms that are highlighted by this measurement.

In order to answer the former question, it is useful to reconsider the different contributions that determine the resistivity of a material. In section 4 we saw that the two dominant terms in the resistivity are phononic scattering at high temperature and impurities scattering at low temperatures. Those terms are linear and independent¹ of temperature respectively. As a consequence they cancel in the differential measuring protocol and do not give any contribution to the *MDR* signal that will be mainly determined by the temperature dependent scattering on magnetic impurities[Serr 06, Grav 07]. .

As a result this measurement is more strict than *MR*, in the sense that it cannot be reproduced by an approximative model, and can then be used to study finer phenomena related magnetic scattering.

In particular we claim that *MDR* allows to highlight the effects of spin-mixing scattering, i.e. of those scattering events that imply a change in the spin state of the conduction electron and that, in *MR*, are normally hidden by spin-conserving events. In the following section a description of the mechanisms giving rise to spin-mixing is given and an interpretation of *MDR* in terms of interplay between spin-current is presented.

8.3 *MDR* and Spin-Mixing

Already in the seventies it was argued that spin-mixing effects can occur in magnetic system and, in the case of granular inhomogeneous materials, can play an important role in the resistivity [Fert 76, Jaou 77, Xing 93].

The processes giving rise to a coupling between spin-up and spin-down channels can be different depending on the nature and the temperature of the sample.

- The principal spin-mixing mechanism is the collisions with spin waves or other collective states. It implies a momentum exchange (inelastic scattering) and vanishes at $T = 0$, since no spin wave excitation survives [De G 58, Fert 69] when the temperature is decreased.
- Another source of spin-mixing at finite temperature are collisions between spin-up and spin-down electrons. This contribution is however negligible [Bour 68].
- Finally spin-flip can occur because of scattering on a magnetic impurity. This term does not vanish at zero temperature but its cross section is about two orders of magnitude smaller than spin-conserving scattering ($SC - S$) from the same impurity

¹I refer here to non magnetic impurities or lattice defects. Obviously this is not the case for magnetic impurities, that are taken into account in the next.

[Mono 68] and thus it can be neglected in materials presenting a residual normal¹ resistivity higher than $1\mu\Omega cm$ [Fert 76].

Normally only the first and the last mechanisms are considered and they are referred to as *spin-mixing* ($SM - S$) and *spin-flip* ($SF - S$) respectively. However in the case of our samples that have a relatively high residual resistivity² spin-flip events can also be neglected and the only mechanism coupling the spin-channels is spin-mixing.

Even if spin-mixing effects have attracted some attention in the case of multilayers in CPP configuration [Vale 93, Yang 94] and in granular systems [Wang 95], they are usually neglected in the description of magneto-transport, as it is the case for the Zhang-Levy model. Such approximation, as discussed in the previous chapter gives satisfactory results as far as MR is concerned. On the other hand, when the MDR is considered, the effect of intermixing between spin channels comes to light since the temperature independent part $SC - S$ is cancelled by the differential measurement protocol. That is the reason why it is expected that this measurement can be a useful tool to study the details of spin conduction in magnetic materials.

Resistivity in the presence of spin mixing and spin-flip scattering has been calculated by A. Fert [Fert 69, Fert 76] in the framework of Boltzmann theory of transport, obtaining the following expression³:

$$\rho = \frac{\rho_{\uparrow}\rho_{\downarrow} + \rho_{\uparrow\downarrow}(\rho_{\uparrow} + \rho_{\downarrow})}{\rho_{\uparrow} + \rho_{\downarrow} + 4\rho_{\uparrow\downarrow}} \quad (8.1)$$

where τ_{\uparrow} and τ_{\downarrow} are the relaxation time for each spin channel and

$$\rho_{\uparrow\downarrow} = \frac{m^*}{e^2 n \tau_{\uparrow\downarrow}}$$

is the term coupling the two currents. The relaxation times for $SM - S$ and $SF - S$ are actually hidden in τ_{\uparrow} , τ_{\downarrow} and $\tau_{\uparrow\downarrow}$. The effect of spin-mixing is a depolarization of the electrical current and it will thus reduce the MR amplitude since the decreasing of resistance is the result of a spin-polarization of conduction electrons.

The origin of spin mixing in granular samples is still a topic of discussion. The main spin mixing mechanism is usually assumed to be electron-magnon collisions [Fert 69, Pira 93]. Because of the presence of correlation and the subsequent formation of the spin-glass state, collective excitations can exist in the samples under study. As a consequence, spin-mixing might be caused by scattering events implying the annihilation or creation of these excitations of the correlated spin-glass state.

In cluster assembled materials, however, spin mixing might be produced by a different mechanism. It has been proposed [Serr 06] that the spins of the conduction electrons precess

¹With *normal* resistivity I refer to the one due to spin-conserving events.

²Typical resistances for a $1 \times 0.1 \times 50 \cdot 10^{-7} cm^3$ sample are of the order of 30Ω , corresponding to $\rho \sim 1 \cdot 10^{-5} \Omega cm$.

³The derivation can be found in appendix B.

about the exchange field as they pass through the magnetic grains. This mechanism is called *Jitterbug spin channel mixing* [Gehr 95] and is represented schematically in fig.8.9. Consider two clusters in position i and j having misaligned magnetic moments. An electron

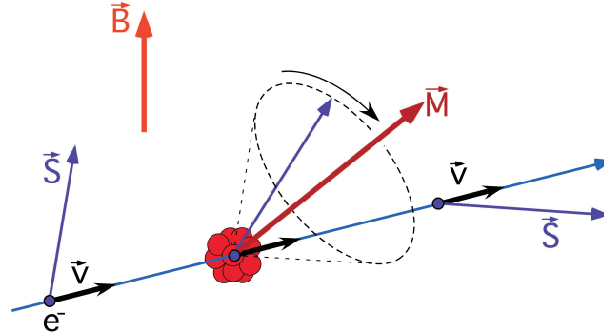


Figure 8.9 – Schematics of the Jitterbug mechanism. When a conduction electron traverses a magnetic cluster, its spin is induced to precess and in the end the electron can be found in a different spin state with respect to the quantization axis defined by the external field.

incident on i will undergo precession and the cluster will act as a spin filter producing a polarized current. Since the scattering probability depends on the spin state of the electron, the filtering action of cluster i will influence the scattering on the site j . The effect of the mechanism is hence stronger for stronger misalignment of neighbouring magnetic moments. At zero field the magnetic moments of clusters are randomly oriented, consequently the jitterbug precession is completely symmetric. As a finite field is applied this symmetry is broken and the mechanism will become effective. If the magnetic field is increased further, the increasing alignment of the moments will again reduce the spin-mixing, however, since this mechanism is very sensitive to small deviations in orientation, it can be observed even at high fields in regions where the clusters are almost completely saturated. Furthermore a strong dependence on inter-granular distance is expected since the effect is maximized if such distance is of the order of the electron spin diffusion length¹.

8.4 Conclusions

The importance of *MDR* for a complete understanding of transport in magnetic cluster assembled materials has been discussed. Such measurement technique, based on the differentiation of the resistance with respect to temperature, allows to focus on those mechanisms that are normally hidden in *MR*.

As a result *MDR* curves show a clear failure of models introduced in the previous chapter. Those models are based on two major hypothesis: the superparamagnetic behaviour of clusters and a two parallel currents conduction mechanism. It can be consequently stated

¹In a matrices such as those considered here, the spin diffusion length is of the order of $\sim 50nm$ [Doud 96]

that at least one of these two hypothesis is not satisfied in the systems under study. The presence of interactions and their importance, inducing the failure of superparamagnetism-based models, have been already demonstrated and discussed in analysing the MR results and they surely play a role in the form of the MDR .

However, we claim that this measurement allows to observe the failure of the second hypothesis: the assumption that spin channels are separated. In fact spin-mixing scattering effects are known to exist, though playing a minor role, in granular systems. The experimental behaviour observed for MDR seems to confirm the existence of a relation between the mechanisms detected by this measurement and spin-mixing. In particular the observed slow saturation is in agreement with the fact that spin-mixing depends on the angle between neighbouring moments and even a small misalignment, negligible with respect to the total magnetization, can induce an effect.

The greater sensitivity of MDR with respect to MR could underline phenomena due to spin-mixing and allow to get a deeper insight on the mechanisms governing magneto transport.

Conclusions and Perspectives

The aim of this work was to study the evolution of magnetic properties of cluster assembled materials by means of transport measurements. In order to specifically tailor the properties of those materials, it should be possible to control the chemical composition, size and concentration of the clusters independently.

For this purpose, an innovative set-up for the production of cluster assembled materials has been built. Clusters are produced in a magnetron-sputtering aggregation source that allows the growing of small ionized aggregates with masses ranging from the dimer to several thousands of atoms. The beam can then be characterized with a time-of-flight mass spectrometer and mass selected prior to deposition. It is also possible to reduce the kinetic energy of the ions in order to achieve a soft landing on the substrate and preserve the clusters from fragmentation. A matrix of a different material is evaporated and deposited on the substrate simultaneously with the beam. A suited evaporation rate of the matrix defines the cluster dilution in the sample. With this growth technique, metallic films of $50nm$ thickness containing cobalt clusters with different sizes and concentrations have been produced.

The samples have been then investigated by means of a set of magnetotransport measurements: magneto-resistance (MR), Hall effect and magneto differential resistance (MDR). The latter measurement protocol consists in recording the magnetic-field dependent response in resistivity to a temperature fluctuation induced by shining a diode laser on the sample; as a matter of fact, this procedure corresponds to the detection of the derivative with respect to temperature of the resistance, measured as a function of the magnetic field.

MR , Hall voltage and MDR have been measured for samples with different cluster sizes and concentrations as a function of a magnetic field from -5 to $5T$ at temperatures between 3 and $300K$. The results are in good agreement with similar measurement reported in literature and can be described on a qualitative basis with theories relying on the hypothesis of non interacting particles, as the superparamagnetic behaviour of magnetization and the Zhang and Levy model for magneto-resistance. However the quantitative results obtained using these models are unphysical. In particular the value of the clusters macrospin shows a strong temperature dependance and a value of the order of $10\mu_B$ per atom is found at

300K. Furthermore it was observed that the parabolic expression of MR , $MR \propto (1 - m^2)$, is not satisfied, especially at low temperatures or at high cluster concentration. From these results it can be deduced that the condition of non-interacting particles is not fulfilled in the case of our clusters even at cobalt atomic concentrations lower than 1%. Such a conclusion is not surprising and can be understood considering that, for a fixed atomic concentration, the average inter-cluster distance is much shorter as the size of the clusters is reduced. Consequently, in the regime of very small sizes considered here, the average distance is sufficiently small to allow the appearance of interaction effects even in very diluted samples.

However, even though interactions appear, no coercivity is observed. This is due to the nature of the interaction: estimating the strength of each possible coupling mechanism, it was deduced that the main cause is probably an indirect exchange mediated by the conduction electrons of the matrix ($RKKY$ coupling). In this case the coupling constant is known to oscillate in sign as a function of the distance between the moments. Since the clusters are randomly distributed, the interaction forces acting on a cluster will not have necessarily all the same sign, giving rise to a frustration of the macrospin. In such a case, the system can become a correlated spin glass. A qualitative interpretation of the experimental results, based on the temperature evolution of the low-field susceptibility and on the form of the magneto-resistance seems to confirm this hypothesis, however further experiment are required in order to give a more accurate proof.

Even if interacting macrospins present a variety of fascinating behaviour, it would be of great interest to obtain samples in which no interaction between clusters occur. In this case, it would be possible to apply the superparamagnetic model in order to extract the value of the clusters macrospin. Since the samples produced with the set-up presented in this work contain nanoparticles with a very sharp mass distribution, this measurement would allow to study the evolution of the magnetic moment as a function of cluster size.

Furthermore, the absence of interactions allows to compare directly the two-parallel current model for electrical conduction with MR data: in such a case, an eventual difference between the theory and the experimental results could be attributed unambiguously to scattering mechanisms that are not taken into account in the two-parallel current model. Another subject that has been discussed, is indeed the nature of the scattering mechanisms giving rise to magneto-transport phenomena. Several magnetotransport models, as the Zhang-Levy theory, describe the electrical conduction with the hypothesis of two separate independent spin-channels. Nevertheless some scattering events might result in a flip of the spin of the electron and, hence, in a coupling between the two channels. This effect, often referred to as spin-mixing, might become important in cluster assembled material and it was shown that the novel MDR measurement protocol might be a good tool for investigating it. This is due to the fact that the differential nature of the MDR technique allows to eliminate the dominant contribution to the resistivity and to focus on those

mechanisms that are not easy to observe in MR curves. At the moment it is not possible to determine if the observed results are due to spin-mixing or to the effect of magnetic interactions. Consequently, also in this case, further investigation is necessary in order to obtain a more reliable interpretation of the experimental results.

Outlook

Apart from the further investigation on the transport properties of magnetic cluster-assembled materials, that has been already discussed, several other experiments can be foreseen.

First of all, other measurement techniques could be used to study the magnetic properties of clusters. In particular the evolution of the magnetic moment, as well as the partition between orbital and spin moment as a function of size, could be measured using x-ray magnetic circular dichroism (XMCD) [Schr 97, Faut 04a]. Another magneto-optical technique that can be used to study this kind of magnetic samples is the Kerr effect [Gibb 85].

Furthermore, the great versatility of the set-up for samples preparation allows to imagine experiments on different kinds of materials. It would be of great interest to study the effect of the matrix on the magnetic properties and in particular to use a semiconductive matrix in order to produce magnetic semiconductors [Mats 01]. The material clusters are made of, can also be changed. It is thus possible to compare different combinations of elements, in order to produce tailored composites with peculiar magnetic properties.

Finally, properties different from magnetism can also be studied. In particular the system allows the evaporation of dielectric matrices that are well suited for the optical characterization of clusters [Hill 07a]. The absorption and fluorescence spectra of small, mass selected clusters [Peys 01] could be studied following this strategy.

General remarks on the measurement technique

In this appendix I discuss some technical aspects of the measurement that need to be considered in order to exclude systematic errors or parasitic effects.

Substrate and matrix

First of all it is necessary to avoid any spurious signal from the substrate and for this reason a sheet of slightly conductive kapton was used as substrate: this choice allows an easy control of soft landing and neutralization during deposition and at the same time does not have any significant effect on the transport measurement since the kapton resistance is much greater than that of the sample and the two add in parallel. Characteristics of kapton and of a silver film deposited on kapton are shown in fig.A and it is verified that no magnetic effects, i.e. MR or MDR , occur.

Influence of current intensity and sampling frequency

Another important check is the determination of the region in which a linear relation exists between current and voltage, since it is necessary to be in this range of current to assure that the sample is ohmic and the resistance can be directly extracted from the voltage measurement. As can be seen in fig.A, this condition is achieved for currents much higher than those used in experiments. On the other hand, as shown in fig.A, the MDR signal gets much more intense (in terms of absolute value) if the current is increased. However a high current produces a variation of the sample temperature through Joule heating and a consequent change in the signal form. Hence a compromise has to be found to guarantee both reliability and intensity of the signal, and for these reason the current was kept lower than 5 mA .

An other parameter whose effect has been analysed, is the frequency of the laser diode in the MDR measurement: decreasing such frequency increases the signal intensity until a plateau is reached at about 5 Hz . These effect is probably due to the fact that the system

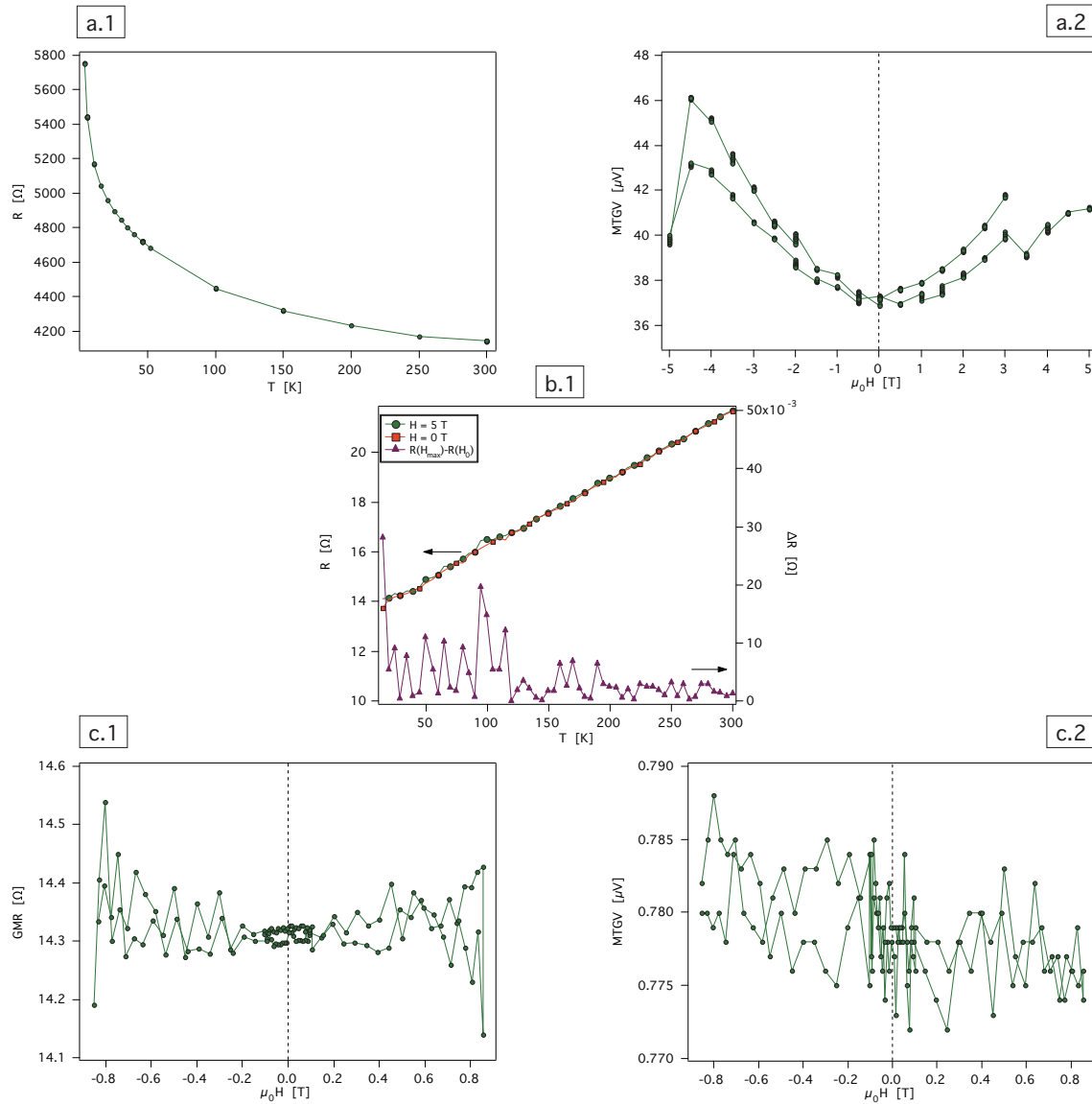


Figure A.1 – a.1) Resistance as a function of temperature of a kapton film: the behaviour is semiconductor-like and values are two orders of magnitude greater than typical sample resistances (cf. b.1). a.2) MDR signal of a kapton film: a response to the magnetic field can be observed, however such response is short-cut by the conducting deposited film. b.1) Resistance of a 50 nm Ag film grown on kapton: resistance has been measured at zero and 5 T magnetic field, the difference shows that no MR occurs. c.1) and c.2) MR and MDR of the same Ag film: no magnetic response is observed.

requires a certain time to completely thermalize at the two extremal temperatures. Is the frequency is not low enough, an intermediate value is achieved and the signal is not maximized. However this intensity variation is not related to a modification of the observed MDR mechanism, as it is confirmed by the fact that the form of the signal is not affected.

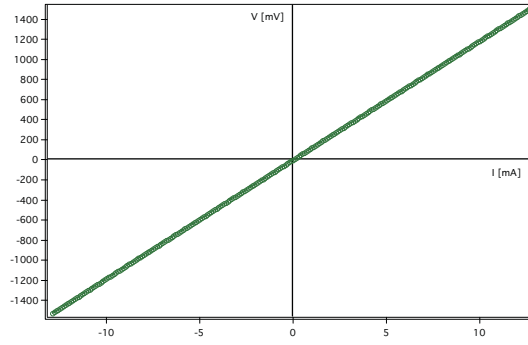


Figure A.2 – *I-V characteristic for a typical sample. A linear behaviour is observed up to 12 mA, while in the experiments the current was always kept lower than 5 mA.*

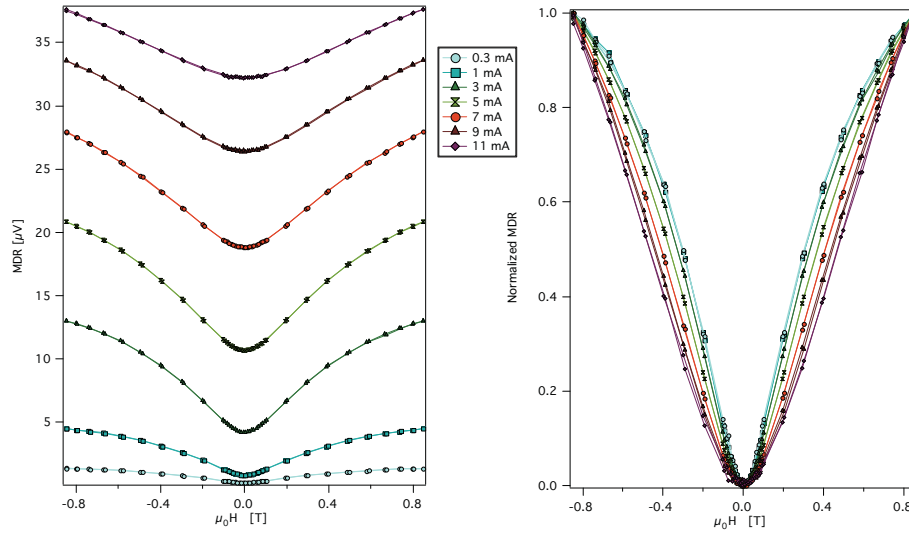


Figure A.3 – *Variation of the MDR signal with current intensity for a sample containing Co clusters with an average size of 23 atoms at an atomic concentration of 1.7%. A strong dependence of both intensity and form can be observed.*

Amplitude of temperature oscillation

A final remark concerns the temperature oscillation induced by illuminating the sample with the laser. It should be first of all remarked that any unambiguous determination is out of reach since too many experimental parameters, such as the laser distance and focalization or the thermal contact, play an important role on it. However an estimation of the order of magnitude can still be made comparing the *MDR* signal to corresponding variation of resistance with temperature. We assume here that the *MR* signal can be described by

$$MR(H, T) = R_0 + \Delta R(1 - \mathcal{L}^2(H, T)) \quad (\text{A.1})$$

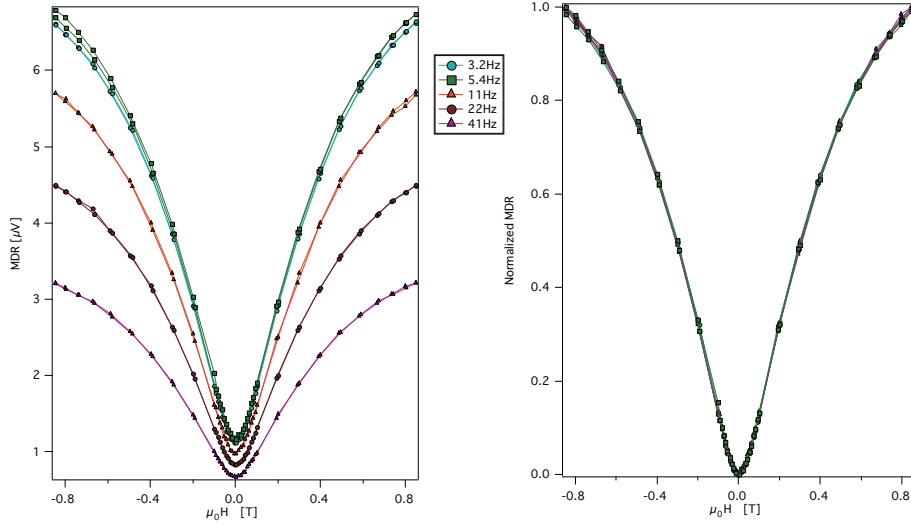


Figure A.4 – Variation of the MDR signal with laser frequency for a sample containing Co clusters with an average size of 23 atoms at an atomic concentration of 1.7%. The intensity of the signal increases with decreasing frequency until a maximum is reached at about 5 Hz. The form of the signal is however not affected, as can be seen in the normalized curves.

where \mathcal{L} is the Langevin function¹ The MDR being the derivative with respect to T , one finds²:

$$MDR(H, T) = \left(MDR_{offset} + 2I\Delta R\mathcal{L}(H, T)\frac{d\mathcal{L}}{dT} \right) \Delta T$$

There are now two different ways of reasoning:

- the amplitude of the MR (ΔR) can be compared to the amplitude of the MDR;
- the offset of the MDR can be compared with the zero field $\frac{dR}{dT}$.

Both procedures imply strong approximation: in the first case the superparamagnetic model used, doesn't completely agree with the experimental data and, for what concerns the second one, the value of MDR_{offset} is strongly affected by parasite effects coming mostly from the electrical contacts. Anyway the values extracted are in good qualitative agreement and of the order of $5 \times 10^{-2} K$.

¹A complete discussion on the form of GMR will follow in the III part.

²Note that the MDR signal is a voltage, that is why the current I is introduced.

Boltzmann equation of spin-dependent electronic transport

The Boltzmann equation describes the evolution of a statistical ensemble of particles under the action of generalized forces (as an electromagnetic field or a temperature gradient). The system is described through its distribution function $g(\mathbf{r}, \mathbf{k}, t)$ ¹, and its evolution is determined according to the semiclassical equations of motions:

$$\begin{aligned}\dot{\mathbf{r}} &= \mathbf{v}(\mathbf{k}) \\ \hbar\dot{\mathbf{k}} &= \mathbf{F}(\mathbf{r}, \mathbf{k}).\end{aligned}$$

In the hypothesis that no collisions occur during an infinitesimal interval of time dt , we can solve these equations to linear order in dt :

$$\begin{aligned}\mathbf{r}(t + dt) &= \mathbf{r}(t) + \mathbf{v}(\mathbf{k})dt \\ \mathbf{k}(t + dt) &= \mathbf{k}(t) + \frac{\mathbf{F}(\mathbf{r}, \mathbf{k})}{\hbar}dt.\end{aligned}$$

Since the volume of phase space is conserved during time evolution, we obtain for the distribution function:

$$g(\mathbf{r}, \mathbf{k}, t) = g(\mathbf{r} - \mathbf{v}(\mathbf{k})dt, \mathbf{k} - \frac{\mathbf{F}(\mathbf{r}, \mathbf{k})}{\hbar}dt, t - dt).$$

In order to relax the hypothesis of no collisions, we need to add a term that will describe the effect of scattering on the distribution function:

$$g(\mathbf{r}, \mathbf{k}, t) = g(\mathbf{r} - \mathbf{v}(\mathbf{k})dt, \mathbf{k} - \frac{\mathbf{F}(\mathbf{r}, \mathbf{k})}{\hbar}dt, t - dt) + \left(\frac{\partial g(\mathbf{r}, \mathbf{k}, t)}{\partial t} \right)_{coll} dt.$$

At this point we can expand our result to the first order in dt and end up with the general form of the Boltzmann equation:

$$\frac{\partial g}{\partial t} + \mathbf{v} \cdot \frac{\partial g}{\partial \mathbf{r}} + \frac{1}{\hbar} \mathbf{F} \frac{\partial g}{\partial \mathbf{k}} = \left(\frac{\partial g}{\partial t} \right)_{coll}. \quad (\text{B.1})$$

¹In the following the distribution function will be chosen to be spin-dependent, $g_s(\mathbf{r}, \mathbf{k}, t)$, in order to take into account the difference in conduction of the two spin channels.

This equation is the fundamental means of investigation of transport properties in solids. The collision term describes the microscopic mechanisms through which the system relaxes when a perturbation is applied. A general expression for such term can be obtained in terms of the probability $P_{i,f}$ for a particle in a state i to be scattered in a state f during the time interval dt .

Since we are concerned with electronic transport in solids, the particles we are interested in are electrons and their states are defined by a wave vector \mathbf{k} and a spin s . The probability to have a collision bringing the electron from the state (\mathbf{k}, s) to the state (\mathbf{k}', s') during dt reads:

$$\frac{P_{\mathbf{k},s;\mathbf{k}',s'} dt d\mathbf{k}}{(2\pi)^3}.$$

Furthermore it has to be considered that electrons are fermionic particles and consequently they are subject to the Pauli exclusion principle. So the probability of having collisions should be reduced by the fraction of initial levels that are occupied, $g_s(\mathbf{k})$, and by that of final levels that are unoccupied, $(1 - g_{s'}(\mathbf{k}'))$. The collision term takes the form:

$$\left(\frac{dg_s(\mathbf{k})}{dt}\right)_{coll} = - \int \frac{d\mathbf{k}'}{(2\pi)^3} g_s(\mathbf{k}) [1 - g_{s'}(\mathbf{k}')] P_{\mathbf{k},s;\mathbf{k}',s'} - g_{s'}(\mathbf{k}') [1 - g_s(\mathbf{k})] P_{\mathbf{k}',s';\mathbf{k},s} \quad (\text{B.2})$$

Assuming that the statistical weight of the initial state is the same for both spin values, we have $P_{\mathbf{k}',s';\mathbf{k},s} = P_{\mathbf{k},s;\mathbf{k}',s'}$ and equation B.2 reduces to:

$$\left(\frac{dg_s(\mathbf{k})}{dt}\right)_{coll} = \sum_{s'=\uparrow,\downarrow} \int \frac{d\mathbf{k}'}{(2\pi)^3} g(\mathbf{k}) [g_{s'}(\mathbf{k}') - g_s(\mathbf{k})] P_{\mathbf{k}',s';\mathbf{k},s} \quad (\text{B.3})$$

In order to separate spin-flip events from spin-conserving ones, we rewrite the expression as:

$$\begin{aligned} \left(\frac{dg_s(\mathbf{k})}{dt}\right)_{coll} &= [g_{-s}(\mathbf{k}) - g_s(\mathbf{k})] P_{\mathbf{k},-s;\mathbf{k},s} + \\ &+ \int \frac{d\mathbf{k}'}{(2\pi)^3} [g_s(\mathbf{k}') - g_s(\mathbf{k})] P_{\mathbf{k}',s;\mathbf{k},s} + \\ &+ \int \frac{d\mathbf{k}'}{(2\pi)^3} [g_{-s}(\mathbf{k}') - g_s(\mathbf{k})] P_{\mathbf{k}',-s;\mathbf{k},s} \end{aligned} \quad (\text{B.4})$$

where the first and last term describe spin-flip and spin-mixing scattering respectively.

It is important to remark that this expression of the collision term, contains the distribution function, so that, when the expression is replaced in the Boltzmann equation (B.1), the result is a non-linear integrodifferential expression that requires sophisticated techniques and approximations in order to be solved.

The simplest of this approximation replaces the collision term by a *relaxation time* $\tau(\mathbf{k})$ that is a specified function of \mathbf{k} and that does not depend on the distribution. Such approximation consists of assuming that each collision seeks to return the system to the equilibrium configuration described by $g^0(\mathbf{r}, \mathbf{k})$, and hence no correlation exists between

successive events. To give an expression for τ we need then to consider the time evolution of the distribution function:

$$g_s(\mathbf{r}, \mathbf{k}, t) = g_s^0(\mathbf{r}, \mathbf{k}) + \alpha_s \left(\mathbf{k} \frac{\partial \bar{\mu}_s(\mathbf{r})}{\partial \mathbf{r}} \frac{\partial g_s^0(\epsilon(\mathbf{k}))}{\partial \epsilon} \right)$$

where $\bar{\mu}_s = \mu_s - eV$ is the spin-dependent electrochemical potential, containing both the chemical potential and the applied electrostatic field, and α_s takes into account the differences between the minority and majority spin channels.

In the additional hypothesis of elastic collisions, three different relaxation times can be obtained from eq.B.4:

$$\begin{aligned} \frac{1}{\tau_{\uparrow\downarrow}} &= P_{\mathbf{k}, -s; \mathbf{k}, s} \\ \frac{1}{\tau_s} &= \int \frac{d\mathbf{k}'}{(2\pi)^3} (1 - \cos \theta_{\mathbf{k}\mathbf{k}'}) P_{\mathbf{k}', s; \mathbf{k}, s} \\ \frac{1}{\tau_{sf}} &= \int \frac{d\mathbf{k}'}{(2\pi)^3} \frac{\alpha_{-s}}{\alpha_s} (1 - \cos \theta_{\mathbf{k}\mathbf{k}'}) P_{\mathbf{k}', -s; \mathbf{k}, s} \end{aligned}$$

where all τ are implicit functions of \mathbf{k} . Hence, using these relaxation times, the collision term of the Boltzmann equation B.1 takes the form [Fert 68]:

$$\mathbf{k} \frac{\partial \bar{\mu}_s(\mathbf{r})}{\partial \mathbf{r}} \frac{\partial g_s^0(\epsilon(\mathbf{k}))}{\partial \epsilon} = - \left(\frac{1}{\tau_s} + \frac{1}{\tau_{sf}} \right) [g_s(\mathbf{k}, \mathbf{r}) - g_s^0(\mathbf{k}, \mathbf{r})] + \frac{g_{-s}(\mathbf{k}, \mathbf{r}) - g_s(\mathbf{k}, \mathbf{r})}{\tau_{\uparrow\downarrow}} \quad (\text{B.5})$$

At this point it is possible to use the previous formula to calculate the transport coefficient and, in our case, the electrical conductivity. In fact the electronic current, in the presence of a constant electric field can be calculated as:

$$\mathbf{j}_s = \int \frac{d^3k}{(2\pi)^3} g_s(\mathbf{k}, \mathbf{r}) e\mathbf{v}$$

Multiplying both sides of B.5 by $e\mathbf{v}$ and integrating over all \mathbf{k} , \mathbf{j}_s and \mathbf{j}_{-s} can be identified. It should be also considered that all the terms containing the equilibrium distribution $g_s^0(\mathbf{k}, \mathbf{r})$ do not contribute to the conduction since only the electrons close to the Fermi energy participate to the conduction process and, as a consequence, only the deformation of the Fermi surface produced by the external field gives a non zero contribution in the calculation. The following expression is hence obtained for the current:

$$- \frac{1}{e} \frac{\partial \bar{\mu}_s(\mathbf{r})}{\partial \mathbf{r}} \frac{e^2 k_F^2 \epsilon_F}{3\pi^2 m} = \left(\frac{1}{\tau_s} + \frac{1}{\tau_{sf}} + \frac{1}{\tau_{\uparrow\downarrow}} \right) \mathbf{j}_s(\mathbf{r}) - \frac{1}{\tau_{\uparrow\downarrow}} \mathbf{j}_{-s}(\mathbf{r}) \quad (\text{B.6})$$

Now the resistivities of each channel, as well as that relative to the spin-flip process can be identified:

$$\begin{aligned} \rho_s &= \frac{3\pi^2 m}{e^2 k_F^2 \epsilon_F} \left(\frac{1}{\tau_s} + \frac{1}{\tau_{sf}} \right) \\ \rho_{\uparrow\downarrow} &= \frac{3\pi^2 m}{e^2 k_F^2 \epsilon_F} \frac{1}{\tau_{\uparrow\downarrow}} \end{aligned}$$

and eq. B.6 can be rewritten separating the two spin channels as:

$$\begin{pmatrix} -\frac{\partial}{\partial \mathbf{r}}(V(\mathbf{r}) - \frac{1}{e}\mu_{\uparrow}(\mathbf{r})) \\ -\frac{\partial}{\partial \mathbf{r}}(V(\mathbf{r}) - \frac{1}{e}\mu_{\downarrow}(\mathbf{r})) \end{pmatrix} = \begin{pmatrix} \rho_{\uparrow} + \rho_{\uparrow\downarrow} & -\rho_{\uparrow\downarrow} \\ -\rho_{\uparrow\downarrow} & \rho_{\downarrow} + \rho_{\uparrow\downarrow} \end{pmatrix} \begin{pmatrix} \mathbf{j}_{\uparrow}(\mathbf{r}) \\ \mathbf{j}_{\downarrow}(\mathbf{r}) \end{pmatrix} \quad (\text{B.7})$$

Inverting B.7 and dropping the term corresponding to the chemical potential¹ we obtain:

$$\begin{pmatrix} \mathbf{j}_{\uparrow}(\mathbf{r}) \\ \mathbf{j}_{\downarrow}(\mathbf{r}) \end{pmatrix} = -\frac{1}{\rho_{\uparrow}\rho_{\downarrow} + \rho_{\uparrow\downarrow}(\rho_{\uparrow} + \rho_{\downarrow})} \begin{pmatrix} \rho_{\uparrow} + \rho_{\uparrow\downarrow} & \rho_{\uparrow\downarrow} \\ \rho_{\uparrow\downarrow} & \rho_{\downarrow} + \rho_{\uparrow\downarrow} \end{pmatrix} \begin{pmatrix} -\nabla V(\mathbf{r}) \\ -\nabla V(\mathbf{r}) \end{pmatrix}$$

The total current is then:

$$\mathbf{j} = \frac{\rho_{\uparrow} + \rho_{\downarrow} + 4\rho_{\uparrow\downarrow}}{\rho_{\uparrow}\rho_{\downarrow} + \rho_{\uparrow\downarrow}(\rho_{\uparrow} + \rho_{\downarrow})} (-\nabla V) \quad (\text{B.8})$$

¹We assume here that the material is homogeneous. Since the spatial dependence of the chemical potential decays over a characteristic length, in an homogeneous material it can be considered constant over the all sample.

Bibliography

- [Abe 82] H. Abe, K. P. Charle, B. Tesche, and W. Schulze. “Surface plasmon absorption of various colloidal metal particles”. *Chemical Physics*, Vol. 68, No. 1-2, pp. 137–141, June 1982.
- [Al O 95] I. A. Al-Omari and D. J. Sellmyer. “Magnetic properties of nanostructured CoSm/FeCo films”. *Phys. Rev. B*, Vol. 52, No. 5, pp. 3441–3447, Aug 1995.
- [Alam 92] G. Alameddin, J. Hunter, D. Cameron, and M. Kappes. “Electronic and geometric structure in silver clusters”. *Chem. Phys. Lett.*, Vol. 192, p. 122, 1992.
- [Alay 75] R. Alayan, A. Arnaud, L. Bourgey, E. Broyer, M. Cottancin, J. Huntzinger, J. Lerm, J. Vialle, M. Pellarin, and G. Guiraud. “Application of a static quadrupole deviator to the deposition of size-selected cluster ions from a laser vaporization source”. *Rev.Sci.Instrum.*, Vol. 2004, p. 2461, 75.
- [Albe 78] R. Alben, J. J. Becker, and M. C. Chi. “Random anisotropy in amorphous ferromagnets”. *Journal of Applied Physics*, Vol. 49, No. 3, pp. 1653–1658, 1978.
- [Alli 01] P. Allia, M. Coisson, P. Tiberto, F. Vinai, M. Knobel, M. A. Novak, and W. C. Nunes. “Granular Cu-Co alloys as interacting superparamagnets”. *Phys. Rev. B*, Vol. 64, No. 14, p. 144420, Sep 2001.
- [Alli 95] P. Allia, M. Knobel, P. Tiberto, and F. Vinai. “Magnetic properties and giant magnetoresistance of melt-spun granular $Cu_{100-x} - Co_x$ alloys”. *Phys. Rev. B*, Vol. 52, No. 21, pp. 15398–15411, Dec 1995.
- [Alli 99] P. Allia, M. Coisson, M. Knobel, P. Tiberto, and F. Vinai. “Magnetic hysteresis based on dipolar interactions in granular magnetic systems”. *Phys. Rev. B*, Vol. 60, No. 17, pp. 12207–12218, Nov 1999.
- [Altb 96] D. Altbir, J. d’Albuquerque e Castro, and P. Vargas. “Magnetic coupling in metallic granular systems”. *Phys. Rev. B*, Vol. 54, No. 10, pp. R6823–R6826, Sep 1996.

- [Ashc 76] N. Ashcroft and N. Mermin. *Solid State Physics*. Saunders College Publishing, 1976.
- [Baib 88] M. N. Baibich, J. M. Broto, A. Fert, F. N. Van Dau, F. Petroff, P. Eitenne, G. Creuzet, A. Friederich, and J. Chazelas. “Giant Magnetoresistance of (001)Fe/(001)Cr Magnetic Superlattices”. *Phys. Rev. Lett.*, Vol. 61, No. 21, pp. 2472–2475, Nov 1988.
- [Beck 56] E. Becker, K. Bier, and W. Henkes. “Strahlen aus kondensierten Atomen und Molekeln in Hochvakuum”. *Z. Physik*, Vol. 146, p. 333, 1956.
- [Ben 05] A. Ben-Bassat. “Sluggish data transport is faster than ADSL”. *Ann. of Impr. Research*, Vol. 11, p. 4, 2005.
- [Berg 70] L. Berger. “Side Jump mechanism for the Hall Effect of ferromagnets”. *Phys. Rev. B*, Vol. 2, p. 4559, 1970.
- [Berk 92] A. E. Berkowitz, J. R. Mitchell, M. J. Carey, A. P. Young, S. Zhang, F. E. Spada, F. T. Parker, A. Hutten, and G. Thomas. “Giant magnetoresistance in heterogeneous Cu-Co alloys”. *Phys. Rev. Lett.*, Vol. 68, No. 25, pp. 3745–3748, Jun 1992.
- [Berr] M. Berry and A. Geim. “Levitation without Meditation”. IgNobel Prize in Physics 2000.
- [Bill 93] I. Billas, J. A. Becker, A. Chtelain, and W. de Heer. “Magnetic moments of Iron clusters with 25 tot 700 atoms and their dependence on temperature”. *Phys. Rev. Lett.*, Vol. 71, p. 4067, 1993.
- [Bill 94] I. Billas, A. Chtelain, and W. de Heer. “Magnetism from the atom to the bulk in iron, cobalt and nickel clusters”. *Science*, Vol. 265, p. 1682, 1994.
- [Bill 95] I. Billas. *Magnetism of iron, cobalt and nickel clusters studied in molecular beams*. PhD thesis, EPFL, 1995.
- [Bina 89] G. Binasch, P. Grünberg, F. Saurenbach, and W. Zinn. “Enhanced magnetoresistance in layered magnetic structures with antiferromagnetic interlayer exchange”. *Phys. Rev. B*, Vol. 39, No. 7, pp. 4828–4830, Mar 1989.
- [Bind 86] K. Binder and A. Young. “Spin glasses: Experimental facts, theoretical concepts, and open questions”. *Rev. Mod. Phys.*, Vol. 58, p. 801, 1986.
- [Binn 02a] C. Binns, M. J. Maher, Q. A. Pankhurst, D. Kechrakos, and K. N. Trohidou. “Magnetic behavior of nanostructured films assembled from preformed Fe clusters embedded in Ag”. *Phys. Rev. B*, Vol. 66, No. 18, p. 184413, Nov 2002.

- [Binn 02b] C. Binns and M. Maher. “Magnetic behaviour of thin films produced by depositing pre-formed Fe and Co nanoclusters”. *N.J.P.*, Vol. 4, p. 85, 2002.
- [Blau 98] K. Blaum, C. Geppert, P. Müller, W. Nörtershäuser, E. Otten, A. Schmitt, N. Trautmann, K. Wendt, and B. Bushaw. “Properties and performance of a quadrupole mass filter used for resonance ionization mass spectrometry”. *Int. J. of Mass. Spect.*, Vol. 181, p. 67, 1998.
- [Bour 68] A. Bourquart, E. Daniel, and A. Fert. *Phys. Lett.*, Vol. 26A, p. 260, 1968.
- [Bran 83] B. Bransden and C. Joachain. *Physics of Atoms and Molecul.* Longman, 1983.
- [Brom 96] K. Bromann, C. Félix, H. Brune, W. Harbich, R. Monot, J. Buttet, and K. Kern. “Controlled deposition of size-selected silver nanoclusters”. *Science*, Vol. 274, No. 5289, pp. 956–8, 1996.
- [Brow 68] W. Brown and E. Frei. *J.Appl.Phys.*, Vol. 39, p. 993, 1968.
- [Camp 70] I. Campbell, A. Fert, and O. Jaoul. *Solid State Phys.*, Vol. Suppl.1, p. S95, 1970.
- [Chud 86] E. M. Chudnovsky, W. M. Saslow, and R. A. Serota. “Ordering in ferromagnets with random anisotropy”. *Phys. Rev. B*, Vol. 33, No. 1, pp. 251–261, Jan 1986.
- [Chud 88] E. M. Chudnovsky. “Magnetic properties of amorphous ferromagnets”. *J. Appl. Phys.*, Vol. 64, p. 5770, 1988.
- [Chud 89] E. Chudnovsky. “dependence of the magnetization law on structural disorder in amorphous ferromagnets”. *J. Magn. Magn. Mater.*, Vol. 79, p. 127, 1989.
- [Chud 95] E. M. Chudnovsky. *The magnetism of amorphous metals and alloys.* 1995.
- [Coeh 88] R. Coehoorn, D. Mooij, J. Duchateau, and K. Bushow. *J. Physique Coll.*, Vol. 49, p. 669, 1988.
- [Cox 85] D. Cox, D. Trevor, R. Whetten, E. Rohlfiing, and A. Kaldor. “Magnetic behavior of free-iron and iron oxide clusters”. *Phys.Rev.B*, Vol. 32, p. 7290, 1985.
- [Datt 90] S. Datta and B. Das. “Electronic analog of the electro-optic modulator”. *Applied Physics Letters*, Vol. 56, No. 7, pp. 665–667, 1990.
- [Daug 97] J. M. Daughton. “Magnetic tunneling applied to memory (invited)”. *The 41st annual conference on magnetism and magnetic materials*, Vol. 81, No. 8, pp. 3758–3763, 1997.
- [De G 58] P. De Gennes and J. Friedel. “Anomalies de résistivité dans certains métaux magnétique”. *J.Phys.Chem.Solids*, Vol. 4, p. 71, 1958.

- [Dien 92] B. Dieny, P. Humbert, V. S. Speriosu, S. Metin, B. A. Gurney, P. Baumgart, and H. Lefakis. “Giant magnetoresistance of magnetically soft sandwiches: Dependence on temperature and on layer thicknesses”. *Phys. Rev. B*, Vol. 45, No. 2, pp. 806–813, Jan 1992.
- [Doud 96] B. Doudin, A. Blondel, and J.-P. Ansermet. “Arrays of multilayered nanowires (invited)”. *The 40th annual conference on magnetism and magnetic materials*, Vol. 79, No. 8, pp. 6090–6094, 1996.
- [Doug 05] D. Douglas, A. Frank, and D. Mao. “Linear ion traps in mass spectrometry”. *Mass Spect. Rev.*, Vol. 24, p. 1, 2005.
- [Doug 93] D. Douglass, D. Cox, J. Bucher, and L. Bloomfield. *Phys. Rev. B*, Vol. 47, p. 12874, 1993.
- [Dupu 04] V. Dupuis, L. Favre, S. Stanescu, J. Tuaille, E. Bernstein, and A. Perez. “Magnetic assembled nanostructures from pure and mixed Co-based clusters.”. *J. Phys.: Condens. Matter*, Vol. 16, p. s2231, 2004.
- [Dupu 97] V. Dupuis, J. Tuaille, B. Prevel, A. Perez, and P. Melinon. “Magnetic interactions in transition metal clusters embedded in matrices prepared by LECBD technique”. *Z. Phys. D*, Vol. 40, p. 155, 1997.
- [East 97] D. Eastham, Y. Qiang, T. Maddock, J. Kraft, J.-P. Schille, G. Thompson, and H. Haberland. “Quenching of ferromagnetism in cobalt clusters embedded in copper”. *J. Phys.: Condens. Matter*, Vol. 9, p. L497, 1997.
- [Ekar 85] W. Ekardt. “Size-dependent photoabsorption and photoemission of small metal particles”. *Phys. Rev. B*, Vol. 31, No. 10, pp. 6360–6370, May 1985.
- [Faut 04a] K. Fauth, E. Goering, G. Schütz, and L. T. Kuhn. “Probing composition and interfacial interaction in oxide passivated core-shell iron nanoparticles by combining x-ray absorption and magnetic circular dichroism”. *Journal of Applied Physics*, Vol. 96, No. 1, pp. 399–403, 2004.
- [Faut 04b] K. Fauth, S. Gold, M. He[ss]ler, N. Schneider, and G. Schutz. “Cluster surface interactions: small Fe clusters driven nonmagnetic on graphite”. *Chemical Physics Letters*, Vol. 392, No. 4-6, pp. 498–502, July 2004.
- [Fedr 93] S. Fedrigo, W. Harbich, and J. Buttet. “Collective dipole oscillations in small silver clusters embedded in rare-gas matrices”. *Phys. Rev. B*, Vol. 47, No. 16, pp. 10706–10715, Apr 1993.
- [Feli 01] C. Félix, C. Sieber, W. Harbich, J. Buttet, I. Rabin, W. Schulze, and G. Ertl. “Ag₈ Fluorescence in Argon”. *Phys. Rev. Lett.*, Vol. 86, No. 14, pp. 2992–2995, Apr 2001.

- [Ferr 97] E. Ferrari, F. da Silva, and M. Knobel. “Influence of the distribution of magnetic moments on the magnetization and magnetoresistance in granular alloys”. *Phys. Rev. B*, Vol. 56, p. 6086, 1997.
- [Fert 68] A. Fert and I. Campbell. “Two-Current conduction in Nickel”. *Phys. Rev. Lett.*, Vol. 21, p. 1190, 1968.
- [Fert 69] A. Fert. “Two-current conduction in ferromagnetic metals and spin wave-electron collisions”. *J. Phys. C*, Vol. 2, p. 1784, 1969.
- [Fert 76] A. Fert and I. Campbell. “Electrical resistivity of ferromagnetic nickel and iron based alloys”. *J. Phys. F*, Vol. 6, p. 849, 1976.
- [Fish 88] D. S. Fisher and D. A. Huse. “Equilibrium behavior of the spin-glass ordered phase”. *Phys. Rev. B*, Vol. 38, No. 1, pp. 386–411, Jul 1988.
- [Full 98] E. E. Fullerton, J. S. Jiang, C. H. Sowers, J. E. Pearson, and S. D. Bader. “Structure and magnetic properties of exchange-spring Sm–Co/Co superlattices”. *Applied Physics Letters*, Vol. 72, No. 3, pp. 380–382, 1998.
- [Gamb 03] P. Gambardella, S. Rusponi, M. Veronese, S. Dhesi, C. Grazioli, A. Dallmeyer, I. Cabria, R. Zeller, P. Dederichs, K. Kern, C. Carbone, and H. Brune. “Giant Magnetic Anisotropy of Single Cobalt Atoms and Nanoparticles”. *Science*, Vol. 300, p. 1130, 2003.
- [Gan 03] L. Gan, R. Gomez, C. Powell, R. McMichael, P. Cheng, and W. J. Egelhoff. “Thin Al, Au, Cu, Ni, Fe, and Ta films as oxidation barriers for Co in air”. *J. App. Phys.*, Vol. 93, p. 8731, 2003.
- [Gang 93] S. Gangopadhyay, G. C. Hadjipanayis, C. M. Sorensen, and K. J. Klabunde. “Exchange anisotropy in oxide passivated Co fine particles”. pp. 6964–6966, AIP, 1993.
- [Garc 00] J. García-Otero, M. Porto, J. Rivas, and A. Bunde. “Influence of Dipolar Interaction on Magnetic Properties of Ultrafine Ferromagnetic Particles”. *Phys. Rev. Lett.*, Vol. 84, No. 1, pp. 167–170, Jan 2000.
- [Gehr 95] G. Gehring, J. Gregg, S. Thompson, and M. Watson. “Electron spin depolarisation in granular magnetic systems”. *Journal of Magnetism and Magnetic Materials*, Vol. 140-144, No. Part 1, pp. 501–502, Feb. 1995.
- [Gerl 22] W. Gerlach and O. Stern. *Z. Physik*, Vol. 9, p. 349, 1922.
- [Gibb 85] D. Gibbs, D. E. Moncton, K. L. D’Amico, J. Bohr, and B. H. Grier. “Magnetic x-ray scattering studies of holmium using synchrotron radiation”. *Phys. Rev. Lett.*, Vol. 55, No. 2, pp. 234–237, Jul 1985.

-
- [Gil 05] W. Gil, G. D., M. Horisberger, and J. Kotzler. “Magnetoresistance anisotropy of polycrystalline cobalt films: Geometrical-size and domain effects”. *Physical Review B (Condensed Matter and Materials Physics)*, Vol. 72, No. 13, p. 134401, 2005.
- [Gilb 00] W. Gilbert. *De Magnete*. London, 1600.
- [Glei 95] H. Gleiter. “Nanostructured Materials: state of the art and perspectives”. *Nanostruct. Mater.*, Vol. 6, p. 3, 1995.
- [Gran 97] A. Granovsky, F. Brouers, A. Kalitsov, and M. Chshiev. “Extraordinary Hall effect in magnetic granular alloys”. *Journal of Magnetism and Magnetic Materials*, Vol. 166, No. 1-2, pp. 193–200, Feb. 1997.
- [Gras 71] A. Grassie, G. Swallow, G. Williams, and J. Loram. “Magnetoresistance in dilute Pd-based alloys”. *Phys. Rev. B*, Vol. 3, p. 4154, 1971.
- [Grav 05] L. Gravier, S. Serrano-Guisan, and J.-P. Ansermet. “Spin-dependent Peltier effect in Co/Cu multilayer nanowires”. *J.App.Phys.*, Vol. 97, p. 105501, 2005.
- [Grav 07] L. Gravier, S. Serrano-Guisan, G. Di Domenicantonio, M. Abid, M. Hillenkamp, C. Flix, and J.-P. Ansermet. “Spin mixing processes in magnetic nanostructures detected by thermoelectric measurements”. *Europhys. Lett.*, Vol. 77, p. 17002, 2007.
- [Greg 94] J. F. Gregg, S. M. Thompson, S. J. Dawson, K. Ounadjela, C. R. Staddon, J. Hamman, C. Fermon, G. Saux, and K. O’Grady. “Effect of magnetic interactions and multiple magnetic phases on the giant magnetoresistance of heterogeneous cobalt-silver thin films”. *Phys. Rev. B*, Vol. 49, No. 2, pp. 1064–1072, Jan 1994.
- [Gu 96] R. Y. Gu, L. Sheng, D. Y. Xing, Z. D. Wang, and J. M. Dong. “Macroscopic theory of giant magnetoresistance in magnetic granular metals”. *Phys. Rev. B*, Vol. 53, No. 17, pp. 11685–11691, May 1996.
- [Habe 94] H. Haberland, M. Mall, M. Moseler, y. Quiang, T. Reiners, and Y. Thrner. *J. Vac.Sci.Technol.*, Vol. 12, pp. 2925–2931, 1994.
- [Habe 95] H. Haberland. *Clusters of Atoms and Molecules*. Vol. 52 of *Springer series in Chemical Physics*, Springer, Berlin, 1995.
- [Hadj 99] G. Hadjiipanayis. “Nanophase hard magnets”. *JMMM*, Vol. 200, p. 373, 1999.
- [Hama 00] H. Hamakake, M. Wakairo, M. Ishikawa, and K. Ishii. “Magnetic and GMR properties of magnetic granular films prepared by low-energy cluster deposition”. *IEEE trans. on mag.*, Vol. 36, p. 2875, 2000.

- [Harr 73] R. Harris, M. Plischke, and M. J. Zuckermann. “New Model for Amorphous Magnetism”. *Phys. Rev. Lett.*, Vol. 31, No. 3, p. 160, Jul 1973.
- [Hilg 00] A. Hilger, N. Cüppers, M. Tenfelde, and U. Kreibig. “Surface and interface effects in the optical properties of silver nanoparticles”. *Eur. Phys. J. D - Atomic, Molecular, Optical and Plasma Physics*, Vol. 10, No. 1, pp. 115–118, March 2000.
- [Hill 06] M. Hillenkamp, G. Di Domenicantonio, and C. Félix. “Monodispersed metal clusters in solid matrices: a new experimental setup”. *Rev.Sci.Instrum.*, Vol. 77, p. 025104, 2006.
- [Hill 07a] M. Hillenkamp, G. Di Domenicantonio, O. Eugster, and C. Félix. “Instability of Ag nanoparticles in SiO₂ at ambient conditions”. *Nanotech.*, Vol. 18, p. 015702, 2007.
- [Hill 07b] M. Hillenkamp, G. Di Domenicantonio, C. Félix, L. Gravier, S. Serrano-Guisan, and J.-P. Ansermet. “Spin-dependent transport in cluster-assembled nanostructures: influence of cluster size and matrix material”. *Eur. Phys. J. B*, 2007.
- [Hohe 64] P. Hohenberg and W. Kohn. “Inhomogeneous electron gas”. *Phys.Rev.*, Vol. 136, p. B864, 1964.
- [Hurd 72] C. Hurd. *The Hall effect in Metals and Alloys*. Plenum Press, New York, 1972.
- [Imry 75] Y. Imry and S. Ma. “Random field instability of the ordered state of continuous symmetry”. *Phys. Rev. Lett.*, Vol. 35, p. 1399, 1975.
- [Jame 01a] M. Jamet, M. Négrier, V. Dupuis, J. Tuaille-Combes, P. Mélinon, A. Pérez, W. Wernsdorfer, B. Barbara, and B. Baguenard. “Interface magnetic anisotropy in cobalt clusters embedded in a platinum matrix”. *Journal of Magnetism and Magnetic Materials*, Vol. 237, pp. 293–301, Dec. 2001.
- [Jame 01b] M. Jamet, W. Wernsdorfer, C. Thirion, D. Maily, V. Dupuis, and P. Mélinon. “Magnetic anisotropy of a single cobalt nanocluster”. *Phys. Rev. Lett.*, Vol. 86, p. 4676, 2001.
- [Jaou 77] O. Jaoul, I. Campbell, and A. Fert. “Spontaneous resistivity anisotropy in Ni Alloys”. *JMMM*, Vol. 5, p. 23, 1977.
- [Jena 96] P. Jena, S. Khanna, and B. Rao. “Stability and Electronic Structure of Cluster Assembled Materials”. *Materials Science Forum*, Vol. 232, p. 1, 1996.
- [John 98] R. Johnston. “The development of metallic bonding in clusters”. *Phil.Trans.RoyalSoc.London*, Vol. A356, p. 211, 1998.

- [Kitt 46] C. Kittel. “Theory of the Structure of Ferromagnetic Domains in Films and Small Particles”. *Phys.Rev.*, Vol. 70, p. 965, 1946.
- [Knig 84] W. D. Knight, K. Clemenger, W. A. de Heer, W. A. Saunders, M. Y. Chou, and M. L. Cohen. “Electronic Shell Structure and Abundances of Sodium Clusters”. *Phys. Rev. Lett.*, Vol. 52, No. 24, pp. 2141–2143, Jun 1984.
- [Koch 05] S. Koch, G. Plasantzas, T. Vystavel, J. De Hosson, C. Binns, and S. Louch. “Magnetic and structural properties of Co nanocluster thin films”. *Phys. Rev. B*, Vol. 71, p. 85410, 2005.
- [Kohn 65] W. Kohn and L. Sham. “Self-Consistent Equations Including Exchange and Correlation Effects”. *Phys.Rev.*, Vol. 140, p. A1133, 1965.
- [Krei 95] U. Kreibig and M. Vollmer. “Springer Series in Material Sciences”. In: *Optical properties of metal clusters*, Springer Verlag, Berlin, 1995.
- [Kres 92] V. V. Kresin. “Collective resonances and response properties of electrons in metal clusters”. *Physics Reports*, Vol. 220, No. 1, pp. 1–52, Nov. 1992.
- [Kund 93] A. Kundt. “On the Hall effect in ferromagnetic materials”. *Wied. Ann.*, Vol. 49, p. 257, 1893.
- [Lau 02] T. Lau, J. A. Föhlisch, R. Nietubyc`, M. Reif, and W. Wurth. “Size-Dependent Magnetism of Deposited Small Iron Clusters Studied by X-Ray Magnetic Circular Dichroism”. *Phys. Rev. Lett.*, Vol. 89, No. 5, p. 057201, Jul 2002.
- [Laur 91] G. Lauritsch, P. G. Reinhard, J. Meyer, and M. Brack. “Triaxially deformed sodium clusters in a self-consistent microscopic description”. *Physics Letters A*, Vol. 160, No. 2, pp. 179–183, Nov. 1991.
- [Levy 90] P. M. Levy, S. Zhang, and A. Fert. “Electrical conductivity of magnetic multilayered structures”. *Phys. Rev. Lett.*, Vol. 65, No. 13, pp. 1643–1646, Sep 1990.
- [Liu 00] J. Liu, R. Skomski, Y. Liu, and D. Sllmyer. “Temperature dependence of magnetic hysteresis of RCox:Co nanocomposites (R=Pr and Sm)”. *J.App.Phys.*, Vol. 87, p. 6740, 2000.
- [Lope 02] J. V. Lopes, J. M. B. Lopes dos Santos, and Y. G. Pogorelov. “Dipolar interactions and anisotropic magnetoresistance in metallic granular systems”. *Phys. Rev. B*, Vol. 66, No. 6, p. 064416, Aug 2002.
- [Luis 06] F. Luis, F. Bartolomé, F. Petroff, J. Bartolomé, L. M. Garcia, C. Deranlot, H. Jaffrès, M. Marinez, P. Bencok, F. Wilhelm, A. Rogalev, and N. Brookes. “Tuning the magnetic anisotropy of Co nanoparticles by metal capping”. *Europhys. Lett.*, Vol. 76, p. 10242, 2006.

- [Lutt 58] J. Luttinger. “Skew Scattering”. *Phys. Rev.*, Vol. 112, p. 739, 1958.
- [Mart 85] J. L. Martins, J. Buttet, and R. Car. “Electronic and structural properties of sodium clusters”. *Phys. Rev. B*, Vol. 31, No. 4, pp. 1804–1816, Feb 1985.
- [Mart 96] T. Martin. “Shells of atoms”. *Physics Reports*, Vol. 273, p. 199, 1996.
- [Mats 01] Y. Matsumoto, M. Murakami, T. Shono, T. Hasegawa, T. Fukumora, M. Kawasaki, P. Ahmet, T. Chikyow, S. Koshihara, and H. Koinuma. “Room-temperature ferromagnetism in transparent transition metal-doped titanium dioxide”. *Science*, Vol. 291, p. 854, 2001.
- [Moli 03] R. Molina, D. Weinmann, and R. Jalabert. “Oscillatory behavior and enhancement of the surface plasmon linewidth in embedded noble metal nanoparticles”. *Europ. Phys. J. D - Atomic, Molecular, Optical and Plasma Physics*, Vol. 24, No. 1, p. 127, June 2003.
- [Mono 68] P. Monod and S. Schultz. “Transmission Electron Spin Resonance in Dilute Copper-Chromium Alloys”. *Phys. Rev.*, Vol. 173, p. 645, 1968.
- [Mott 64] N. Mott. “Electrons in transition metals”. *Adv. Phys.*, Vol. 13, p. 325, 1964.
- [Mydo 93] J. Mydosh. *Spin glasses: an experimental introduction*. Taylor&Francis, 1993.
- [Pare 97] F. Parent, J. Tuaille, L. B. Stern, V. Dupuis, B. Prevel, A. Perez, P. Melinon, G. Guiraud, R. Morel, A. Barthélémy, and A. Fert. “Giant magnetoresistance in Co-Ag granular films prepared by low-energy cluster beam deposition”. *Phys. Rev. B*, Vol. 55, No. 6, pp. 3683–3687, Feb 1997.
- [Pere 97] A. Perez, P. Melinon, V. Dupuis, P. Jensen, B. Prevel, J. Tuaille, L. Bardotti, C. Martet, M. Treilleux, M. Broyer, M. Pellarin, J. Vaille, B. Palpant, and J. Lerme. “Cluster assembled materials: a novel class of nanostructured solids with original structures and properties.”. *J. Phys. D: Appl. Phys.*, Vol. 30, p. 709, 1997.
- [Peys 01] L. Peyser, A. Vinson, A. Bartko, and R. Dickson. “Photoactivated fluorescence from individual silver nanoparticles”. *Science*, Vol. 291, p. 5501, 2001.
- [Pira 93] L. Piraux, M. Cassart, J. S. Jiang, J. Q. Xiao, and C. L. Chien. “Magnetothermal transport properties of granular Co-Ag solids”. *Phys. Rev. B*, Vol. 48, No. 1, pp. 638–641, Jul 1993.
- [Prat 91] W. P. Pratt, S.-F. Lee, J. M. Slaughter, R. Loloee, P. A. Schroeder, and J. Bass. “Perpendicular giant magnetoresistances of Ag/Co multilayers”. *Phys. Rev. Lett.*, Vol. 66, No. 23, pp. 3060–3063, Jun 1991.

- [Resp 98] M. Respaud, J. M. Broto, H. Rakoto, A. R. Fert, L. Thomas, B. Barbara, M. Verelst, E. Snoeck, P. Lecante, A. Mosset, J. Osuna, T. O. Ely, C. Amiens, and B. Chaudret. “Surface effects on the magnetic properties of ultrafine cobalt particles”. *Phys. Rev. B*, Vol. 57, No. 5, pp. 2925–2935, Feb 1998.
- [Rubi 98] S. Rubin, M. Holdenried, and H. Micklitz. “Well-defined Co clusters embedded in an Ag matrix: A model system for the giant magnetoresistance in granular films”. *Eur. Phys. J. B*, Vol. 5, p. 23, 1998.
- [Sanc 99] A. Sanchez, S. Abbet, U. Heiz, W. Schneider, H. Hakkinen, R. Barnett, and U. Landman. “When gold is not noble: nanoscale gold catalysts”. *J. Phys. Chem.*, Vol. 48, p. 9573, 1999.
- [Sche 06] A. Scheffel, M. Gruska, D. Faivre, A. Linaroudis, J. Plitzko, and D. Schuler. “An acidic protein aligns magnetosomes along a filamentous structure in magnetotactic bacteria”. *Nature*, Vol. 440, p. 110, 2006.
- [Schm 98] M. Schmidt, R. Kusche, B. von Issendorff, and H. Haberland. “Irregular variations in the melting point of size-selected atomic clusters”. *Nature*, Vol. 393, No. 6682, pp. 238–240, May 1998.
- [Schr 97] A. Schreyer, C. F. Majkrzak, T. Zeidler, T. Schmitte, P. Bödeker, K. Theis-Bröhl, A. Abromeit, J. A. Dura, and T. Watanabe. “Magnetic Structure of Cr in Exchange Coupled Fe/Cr(001) Superlattices”. *Phys. Rev. Lett.*, Vol. 79, No. 24, pp. 4914–4917, Dec 1997.
- [Scol 88] G. Scoles. *Atomic and Molecular Beam Methods*. Oxford University Press, Oxford, 1988.
- [Serr 06] S. Serrano-Guisan, G. Di Domenicantonio, M. Abid, J.-P. Abid, M. Hillenkamp, L. Gravier, J.-P. Ansermet, and C. Flix. “Enhanced magnetic field sensitivity of spin-dependent transport in cluster-assembled metallic nanostructures”. *Nat.Mat.*, Vol. 5, p. 730, 2006.
- [Shen 03] L. Sheng, D. Y. Xing, H. Y. Teng, and D. N. Sheng. “Random walk simulation of magnetotransport in magnetic granular systems”. *Phys. Rev. B*, Vol. 68, No. 13, p. 132401, Oct 2003.
- [Shi 93] J. Shi, E. Kita, L. Xing, and M. Salomon. *Phys. Rev. B*, Vol. 69, p. 16119, 1993.
- [Skom 93] R. Skomski and J. M. D. Coey. “Giant energy product in nanostructured two-phase magnets”. *Phys. Rev. B*, Vol. 48, No. 21, pp. 15812–15816, Dec 1993.
- [Skom 99] R. Skomski and J. Coey. *Permanent magnetism*. Bristol Institute of Physics Publishing, 1999.

- [Teja 91] J. Tejada, B. Martinez, A. Labarta, and E. M. Chudnovsky. “Correlated spin glass generated by structural disorder in the amorphous $Dy_6Fe_{74}B_{20}$ alloy”. *Phys. Rev. B*, Vol. 44, No. 14, pp. 7698–7700, Oct 1991.
- [Thom 57] W. Thomson. *Proc. Roy. Soc.*, Vol. 8, p. 546, 1857.
- [Tuai 04] J. Tuaille-Combes, O. Boisron, E. Bernstein, G. Guiraud, A. Gerber, A. Milner, P. Melinon, and A. Perez. “Extraordinary Hall effect and X-ray photoemission studies of two dimensional films of magnetic nanoclusters”. *Applied Surface Science*, Vol. 226, No. 1-3, pp. 321–326, March 2004.
- [Vale 93] T. Valet and A. Fert. “Theory of the perpendicular magnetoresistance in magnetic multilayers”. *Phys. Rev. B*, Vol. 48, No. 10, pp. 7099–7113, Sep 1993.
- [Vere 99] M. Verelst, T. Ely, C. Amiens, E. Snoeck, P. Lecante, A. Mosset, M. Respaud, J. Broto, and B. Chaudret. “Synthesis and Characterization of CoO , Co_3O_4 and Mixed Co/CoO Nanoparticles”. *Chem. Mater.*, Vol. 11, p. 2702, 1999.
- [Walk 84] M. Walker, J. Kirschvink, S.-B. R. Chang, and D. A.E. “A candidate magnetic sense organ in the yellowfin tuna, *thunnus albacares*”. *Science*, Vol. 224, p. 751, 1984.
- [Wang 94a] J.-Q. Wang and G. Xiao. *Phys. Rev. B*, Vol. 49, p. 3982, 1994.
- [Wang 94b] J.-Q. Wang and G. Xiao. *Phys. Rev. B*, Vol. 50, p. 3423, 1994.
- [Wang 95] J.-Q. Wang and G. Xiao. “Large finite-size effect of giant magnetoresistance in magnetic granular thin films”. *Phys. Rev. B*, Vol. 51, No. 9, pp. 5863–5867, Mar 1995.
- [Wile 55] W. Wiley and I. McLaren. “Time-of-Flight Mass Spectrometer with Improved Resolution”. *Rev.Sci.Instru.*, Vol. 26, pp. 1150–1157, 1955.
- [Xiao 92] J. Xiao, J. Jiang, and C. Chien. *Phys. Rev. Lett.*, Vol. 68, p. 3749, 1992.
- [Xing 93] L. Xing and Y.-C. Chang. “Theory of giant magnetoresistance in magnetic granular systems”. *Phys. Rev. B*, Vol. 48, p. 4156, 1993.
- [Xion 92] P. Xiong, G. Xiao, J. Q. Wang, J. Q. Xiao, J. S. Jiang, and C. L. Chien. “Extraordinary Hall effect and giant magnetoresistance in the granular Co-Ag system”. *Phys. Rev. Lett.*, Vol. 69, No. 22, pp. 3220–3223, Nov 1992.
- [Xu 05] X. Xu, S. Yin, R. Moro, and W. A. de Heer. “Magnetic Moments and Adiabatic Magnetization of Free Cobalt Clusters”. *Physical Review Letters*, Vol. 95, No. 23, p. 237209, 2005.

- [Yang 94] Q. Yang, P. Holody, S.-F. Lee, L. L. Henry, R. Loloee, P. A. Schroeder, W. P. Pratt, and J. Bass. “Spin flip diffusion length and giant magnetoresistance at low temperatures”. *Phys. Rev. Lett.*, Vol. 72, No. 20, pp. 3274–3277, May 1994.
- [Zhan 05] H. Zhang and X. Chen. “Controlled synthesis and anomalous magnetic properties of relatively monodisperse CoO nanocrystals.”. *Nanotech.*, Vol. 16, p. 2288, 2005.
- [Zhan 93] S. Zhang and P. Levy. “Conductivity and magnetoresistance in magnetic granular films (invited)”. *J. Appl. Phys.*, Vol. 73, p. 5315, 1993.
- [Zhan 95] S. Zhang and P. Levy. “Spin-transport theory of magnetically inhomogeneous systems”. *Mat. Sci. Eng. B*, Vol. 31, p. 157, 1995.
- [Zima 60] J. Ziman. *Electrons and Phonons*. Ed. Oxford at the Clarendon Press, 1960.

Acknowledgement

After four years of harsh work and some months of frenetical writing, the time has arrived to thank all those people that have guided and accompanied me during my doctoral experience.

A special thanks goes to all the members of the examination committee: Prof. R. Schaller, Prof. H. Ronnow, Prof. K. Fauth and Dr. V. Dupuis, for accepting the burdensome job of reading and correcting the manuscript and for all the fruitful remarks that allowed the first, coarse edition of the thesis to transform into this final version.

But the thesis is only the written memory of a much longer work. Hence I would like to express all my gratitude to my supervisors: Prof. Christian Félix and Dr. Matthias Hillenkamp. Christian gave me the opportunity to discover the world of cluster physics and he has been an exemplary thesis director, available for any scientific and human advice and for generous encouragement. Matthias has played an extremely important role in my formation and in the development of the present work: he was always there for me, being my reference in the lab, my office mate and even... my neighbour!

A further appreciation for guaranteeing a friendly, collaborative and stimulating spirit, goes to the other members of the cluster group: capitain Alexandre, Sylvain, Wolfgang, Raphaël, Michael, Régis, as well as the former memebbers, Olivier, Gregoire, Tobias and Varlei that deserves a special thanks for giving me the opportunity to start a new working (but not only) adventure.

As this work is not only made of clusters, but also of transport properties, I wish to thank Prof. J-Ph. Ansermet and all the members of his group for the fruitful collaboration and for all the spin-brain-mixing discussions.

The enjoyable atmosphere I found in the group did extend through the whole institute and that is why I'm grateful to all the technical staff and to the secretaries of the IPN: not only they have given a fundamental contribution through their precious work, but they have also cheered me up with their smiles whenever it was necessary.

Furthermore, in order to get a valuable PhD degree, it is necessary to spend a considerable amount of time in all those activities that allow a complete development of the scientific attitude. It is of great importance to be involved in interdisciplinary discussions

(coffee breaks, late breakfasts), in workshops (fish-days, movie-nights, Sunday-afternoon lunches), in collaborations with other researchers (e-mail writing) and in participating to international conferences (seasonal holidays, bike tours). For this reason I wish to thank all those people that showed always enthusiastic in organizing such events, in particular, the Institute Gang and the Italian Network & Co..

I also wish to thank all my pre-doctoral friends for successfully preserving their friendship from the effects of a four-year long-distance relation.

The final thought, as in all respectful acknowledgement, goes to my parents: thank you for always welcoming me home (even when it was not clear where the home was) and for always being present, not too close, not too far.

Curriculum Vitae

Giulia Di Domenicantonio

Born on April 23rd 1979 in Rome, Italy
nationality: Italian

Languages:

Italian: mother tongue

English: fluent written and oral

French: fluent written and oral

Education:

From December 2003: PhD in Physics at *École Polytechnique Fédérale de Lausanne*.

April 2003 to September 2003 CNR research fellowship at *Università di Roma “La Sapienza”*.

March 2003 *Laurea* with honours in Physics at *Università di Roma “La Sapienza”*.

From 1998 to 2002 Under graduate laboratory assistant.

Schools:

September 2003, Palau (Italy) “School on Neutron Scattering”. Prize as best student.

February 2004, Jülich (Germany) 36th Spring School “Magnetism goes Nano”

Conferences:

May 2004, *Euroconference on Cluster Systems and Nanotubes*. Giens (France)

February 2006, *SPS meeting*. Lausanne (Switzerland)

July 2006, *ISSPIC XIII*. Gotheborg (Sweden)

February 2007, *SPS meeting*. Zurich (Switzerland)

March 2007, *Symposium on Size Selected Clusters*. Brand (Austria)

October 2007, *6th International Conference on Fine Particle Magnetism*. Rome (Italy)

Publications:

- **Monodispersed metal clusters in solid matrices: A new experimental setup**
M. Hillenkamp, G. Di Domenicantonio, C. Félix
Rev. Sci. Instrum., **77** (2006) 025104
- **Enhanced magnetic field sensitivity of spin-dependent transport in cluster-assembled metallic nanostructures**
S. Serrano-Guisan, G. Di Domenicantonio, M. Abid, J.P. Abid, M. Hillenkamp, L. Gravier, C. Félix and J.Ph. Ansermet
Nature Materials, **5** (2006) 113103
- **Spin-dependent transport in cluster-assembled nanostructures: influence of cluster size and matrix material**
M. Hillenkamp, G. Di Domenicantonio, C. Félix, L. Gravier, S. Serrano-Guisan and J.Ph. Ansermet
Eur. Phys. J. B, **126** (2007)
- **Instability of Ag nanoparticles in SiO_2 at ambient conditions**
M. Hillenkamp, G. Di Domenicantonio, O. Eugster, C. Félix
Nanotechnology, **18** (2007) 015702
- **Spin-mixing processes in magnetic nanostructures detected by thermoelectric measurements**
L. Gravier, S. Serrano-Guisan, G. Di Domenicantonio, M. Abid, M. Hillenkamp, C. Félix and J.Ph. Ansermet
Europhys. Lett., **77** (2007) 17002
- **Interaction effects in dilute cluster-assembled magnetic nanostructures**
M. Hillenkamp, G. Di Domenicantonio, C. Félix
to be published in Phys. Rev. B